



**This electronic thesis or dissertation has been  
downloaded from Explore Bristol Research,  
<http://research-information.bristol.ac.uk>**

*Author:*  
**Stockdale, Holly S**

*Title:*  
**The Role of Cardiolipin and pH in the Self-Assembly of Bacterial Membrane Mimics**

**General rights**

Access to the thesis is subject to the Creative Commons Attribution - NonCommercial-No Derivatives 4.0 International Public License. A copy of this may be found at <https://creativecommons.org/licenses/by-nc-nd/4.0/legalcode>. This license sets out your rights and the restrictions that apply to your access to the thesis so it is important you read this before proceeding.

**Take down policy**

Some pages of this thesis may have been removed for copyright restrictions prior to having it been deposited in Explore Bristol Research. However, if you have discovered material within the thesis that you consider to be unlawful e.g. breaches of copyright (either yours or that of a third party) or any other law, including but not limited to those relating to patent, trademark, confidentiality, data protection, obscenity, defamation, libel, then please contact [collections-metadata@bristol.ac.uk](mailto:collections-metadata@bristol.ac.uk) and include the following information in your message:

- Your contact details
- Bibliographic details for the item, including a URL
- An outline nature of the complaint

Your claim will be investigated and, where appropriate, the item in question will be removed from public view as soon as possible.



University of  
**BRISTOL**

## **The Role of Cardiolipin and pH in the Self-Assembly of Bacterial Membrane Mimics**

**Holly Shannon Stockdale**

A dissertation submitted to the University of Bristol in accordance with the requirements for  
award of the degree of Research Master of Science in the Faculty of Science, School of  
Chemistry

August 2020

**Supervisor:** Dr Wuge H. Briscoe  
**Section:** Physical and Theoretical Chemistry  
**Project Group:** Soft Matter at Interfaces (Briscoe) Group

**Word Count:** 19,422



## Abstract

---

Cardiolipin is a unique four-tailed pH-responsive lipid found in the mitochondria of animals and in the membranes of bacteria. It has been found to play a role in altering numerous physicochemical properties of bacterial membrane mimics including membrane fluidity, mechanical stability, and thermotropic behaviour, and it is also unique in that its two headgroups have different pKa values (~2.8 and 7.5-9.5), allowing cardiolipin to be either uncharged, or carry one or two negative charges. However, despite these properties there is still relatively little research on its specific function and role in shaping the self-assembly and phase behaviour of bacterial membranes and the response of these membranes to their environment. In light of the rising need for novel strategies for targeting bacteria due to antibiotic resistance, cardiolipin is an important target for investigation in order to gain a deeper understanding of the bacterial membrane and how it can be disrupted.

This project aimed to investigate the effects of cardiolipin and pH on the properties of bacterial membrane mimics, specifically the phase behaviour of mesophases and the stability of liposomes, two models for bacterial membranes. High-pressure small-angle x-ray scattering (HP-SAXS) was used to construct pressure temperature phase diagrams of mesophases consisting of 1,2-dioleoyl-sn-glycero-3-phosphoethanolamine (DOPE) and 1,2-dioleoyl-sn-glycero-3-phospho-(1'-rac-glycerol) (DOPG) in a 78:22 ratio, and DOPE, DOPG and 18:1 cardiolipin in a 70:20:10 ratio, mimicking the membrane of *E. coli*, at pH 1.3, 5.1 and 12.1. Both cardiolipin and pH were found to have an impact on the phase behaviour of the system, with the H<sub>II</sub> phase forming under ambient conditions at pH 1.3 and the L<sub>α</sub> phase forming at pH 5.1 and 12.1. Cardiolipin was found to have an effect on the behaviour of the system, increasing the sensitivity of the coherence length  $L$  to temperature, increasing the  $d$ -

spacing at all temperatures studied at pH 5.1, and increasing the dependence of  $d$ -spacing on pressure at pH 5.1. DOPE/DOPG and DOPE/DOPG/CL liposomes were also used to model the *E. coli* membrane at pH 5.1 and 12.1 and, where cardiolipin and pH were also found to have an effect on the properties of the liposomes. The cardiolipin-containing liposomes did not undergo any significant change in average diameter  $D$  or zeta potential  $\zeta$  between pH 5.1 and 12.1, while the DOPE/DOPG liposomes had both a lower  $D$  and  $\zeta$  at pH 12.1 than at pH 5.1, pointing to a definite role of cardiolipin in mediating the response of the lipids to pH.

## Acknowledgements

Firstly, I would like to express my gratitude towards my supervisor Dr. Wuge H. Briscoe for giving me the opportunity to undertake this research project in the Briscoe group, and for all of his advice and insight throughout. I am very grateful to him for his guidance during the course of my master's and would like to express my thanks to him for his invaluable support without which this thesis would not have been possible. I would also like to thank Dr Avinash Patil for his suggestions and advice during and following my APM, which were greatly helpful in guiding me during the latter half of my master's.

A huge thanks is extended to Dr Tim Snow and the staff at Beamline I22 at Diamond Light Source for all of their help, and I would also like to thank Prof. Steve Mann's research group for training and allowing me to use their DLS machine and to Dr Annela Seddon for allowing me use of her PLM microscope.

A special thanks goes to the Briscoe group, for being so welcoming, helpful, and supportive during the time I spent doing my master's both in the lab, at beamlines and around the office, and for being good fun and making it a great experience that I won't forget. I would particularly like to thank Dr Laura Fox for her help with HP-SAXS and Lauren Matthews for her help with PLM, both of whom were very generous with their time and expertise and went out of their way to do so.

I would also like to thank the members of my office Lauren Matthews, Dr Anna Slstanova and Dajana Gubala for being lovely people, helping me settle into Bristol, for answering all of my random questions, coming with me to buy burritos and for the fun times we had in the office. Thank you to everyone for making my master's a memorable experience.

Finally, I would like to express deep thanks to my parents for their support and encouragement throughout my master's, I could not have done it without them, and to my friends outside of Bristol for always being there for me.

## ***Author's declaration***

I declare that the work in this dissertation was carried out in accordance with the requirements of the University's Regulations and Code of Practice for Research Degree Programmes and that it has not been submitted for any other academic award. Except where indicated by specific reference in the text, the work is the candidate's own work. Work done in collaboration with, or with the assistance of, others, is indicated as such. Any views expressed in the dissertation are those of the author.

SIGNED: Holly Stockdale

DATE: 24/08/2020



# Contents

---

List of figures & tables . . . . .	10
<b>Chapter 1. Introduction . . . . .</b>	<b>14</b>
1.1 Project motivation . . . . .	14
1.2 Antibiotic resistance . . . . .	16
1.3 Introduction to lipids . . . . .	19
1.4 Introduction to self-assembly . . . . .	21
1.5 The cell membrane as a target . . . . .	25
1.6 Introduction to cardiolipin . . . . .	28
1.7 The pH responsiveness of cardiolipin . . . . .	31
1.8 Lipid mesophases . . . . .	33
1.9 Introduction to liposomes . . . . .	34
1.10 Model membranes . . . . .	36
1.11 Project justification . . . . .	37
<b>Chapter 2. Methods &amp; Experimental . . . . .</b>	<b>39</b>
2.1 Introduction to X-rays . . . . .	39
2.2 Introduction to SAXS . . . . .	40
2.3 Synchrotrons and X-ray generation . . . . .	44
2.4 The effect of pressure on lipids and the use of HP-SAXS . . . . .	45
2.5 Introduction to dynamic light scattering . . . . .	48
2.6 Zeta potential . . . . .	50
2.7 Introduction of polarising light microscopy . . . . .	52
2.8 General methods . . . . .	53
2.8.1 Preparation of pH solutions . . . . .	53
2.8.2 Preparation of samples for HP-SAXS . . . . .	53
2.8.3 HP-SAXS measurements . . . . .	54
2.8.4 Preparation of samples for polarising light microscopy . . . . .	54
2.8.5 Preparation of samples for dynamic light scattering and zeta potential measurements . . . . .	55

<b>Chapter 3: HP-SAXS study on the effect of cardiolipin, temperature, pressure and pH on the phase behaviour of a model bacterial membrane</b> .....	56
3.1 Abstract .....	56
3.2 Results & Discussion .....	57
3.2.1 Phase behaviour of lipid systems .....	58
3.2.2 d-spacing of lipid systems .....	66
3.2.3 Coherence length of lipid systems .....	69
3.3 Conclusions .....	72
<b>Chapter 4: DLS studies on the effect of pH and cardiolipin on the stability of liposomes</b> ..	74
4.1 Abstract .....	74
4.2 Results & Discussion .....	75
4.2.1 Effects of pH and cardiolipin on liposome hydrodynamic diameter ...	76
4.2.2 Effects of pH and cardiolipin on liposome zeta potential $\zeta$ .....	78
4.2.3 Effects of pH and cardiolipin on polydispersity index (PDI) of liposomes .	
.....	81
4.3 Conclusions .....	84
<b>Chapter 5: Polarised light microscopy (PLM) images of bacterial membrane mimics</b> .....	87
5.1 Abstract .....	87
5.2 Results & Discussion .....	88
5.2.1 Individual lipids .....	89
5.2.2 Lipid systems .....	93
5.3 Conclusions .....	98
<b>Chapter 6: Conclusions &amp; future work</b> .....	101
<b>References</b> .....	106

## List of Figures

Figure 1: Common phospholipids with tail groups and headgroups indicated . . . . .	19
Figure 2: Illustration of the components of the packing parameter. . . . .	23
Figure 3: Diagram of the structure of a gram-negative bacteria cell envelope . . . . .	26
Figure 4: The structure of cardiolipin . . . . .	28
Figure 5: The effect of decreasing pH on the headgroup of cardiolipin . . . . .	31
Figure 6: The structure of the $L_{\alpha}$ , $L_{\beta}$ and $L_c$ bilayer phases . . . . .	33
Figure 7: Illustration of the general principle of SAXS . . . . .	41
Figure 8: SAXS patterns obtained during this project. (Left) A pattern from a lipid sample in a lamellar phase, showing the characteristic peak ratio 1:2:3:4:5... (Right) A pattern from a lipid sample in the inverse hexagonal phase, showing the characteristic peak ratio 1: $\sqrt{3}$ :2... . . . .	41
Figure 9: illustration of the $H_{II}$ phase with arrows indicating the positions (100), (110) and (010) planes . . . . .	42
Figure 10: Illustration of the forces between headgroups and tail groups of lipids . . . . .	46
Figure 11: The effect of increasing pressure on inverse hexagonal lipid phases . . . . .	47
Figure 12: Illustration of the potentials and layers of charge present around a particle . . . .	50
Figure 13: Illustration of the peak-fitting process in Igor Pro using data collected in this experiment . . . . .	57
Figure 14: (A&C) Pressure-temperature phase diagrams for lipid mesophase systems at pH 5.1. (B&D) SAXS graphs for CON2 and CL2 at pH 5.1 and $T = 20^{\circ}\text{C}$ . (E) Structures of lipids used in samples and diagrams of lipid mixtures used in samples . . . . .	59
Figure 15: SAXS graphs for CL3 at $T = 20^{\circ}\text{C}$ . . . . .	61
Figure 16: (A) Pressure-temperature phase diagram for CL1. (B) Diagram of $H_{II}$ phase . . . .	62
Figure 17: SAXS data for CL1 at $T = 20^{\circ}\text{C}$ . . . . .	64
Figure 18: Effect of pressure, temperature, and lipid composition on the d-spacing of the lamellar mesophases in samples CON2, CL2 and CL3 . . . . .	65
Figure 19: Linear fits carried out for CON2 (A) and CL2 (C) to obtain $\Delta d/\Delta p$ , and $\Delta d/\Delta p$ against temperature for CON2 (B) and CL2 (C) . . . . .	66
Figure 20: Linear fit for CL3 at $20^{\circ}\text{C}$ to obtain $\Delta d/\Delta p$ , and $\Delta d/\Delta p$ . . . . .	67
Figure 21: The effect of pressure on lattice parameter $a$ for sample CL1, with linear fits used to obtain $\Delta d/\Delta p$ , and $\Delta d/\Delta p$ . . . . .	68

Figure 22: The effect of pressure and temperature on the coherence length $L$ of CON2 (A) and CL2 (B) .....	70
Figure 23: Effect of pressure on the coherence length $L$ of CL3 at 20°C .....	71
Figure 24: Effect of temperature and pressure on the coherence length $L$ of sample CL1 ...	72
Figure 25: The mesophase formed by DOPE/DOPG 78:22 and DOPE/DOPG/CL 70:20:10 at pH 1.3 .....	76
Figure 26: Average diameter of DOPE/DOPG (green) and DOPE/DOPG/CL (blue) liposomes at pH 5.1 .....	77
Figure 27: Average diameter of DOPE/DOPG (green) and DOPE/DOPG/CL (blue) liposomes at pH 12.1 .....	78
Figure 28: Average zeta potential $\zeta$ of DOPE/DOPG (green) and DOPE/DOPG/CL (blue) liposomes at pH 5.1 .....	79
Figure 29: Average zeta potential $\zeta$ of DOPE/DOPG (green) and DOPE/DOPG/CL (blue) liposomes at pH 12.1 .....	80
Figure 30: Polydispersity index (PDI) of DOPE/DOPG liposomes at pH 5.1 .....	81
Figure 31: Polydispersity index (PDI) of DOPE/DOPG/CL liposomes at pH 5.1 .....	82
Figure 32: Polydispersity index (PDI) of DOPE/DOPG liposomes at pH 12.1 .....	83
Figure 33: Polydispersity index (PDI) of DOPE/DOPG/CL liposomes at pH 12.1 .....	84
Figure 34: The charging behaviour of cardiolipin at the pH values examined in this thesis ..	85
Figure 35: PLM images of pure cardiolipin at pH 1.3 taken with a 530 nm waveplate inserted, at 10x magnification .....	88
Figure 36: PLM images of pure cardiolipin at pH 5.1 taken with a 530 nm waveplate inserted, at 10x magnification .....	89
Figure 37: PLM images of pure cardiolipin at pH 12.1 taken with a 530 nm waveplate inserted, at 10x magnification .....	90
Figure 38: PLM images of pure DOPG at pH 1.3 taken with a 530 nm waveplate inserted, at 10x magnification .....	91
Figure 39: PLM images of pure DOPG at pH 5.1 taken with a 530 nm waveplate inserted, at 10x magnification .....	92
Figure 40: PLM image of pure DOPG at pH 12.1 taken with a 530 nm waveplate inserted, at 10x magnification .....	92

Figure 41: PLM images of DOPE/DOPG at pH 1.3 taken with a 530 nm waveplate inserted, at 4x magnification (A, B), 10x magnification (C) and 20x magnification (D) . . . . .	93
Figure 42: PLM images of DOPE/DOPG/CL at pH 1.3 taken with a 530 nm waveplate inserted at 4x magnification . . . . .	94
Figure 43: PLM images of DOPE/DOPG at pH 5.1 taken with a 530 nm waveplate inserted, at 4x magnification (A & B) and 10x magnification (C & D) . . . . .	95
Figure 44: PLM images of DOPE/DOPG/CL at pH 5.1 taken with a 530 nm waveplate inserted, at 4x magnification (A & B) and 10x magnification (C) . . . . .	96
Figure 45: PLM images of DOPE/DOPG at pH 12.1 taken with a 530 nm waveplate inserted, at 4x magnification (A) and 10x magnification (B) . . . . .	97
Figure 46: PLM images of DOPE/DOPG/CL at pH 12.1 taken with a 530 nm waveplate inserted, at 4x magnification (A, B & C) and 10x magnification (D) . . . . .	98

## List of Equations

Equation 1: The thermodynamics of the formation of micelles . . . . .	22
Equation 2: The free energy change associated with aggregation from a dilute monomer state . . . . .	22
Equation 3: The packing parameter . . . . .	23
Equation 4: The relation between radius, volume and area per amphiphile . . . . .	23
Equation 5: Bragg's Law . . . . .	40
Equation 6: Calculation of scattering vector $Q$ . . . . .	42
Equation 7: Calculation of d-spacing . . . . .	42
Equation 8: The Scherrer equation . . . . .	43
Equation 9: Calculation of the radius of gyration . . . . .	44
Equation 10: The Clapeyron equation . . . . .	47
Equation 11: The Stokes-Einstein equation . . . . .	49
Equation 12: Calculation of the decay rate in DLS . . . . .	49
Equation 13: Calculation of wave vector $q$ . . . . .	49
Equation 14: The Henry equation . . . . .	51

## List of Tables

Table 1: Lipid structures and mesophases formed according to packing parameter . . . . .	24
Table 2: Characteristic peak ratios produced by various lipid mesophases from SAXS measurements . . . . .	43
Table 3: Samples investigated via HP-SAXS in this work . . . . .	58
Table 4: Summary of DLS results . . . . .	85
Table 5: Phase assignment of lipid samples observed via PLM . . . . .	99

## Chapter 1. Introduction

---

### 1.1 Project Motivation

Antibiotic resistance is a growing global issue. Bacterial infections are predicted to cause an increasing number of deaths over the 21st century as current antibiotics becomes obsolete, making it clear that alternative strategies for killing bacteria need to be developed. As the bacterial membrane is an essential component of the cell and the interface through which they interact with their environment and antibiotic drugs, it is of fundamental importance to understand how and why bacterial membranes behave under differing solution conditions such as pH, temperature and ion concentration.

Cardiolipin is a unique four-tailed lipid present in an enormous array of prokaryotic and eukaryotic species that makes up a significant proportion of bacterial membranes, typically around 10%. It has been demonstrated to have a significant impact on the physicochemical properties of lipid membranes, affecting their thermotropic behaviour, promoting the formation of non-lamellar structures, increasing membrane fluidity, and decreasing membrane mechanical stability.<sup>1-3</sup> However, at the time of writing no pressure-temperature phase diagram had previously been established for a cardiolipin-containing bacterial membrane model. Constructing a phase diagram would provide an overview of the effect of cardiolipin on the response of a bacterial membrane model to pressure and temperature. There have also been few studies examining the effect of pH on cardiolipin in the context of the behaviour of bacterial membrane models.

Cardiolipin is interesting not just because of its previously established impact on lipid membrane properties, but also due to its pH responsiveness. It is unique in that it contains

two phosphate headgroups and four carbon tails, and it has been demonstrated experimentally that these two headgroups have differing  $pK_a$  values (approx. 2.8 and 7.5-9.5, respectively),<sup>4</sup> likely due to intramolecular bonding between the glycerol linker present and one of the headgroups. It carries a single negative charge at physiological pH; however, as the pH decreases, the repulsion between the headgroups is minimised as both headgroups are protonated. It seems likely that changes in head group repulsion could affect the packing parameter and therefore the self-assembly behaviour of cardiolipin, and so obtaining phase diagrams under different pH conditions would provide further insight into the role cardiolipin is playing in bacteria.

In this project, the phase behaviour of mesophases mimicking the composition of bacterial membranes (i.e. the DOPE:DOPG:CL molar ratio at 70:20:10) has been studied via small-angle X-ray scattering (SAXS) at different pH values at Diamond Light Source beamline I22 with the aim to produce pressure-temperature phase diagrams for this system at different pH values. Polarised light microscopy (PLM) images of these mesophases were also obtained in order to complement the SAXS findings, and dynamic light scattering (DLS) measurements of liposomes - another model mimicking the bacterial membrane - of the same lipid composition were carried out at different pH values to assess the effect of cardiolipin on the stability of the liposomes over time.

A greater understanding of the role of cardiolipin in the behaviour of bacterial membranes would contribute to the overall understanding of how bacterial membranes respond to their environment and maintain structural integrity, with a view to better understand how to physically disrupt bacterial membranes in light of the growing global issue of bacterial antibiotic resistance. Chapter 1 of this thesis introduces the context of antibiotic resistance and introduces cardiolipin and its properties, and how cardiolipin is relevant to this



challenge. It also introduces the concept of self-assembly and lipid mesophases and how they are useful for gaining insight into bacterial membranes. Chapter 2 describes the experimental details of the project, introducing the techniques used and detailing how experiments were conducted. Chapter 3 presents the results of the SAXS experiments and their discussion, while Chapters 4 and 5 cover the DLS and PLM results respectively, before conclusions and future work in Chapter 6.

## 1.2 Antibiotic Resistance

With the discovery of penicillin in 1928, medicine entered a new era wherein previously life-threatening infections became treatable. It also greatly improved the outcomes for the immunocompromised, allowing for treatments such as chemotherapy and organ transplants.<sup>5</sup> The ability to effectively treat infections through the use of naturally and then later synthetically-derived compounds saved countless lives across the 20th century and continues to be a key tool in modern medicine in the 21<sup>st</sup>; however, this ability is now under threat. Even at the dawn of the antibiotic era in 1945, Alexander Fleming, the discoverer of penicillin, warned of the possibility of bacteria developing resistance in his Nobel Lecture: *“It is not difficult to make microbes resistant to penicillin in the laboratory by exposing them to concentrations not sufficient to kill them, and the same thing has occasionally happened in the body”*.<sup>6</sup> These fears would be confirmed in 1947 with the observation of penicillin-resistance in staphylococcus pyogenes, the author stating that *“the rate of increase in this hospital at present is so rapid as to be somewhat alarming”*.<sup>7</sup>

Since then, resistance to subsequently discovered antibiotics has continually developed with methicillin-resistant staphylococcus aureus (MRSA) being identified in 1961- two years after the introduction of methicillin; levofloxacin-resistant pneumococcus emerged

in 1996, the same year that levofloxacin was introduced; and ceftaroline-resistant staphylococcus aureus was found in 2011, with ceftaroline having been introduced in 2010.<sup>8</sup> It is clear that antibiotic resistance in bacteria is a growing issue.

In 2015, there were an estimated 671,689 infections and 33,110 deaths in the EU and European Economic Area as a result of antibiotic resistant bacteria,<sup>9</sup> while in the USA there are estimated to be at least 2 million such infections every year with approximately 23,000 resultant deaths.<sup>10</sup> The prevalence of multidrug resistant bacteria has been growing worldwide at a rapid rate, reaching pandemic levels in the past two decades,<sup>10</sup> with 10 million lives projected to be at risk every year by 2050.<sup>11</sup> This makes clear the scale of the issue - especially as the burden of antibiotic resistant bacteria is highest in babies and the elderly in the EU and EEA, indicating that with an ageing population the threat will only increase.<sup>12</sup>

Alongside the rapid increase in the rates of resistance, there is also a 'discovery gap' in research wherein very few new antibiotic drugs are being discovered and approved for use, while resistance against existing drugs continues to rise: between 2005 and 2009, only one new drug – telavancin - was approved by the FDA.<sup>13</sup> At the same time, antibiotics continue to be prescribed inappropriately, which contributes to the development of resistance,<sup>14</sup> as well as being used in veterinary settings and as herbicides and pesticides,<sup>15</sup> making the preservation of their efficacy a challenge.

There are multiple mechanisms through which bacteria can become resistant to antibiotics. Some have inherent resistance to certain drugs, such as the inherent resistance of gram-negative bacteria to many hydrophobic bacteria owing to the structure of their outer membrane.<sup>16</sup> In addition to the case described by Fleming<sup>17</sup> wherein treatment kills all bacteria except those with inherent resistance which then go on to proliferate, bacteria can acquire resistance through horizontal gene transfer via bacteriophages, plasmids or even

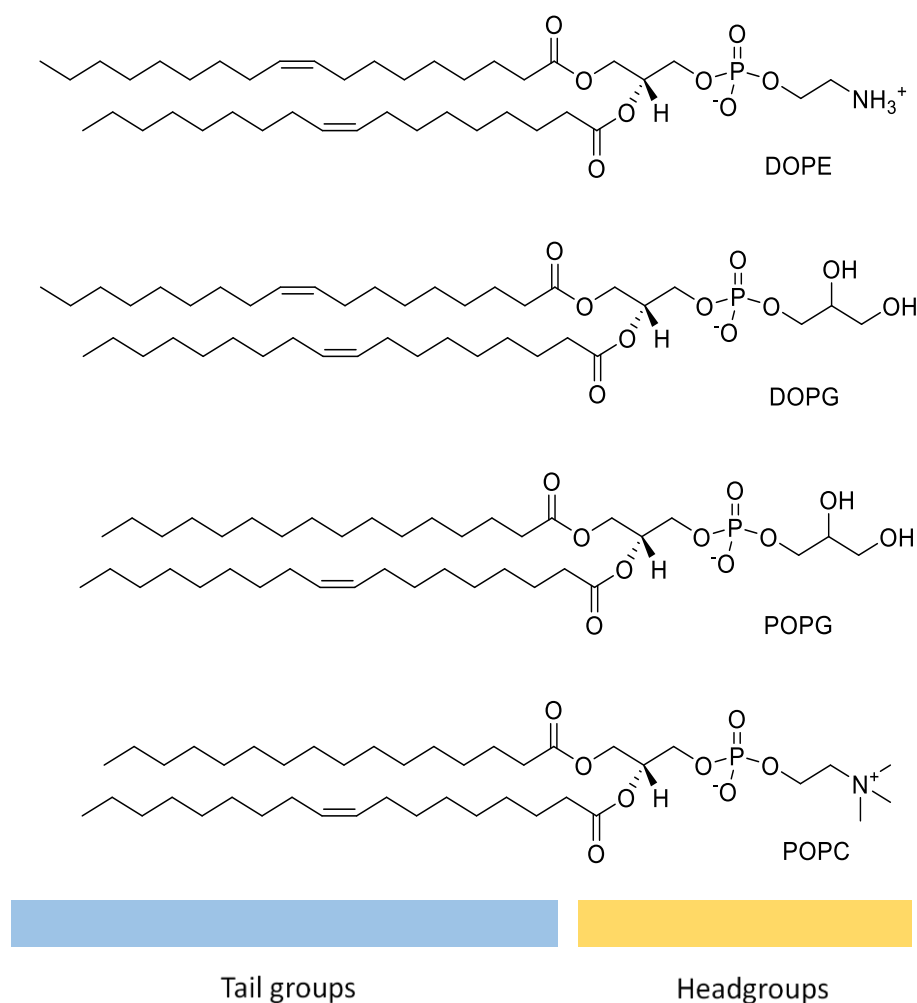
naked DNA (even between bacteria of different taxonomic groups)<sup>18</sup> or undergo spontaneous mutations that grant them resistance.<sup>19</sup> Even so-called 'last resort' antibiotics such as vancomycin, used to treat methicillin-resistant *Staphylococcus aureus* (MRSA) which emerged in 1961, are not guaranteed to remain effective indefinitely; in recent years, vancomycin-intermediate *S. aureus* has emerged worldwide, one of many multidrug- or even pan-resistant species.<sup>20</sup>

The antibiotics discovered in the 'golden age' of discovery in the mid-20th century were almost all found within nature rather than being produced synthetically. However, this eventually led to drugs within the same class being 're-discovered' and an insufficient number of new classes being discovered to keep up with developing resistance. Furthermore, modern antibiotic discovery techniques employed by the pharmaceutical industry since the 1990s such as high-throughput screening have failed to yield significant results.<sup>21</sup> It is clear that, with the seeming inevitability of the development of resistance to conventional antibiotics, there is a necessity for the exploration of alternative strategies to combat bacteria.

There have been several proposed and trialed alternatives to conventional drugs, including antibody therapy,<sup>22</sup> and phage therapy,<sup>23</sup> however, neither have seen wider application in a medical context. While there has been an effort to reduce the rate at which resistance develops to currently used antibiotics through the endorsement of conservative and appropriate use, this is not a strategy that can be counted on to work in the long-term.

### 1.3 Introduction to Lipids

Lipids are a class of amphiphilic biomolecules ubiquitous throughout nature. Amphiphiles are molecules that contain both a hydrophobic and a hydrophilic moiety, and as a result are often soluble in both aqueous and non-aqueous solutions. In the case of lipids, which are soluble in non-polar solvents but not as soluble in water, the hydrophobic moiety consists of fatty acid chains or tails, with both unsaturated chains and saturated chains containing one or more double or triple bonds being present in various species of lipid. Thousands of distinct species have been identified in nature<sup>24</sup>, with a variety of different headgroups, chain lengths and degrees of saturation available. Chain lengths of 12-20 C are common, while a large range of head groups occur including glycerol, choline, serine and inositol.<sup>25</sup> There are eight classes of



**Fig. 1.** Common phospholipids with tail groups and headgroups indicated.

naturally occurring lipids: sphingolipids which have roles in the regulation of various cell processes such as the cell cycle and apoptosis,<sup>26</sup> glycerolipids, glycerophospholipids, sterol lipids, phenol lipid, saccharolipids, and polyketides.<sup>27</sup> They perform a wide range of biological functions, including energy storage, thermal insulation, signaling, and protecting organs from damage.

Phospholipids are defined by the inclusion of a phosphate head group on the linker, and typically have two fatty acid tails. Some phospholipids commonly found in bacteria include 1,2-dioleoyl-sn-glycero-3-phosphoethanolamine (DOPE), 1,2-dioleoyl-sn-glycero-3-phospho-(1'-rac-glycerol) (DOPG), 1-palmitoyl-2-oleoyl-sn-glycero-3-phosphoethanolamine (POPE), and 1-palmitoyl-2-oleoyl-sn-glycero-3-phospho-(1'-rac-glycerol) (POPG) (figure 1).

Phospholipids are notable for being the main component of cell membranes due to their amphiphilic nature, and they self-assemble into a variety of structures in both aqueous and non-aqueous solvents, this being a key feature and essential for life. The formation of bilayers and vesicles allows for the protection of the internal environment of cells and provides a semi-permeable barrier through which ions and essential nutrients can pass. Phospholipids are a constant feature throughout nature, and the composition of lipids present in membranes varies greatly between species and is sensitive to external conditions including pH, temperature, cellular age, availability of nutrients and the presence of pathogens, pointing to their vital and dynamic role in the maintenance of life.<sup>25</sup>

Examples of these qualities include the fact that halophilic and halotolerant bacteria that thrive at high salt concentrations typically contain a larger proportion of anionic lipids compared to non-halophilic species, an adaptation to minimise membrane stress in such an environment,<sup>28</sup> and that temperature has also been found to have an effect on the PE, PG and cardiolipin content of various species of bacteria, such as *Bacillus caldotenax*<sup>29</sup> and

*neurospora crassa*,<sup>30</sup> pointing to the importance of variations and changes in lipid composition in the adaptation of organisms to their surroundings and the necessity of the variety of lipids in nature.

#### **1.4 Introduction to Self-assembly**

As previously mentioned, phospholipids are amphiphilic in nature and contain both a hydrophobic and a hydrophilic moiety. When placed into an aqueous solution, they are subject to the hydrophobic effect, the effect wherein hydrophobic molecules aggregate to minimise their contact with the water, resulting in the formation of self-assembled structures.

When a non-polar substance is present in water, it disrupts the 3-dimensional hydrogen bonding network that exists between the water molecules, causing them to re-orientate around the hydrophobic molecules to maximise their intramolecular hydrogen bonding and causing a decrease in entropy,<sup>31</sup> a phenomenon known as the hydrophobic effect. At the same time, the hydrophobic molecules aggregate in order to maximise their contact with each other and minimise their contact with the water in order to afford an increase in entropy.

In amphiphiles, the molecules are subject to both the hydrophobic effect arising from the fatty acid chains, and the favourability of the interactions between the hydrophilic head groups and the aqueous solvent. As a result, they self-assemble into structures that best satisfy these opposing forces, where an optimal surface area per head group and therefore a minimum free energy per molecule is obtained. In addition, the exact structure formed is influenced by geometric constraints which prevent multiple-chained lipids being able to form micelles and entropic constraints which prevent single-chained lipids from being able to form vesicles and bilayers.<sup>32</sup>

The thermodynamics of the formation of micelles is described by **equation 1**,

$$X_N = N \left( \frac{X_M}{M} \right)^N e^{N(\mu_M^0 - \mu_N^0)/kT} \quad \text{Equation 1}$$

where  $\mu_N^0$  is the free energy per molecule in the micelle,  $k$  is the Boltzmann constant,  $N = 1$  corresponds to isolated molecules or monomers in solution,  $T$  is the temperature,  $X_N$  is the mol fraction of molecules incorporated into micelles of aggregation number  $M$ , and is an arbitrary reference state of micelles with aggregation number  $M$ . When  $\mu_M^0 = \mu_N^0$ , the monomer state is preferred as it is entropically favoured. For aggregation to occur, it must be accompanied by a negative change in free energy.<sup>32</sup>

The free energy change associated with aggregation from a dilute monomer state can be modelled **equation 2**,

$$\left( \frac{\Delta\mu_g^\circ}{kT} \right) = \left( \frac{\Delta\mu_g^\circ}{kT} \right)_{Transfer} + \left( \frac{\Delta\mu_g^\circ}{kT} \right)_{Interface} + \left( \frac{\Delta\mu_g^\circ}{kT} \right)_{Head} \quad \text{Equation 2}$$

with the first term being the negative free energy contribution resulting from the tails coming into contact with one another, a favourable interaction compared to contact with water; the second term being a positive free energy contribution to reflect the fact that the tails are never completely out of contact with water; and the third term being another positive energy contribution reflecting the electrostatic and/or steric repulsion between the head groups as the monomers pack together closely.<sup>33</sup>

Furthermore, the geometric factors involved in self-assembly have been described. The geometric constraints can be quantified and the equilibrium structure predicted using the packing parameter, first described by Israelachvili, Mitchell and Ninham in 1975,

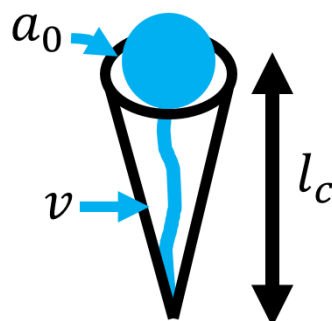
$$\text{Packing parameter} = \frac{v}{a_0 l_c} \quad \text{Equation 3}$$

where  $a_0$  is the optimal area per amphiphile,  $v$  is the volume of the lipid, and  $l_c$  is the length of the hydrocarbon chains.

In a spherical micelle, the radius  $R$ ,  $v$  and  $a$  at the interface between the hydrocarbon chains and water are related by **equation 4**:

$$R = \frac{3v}{a} \quad \text{Equation 4}$$


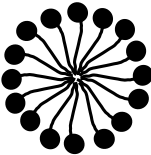

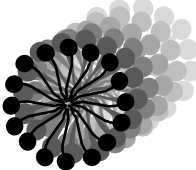



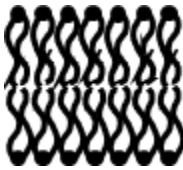

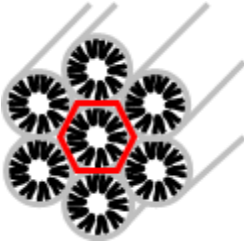
The radius of the molecule cannot exceed  $l_c$ , and so  $\frac{v}{a_0 l_c}$  must be less than or equal to 1/3 for micelles to form unless surface area  $a > a_0$ . When  $\frac{v}{a_0 l_c}$  exceeds 1/3, alternative structures will form, summarised in **table 1**. When the packing parameter is equal to or less than 1/3, micelles form; however, between 1/3 and 1/2, cylindrical micelles are formed, followed by vesicles and flexible bilayers as the packing parameter reaches 1/2 and the space occupied by the lipids takes on a truncated cone shape. When the packing parameter reaches 1 and the



**Fig. 2.** An illustration of the components of the packing parameter.



space occupied by the lipids becomes cylindrical, planar bilayers form, followed by an increasing tendency to form inverted phases as the packing parameter increases beyond 1.<sup>34</sup>

Surfactant Shape	Packing Parameter	Shapes Formed
	$< \frac{1}{3}$	 Spherical micelles
	$\frac{1}{3} - \frac{1}{2}$	 Cylindrical micelles
	$\frac{1}{2} - 1$	 Flexible bilayers and vesicles
	1	 Planar bilayers
	$> 1$	 Inverted hexagonal phase

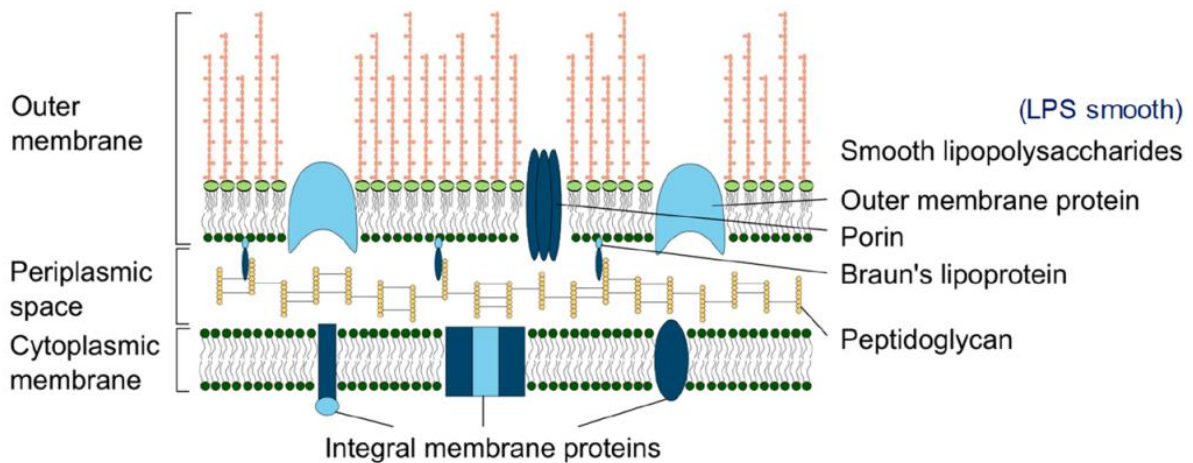
**Table 1.** Lipid structures and mesophases formed according to packing parameter.

## 1.5 The Cell Membrane as a Target

Lipid membranes are a universal feature of all types of cell, including bacteria. They play an essential function in maintaining the structure of the cell, acting as a protective semi-permeable barrier, allowing for the maintenance of concentration gradients essential to life, intracellular communication and recognition, adhesion to surfaces, and other specialised functions.<sup>35</sup> Because the cell membrane is the barrier between the inner workings of the cell and an often changing outside environment, and the interface through which it interacts with its surroundings, its integrity is essential to the survival of the cell, and necessary for the existence of cellular-based life.

The basic composition of a cell membrane is a double layer of phospholipids that supports embedded cholesterol and proteins that carry out functions such as transport of ions and substrates, intercellular communication and cell recognition. Many proteins also bind to the cell membrane in a reversible electrostatic or hydrophobic manner, often requiring the presence of anionic lipids, and smaller species can diffuse through the lipid membrane directly without the use of proteins.<sup>36</sup>

However, bacteria differ significantly from eukaryotic organisms beyond this basic structure. In addition to a cell membrane, bacteria also have a second polysaccharide and peptidoglycan outer membrane or cell wall (**Fig. 3**).<sup>37</sup> Between these two layers is the periplasmic space which contains a range of ions and proteins that are necessary for and facilitate essential cell processes such as electron transport and hydrolysis of substrates.<sup>38</sup> The major lipid species found in bacteria are phosphatidylglycerol (PG, anionic), phosphatidylethanolamine (PE, zwitterionic) and cardiolipin (anionic), with cardiolipin found to form domains within bacterial membranes and PG hypothesised to do the same.<sup>36</sup>



**Fig. 3.** Diagram of a gram-negative bacteria cell envelope (taken from reference 37)

The composition of bacterial membranes varies between species but can be sorted into two main categories: gram-negative and gram-positive. Gram-negative bacteria include species such as *E. coli* and *S. typhimurium* and have an outer membrane where the inner leaflet is composed of phospholipids and the outer membrane is composed of lipopolysaccharides (LPS).<sup>38</sup> The LPS layer also contains magnesium and calcium ions that help maintain its integrity through the bridging of negative charges present on the phosphate groups of the sugars.<sup>39</sup> Gram-positive bacteria on the other hand do not have a second lipid bilayer, and instead have a wall comprised of peptidoglycan that is around 40-80 nm thick, and the periplasmic space is much larger than in gram-negative bacteria.<sup>40</sup> Another difference between the two classes of bacteria is the general lipid composition, with gram-positive bacteria containing a larger proportion of negatively-charged PG, and gram-negative bacteria containing a larger proportion of zwitterionic PE lipids.<sup>38</sup>

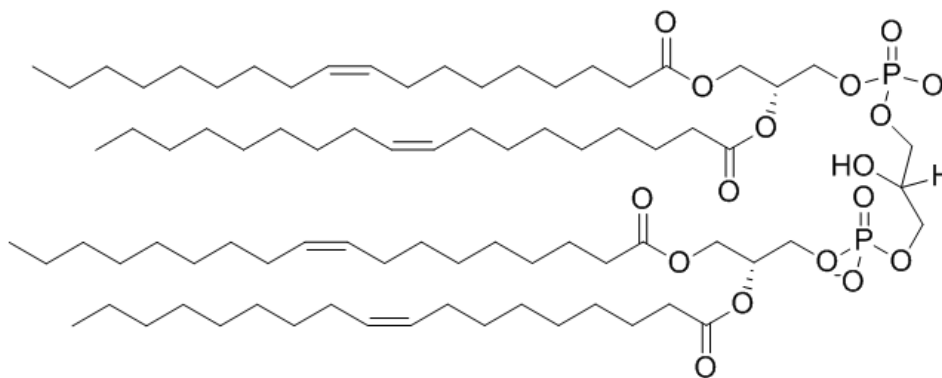
Most conventional antibiotics need to cross the bacterial membrane in order to take effect, as they work by inhibiting the production of proteins, RNA or DNA.<sup>41</sup> The most commercially and medically successful antibiotics include  $\beta$ -lactams, fluoroquinolones, rifampicins and tetracyclines, whose targets are enzymes involved in essential cell processes,

DNA processes, or RNA translation respectively.<sup>42</sup> As all these processes occur within the bacterial cell itself, it is clear that a necessary feature for many antibiotic drugs is the ability to penetrate the bacterial membrane. It has been found that interactions between drugs and lipids have a significant role in shaping key pharmacokinetic properties of drugs including their distribution and accumulation.<sup>43</sup> Some naturally occurring compounds found to have antimicrobial activity are thought to work through disruption or alteration of the bacterial membrane including sesquiterpenes and epigallocatechin gallate, as well as some developed antibiotics such as dalbavancin,<sup>19</sup> while the use of liposomes to enhance drug delivery also relies upon the interactions between the vesicles and the bacterial cell membranes.<sup>44</sup>

In addition, a variety of bactericidal surfaces that kill bacteria mechanically using nanostructures exist in nature and can be produced artificially. These structures can include nanopikes, nanopores and nanopillars, and can both prevent bacterial adhesion and rupture bacterial membranes upon contact,<sup>45</sup> an example being the nanopillar-covered wings of cicadas, which while not able to prevent bacterial adhesion, were found to penetrate all *P. aeruginosa* cells that they came into contact with, and so are highly effective at killing them.<sup>46</sup> Antimicrobial peptides that are thought to physically damage bacterial membranes are also widespread throughout nature, and as their bactericidal ability takes advantage of the structure of the bacterial membrane itself, in order to develop resistance, bacteria would have to develop a new membrane structure. Any strategy that targets the bacterial membrane itself may be able to take advantage of the fact that the development of resistance would require the bacteria to re-organise or change the composition of its membrane, a costly strategy,<sup>39</sup> and so may be a valuable route to explore for developing new ways to target bacteria.

## 1.6 Introduction to Cardiolipin

Cardiolipin (CL) (**Fig. 4**) is an anionic phospholipid found in the membranes of both prokaryotic and eukaryotic species.<sup>47</sup> The name 'cardiolipin' derives from the fact that the discovery of this lipid was first reported in 1942,<sup>48</sup> isolated from beef heart cells, where it was found to be an important component of the inner mitochondrial membrane that is essential for optimal functioning. Alterations in the cardiolipin content or in the acyl chain content of cardiolipin is associated with various dysfunctions and diseases including Barth syndrome, heart failure, hypothyroidism and ischemia,<sup>49</sup> and it has been found to play a role in orientating membrane proteins, receptors and enzymes.<sup>50</sup> It has been found that several proteins involved in oxidative phosphorylation incorporate cardiolipin into their quaternary structure, and cannot function without its presence.<sup>51</sup> It has also been identified in the structures of various bacterial proteins such as succinate dehydrogenase in *E. coli*.<sup>52</sup>



**Fig. 4.** The structure of cardiolipin.

In bacterial membranes, cardiolipin commonly comprises around 10% of the total membrane lipid,<sup>47, 53-55</sup> although it has been observed in some species of bacteria including *E. coli* and *S. aureus* that this proportion increases in response to environmental stress,<sup>56, 57</sup> as well as during the stationary phase of growth (when the number of bacteria in a population

remains stationary, commonly due to a limiting environmental factor such as the availability of an essential nutrient).<sup>58, 59</sup> For example, it was found by Romantsov *et al.* that *E. coli* grown in high-salinity conditions the proportion of CL increased while the PE content decreased, at least partly due to the osmotic induction of the CL synthase gene. The CL/PG ratio was also found to be more than two times higher in the cytoplasmic membrane than in the outer membrane: 0.20 vs 0.09.<sup>60</sup> It is possible that this increase in the CL content in response to stress may indicate that CL plays a role in enhancing the structural integrity of bacterial membranes.<sup>47</sup>

Cardiolipin has an unusual molecular structure, consisting of two phosphate head groups joined by a glycerol linker, and, unlike most membrane lipids, it has four carbon tails, two per head group. Due to this bulky structure, it has a restricted degree of mobility and conformational flexibility and a low capacity for self-shielding, and therefore its head groups are generally more accessible for interactions with drugs, ions, and water compared to most other lipids.<sup>47</sup> Cardiolipin also has a very small head group area relative to its fatty acid tails, comparable to two typical lipid molecules sharing a single head group, which should promote cohesion between the fatty acid chains.<sup>47</sup> Its packing parameter is greater than one, indicating its preference for an inverse curvature and the formation of the inverted hexagonal  $H_{II}$  phase, suggesting that the incorporation of cardiolipin into lipid membranes may increase their propensity for negative curvatures. This effect has been observed in nature, where cardiolipin has been found to exist in greater concentrations in curved regions of the bacterial membrane such as the poles and septum regions.<sup>60</sup>

It is clear that cardiolipin plays a physiological role in membranes. However, the role it plays in shaping the physicochemical properties of membranes is not entirely clear, and as it is so commonly found in bacteria and makes up a significant portion of the membrane,

understanding its role is very relevant to understanding the behaviour and properties of bacterial membranes in general.

Previous studies of the effect of cardiolipin on lipid membranes have shown that cardiolipin plays a role in shaping their physicochemical properties, decreasing the water permeability of vesicles when present in even small amounts. In a paper by Nichols-Smith *et al.*, giant vesicles were prepared with compositions of 99.5% SOPC/0.5% POPS or SOPS, 95% SOPC/5% CL, and 90.8% SOPC/9.2% CL. Compressibility experiments were carried out using the micropipette technique wherein changes in membrane tension are related to vesicle surface area. Surface pressure-average area isotherms were also obtained for mixed egg PC/cardiolipin monolayers, and it was found that on a pure water subphase a mixture of 40% CL/60% egg PC was the most stable, while on a salt subphase this occurs at 60% CL. Cardiolipin appears to decrease the apparent area compressibility modulus and the lysis tension of bilayer structures, suggesting that cardiolipin decreases the lateral tension between monolayer leaflets and lowers the energy required to stretch the membrane.<sup>61</sup>

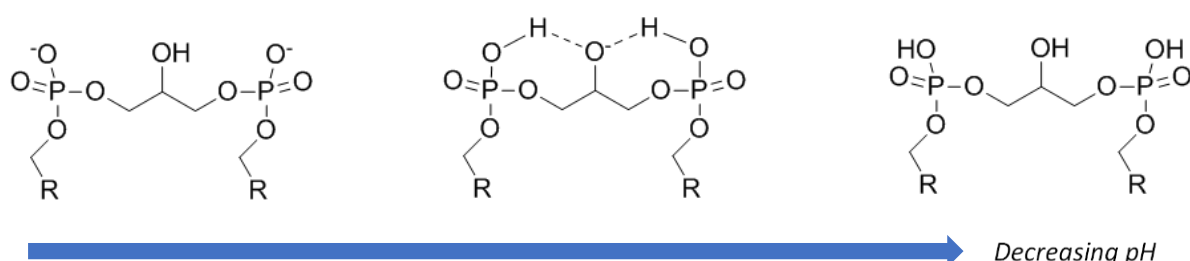
Wydro found that cardiolipin has also been found to weaken interactions between molecules in mixed POPE/POPG/CL and POPE/DPPG/CL films following pressure-area isotherms obtained on a pure water and a 15mM NaCl subphase. It is proposed that this may be due to cardiolipin's large bulk, disturbing the system and disrupting packing, thereby weakening intermolecular interactions.<sup>62</sup> In another study by Etienne *et al.*, GIXD was used to investigate DPPC/CL monolayers and it was demonstrated that the presence of CL increased the lateral pressure in the acyl chain region, which could affect the way that the membrane interacts with proteins such as by facilitating the anchoring of proteins or affecting the structure of membrane proteins.<sup>63</sup> Cardiolipin was also observed by Unsay *et al.* using confocal microscopy, fluorescence correlation spectroscopy and atomic force microscopy to

increase the fluidity and decrease the mechanical stability in planar supported bilayers when present at 5, 10, and 20% with egg PC, and a mitochondrial membrane mimic composed of egg-PC:PE:PI:PS:CL at 48.5:27.2:9.9:10.0:4.4 mol.<sup>1</sup>

Cardiolipin's effects on membrane properties can be observed in mitochondria, where it is found in mammals- it has been observed by Ohtsuka et al. that Chinese hamster ovary cells with a CL content 30% of the normal value showed lacking and disorganised cristae, suggesting that CL may play an important role in regulating the curvature of the membrane.<sup>64</sup>

### 1.7 The pH Responsiveness of Cardiolipin

As well as its unusual structure and restricted conformational flexibility, a key property of cardiolipin is its responsiveness to pH and the subsequent consequences for its behaviour within membranes. Cardiolipin's two headgroups are diastereotopically inequivalent,<sup>65</sup> being esterified at the 1- and 3- positions of the head group glycerol respectively. This is a possible explanation for the observation that cardiolipin's two head groups have very different pKa values- approximately 2.8 and 7.5-9.5 respectively,<sup>66</sup> carrying two negative charges at very basic pH, one negative charge at physiological pH with a single proton trapped in a bicyclic resonance structure (**Fig. 5**) and no negative charge at acidic pH. However, it has also been



**Fig. 5.** The effect of decreasing pH on the headgroup of cardiolipin.



suggested that these two  $pK_a$  values may be the result of an intramolecular hydrogen bond between the proton present on the glycerol head group and one of the phosphate moieties.<sup>67</sup>

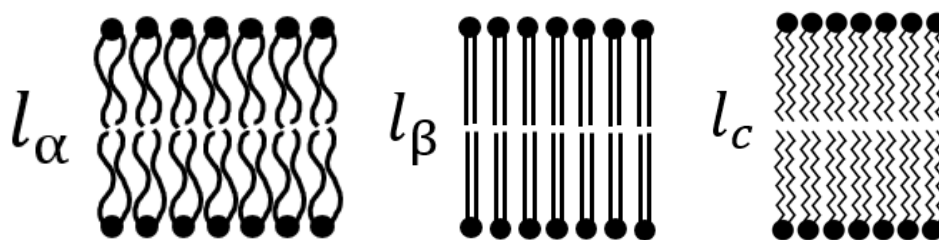
These two differing  $pK_a$  values grant cardiolipin the ability to act as a buffer and a proton sink,<sup>68</sup> and also mean that its properties are to be pH-dependant. At basic pH when both head groups are negatively charged, the repulsion between the two head groups is maximised, leading to a slightly more cylindrical shape. Likewise, when both head groups are protonated, the tails are freer to move around, and the molecule can adopt an inverted truncated cone shape.<sup>69</sup> This effect has been observed both experimentally<sup>70</sup> and computationally,<sup>71</sup> with cardiolipin's propensity to form inverted phases being maximal at a neutral charge. This points to there being consequences for the behaviour of the lipid membranes that contain cardiolipin, affecting the packing and organisation of the molecules within the membrane and therefore the phase behaviour.<sup>68</sup> And so, investigating and understanding the effect is also of vital importance for fully understanding the fundamental impact of cardiolipin within membranes.

This effect has been observed by Khalifat et al., where microinjections of HCl solution delivered to the outside of giant unilamellar vesicles (GUVs) containing cardiolipin caused morphological changes reminiscent of cristae in mitochondria, caused by tighter packing and increased elastic stress at the outer membrane resulting in the observed morphology. The vesicles were composed of PC/PE/CL in a ratio of 60:30:10, representative of a biological membrane. The same effect was not observed in GUVs composed of only PE/PC 66:34, highlighting the role of cardiolipin in this responsiveness to pH.<sup>72</sup> However, little research has been done regarding the effect of pH on cardiolipin-containing membranes that specifically aim to model bacterial membranes, and this information would be valuable in better

understanding how certain bacteria tolerate extreme pH environments, and gaining a deeper fundamental understanding of the role CL plays in the survival of bacteria.

## 1.8 Lipid Mesophases

Lipids are able to self-assemble into a wide range of structures including but not limited to micelles, vesicles and bilayers, known as mesophases- states that are intermediate between liquid and solid. Bilayers themselves can exist in a variety of phases (**Fig. 6**) such as the  $L_\alpha$  or fluid phase, which is most ubiquitous in biology as it allows for the maintenance of structural integrity as well as function.<sup>73</sup> In the  $L_\alpha$  phase, the tail groups are disordered and move more freely than in other bilayer phases. Bilayers can also exist in the  $L_\beta$  or  $L_\beta'$  gel phase. In this phase, lipid tails are more ordered and organised either perpendicular to the plane of the bilayer in the  $L_\beta$  phase or at a tilt in the  $L_\beta'$  phase. The  $L_c$  phase occurs at low temperatures and is the phase in which the lipid tails are the most highly ordered. During some phase transitions there also exists a pretransition  $P_\beta'$  rippled phase as the chains melt from the  $L_\beta$  to the  $L_\alpha$  phase, although this is only known to occur in bilayers containing PC.<sup>74</sup>



**Fig. 6.** The structure of the  $L_\alpha$ ,  $L_\beta$  and  $L_c$  bilayer phases

Beyond bilayers, hexagonal and cubic phases can also form. The hexagonal phases consist of micellar columns packed into a hexagonal lattice, with the water channels either between the columns in the case of the  $H_1$  phase where there is positive curvature with

respect to the lipid chain region, or water channels within the columns in the case of the  $H_{II}$  phase where there is negative curvature with respect to the chains i.e. the tails protrude outwards.<sup>75</sup> Bicontinuous cubic phases are periodic three-dimensional structures consisting of curved bilayers and water channels with a regular structure, sponge phases are similar to bicontinuous cubic phases, however they have a disordered structure and are more fluid.<sup>75</sup>

The mesophases formed by a particular lipid or mixture of lipids depends on a range of factors including pressure, temperature, pH, ion concentration and hydration, and transitions between different phases can be induced by altering these factors and the phase behaviour of a lipid or lipid mixture can be illustrated through phase diagrams, such as temperature-pressure or temperature vs hydration.

## **1.9 Introduction to Liposomes**

Liposomes are a structure commonly formed by the self-assembly of lipids. They are spherical vesicles surrounding an aqueous core, and may be classified according to their size and the number of layers they contain. Unilamellar vesicles (ULVs) consist of only one layer of bilayer and can be further classified according to size- small unilamellar vesicles (SUVs), large unilamellar vesicles (LUVs), and giant unilamellar vesicles (GUVs)- while multilamellar vesicles (MLVs) consist of multiple layers of bilayer separated by thin layers of water. Liposomes can vary in size from 0.025 - 2.5  $\mu\text{m}$ ,<sup>76</sup> with SUVs being less than 1  $\mu\text{m}$  in size, LUVs being 0.1 - 1.0  $\mu\text{m}$ , and MLVs can reach over 500  $\mu\text{m}$  and contain hundreds of layers.<sup>77</sup>

Liposomes can be tuned to carry out specific functions by adjusting their lipid composition to influence properties such as charge and fluidity- for example, saturated, long-chained phospholipids result in a less permeable, more rigid structure, while unsaturated lipids will result in a more permeable but less stable structure.<sup>76</sup> The ability to tune their

properties in this manner makes it easy to produce liposomes for a wide range of different uses, and their potential applications in a range of areas, particularly medicine and pharmaceuticals, has been widely explored.

They have found use in medicine as they provide excellent drug-carrying capabilities. As liposomes are biocompatible and non-toxic, being made of the same substances as cell membranes, and readily fuse with cell membranes,<sup>76</sup> they are an excellent choice for introducing substances into the body. They are able to carry both hydrophobic and hydrophilic drugs in the lipid and water core sections of the liposome, respectively. This ability to control the movement of drugs to their target site allows for lowered exposure of sensitive tissues to drug and the reduction of toxicity, as well as improving the efficacy of the drug as it can be released nearer its target site. The fact that the drug is carried within the liposome itself rather than being exposed directly to the body during administration can also help to improve the drug's stability within the body as it is protected from pH changes, enzyme activity, and other biological processes that may damage it.<sup>78</sup>

Liposomes can be introduced into the body by a variety of routes including injection<sup>79</sup> and inhalation<sup>78</sup> as well as topically,<sup>80</sup> allowing them to be used for a range of purposes and to deliver drugs through the most appropriate route. Overall, liposomes are a versatile tool in medicine, and additionally they have several non-medical applications too including in the formulation of cosmetics and in the food industry, where their ability to sequester harmful compounds and release molecules in a controlled fashion can be applied in processes such as fermentation and controlled release of pesticides.<sup>5</sup>

## 1.10 Model Membranes

Bacterial membranes are complex, dynamic structures containing various embedded and associated proteins and lipids. Which proteins are present and in which quantities can vary greatly between species and, due to the complex nature of the lipid membrane, accurately re-creating a bacterial lipid membrane for use in studies would prove to be highly difficult. Through the selection of the appropriate lipids in the desired quantities, systems mimicking the lipid composition of various biological systems can be constructed fairly easily with a high degree of precision and used to gain insight into the behaviour of these membranes, as they retain the basic lipid bilayer structure while allowing for the investigation of the precise effects of individual components.<sup>81</sup>

Commonly used model membranes include supported lipid bilayers (SLBs) which are readily formed through the fusion of vesicles or deposition of a Langmuir monolayer onto substrates such as mica or silica, and are able to maintain excellent mechanical stability.<sup>82</sup> Lipid monolayers formed on water/buffer surfaces in Langmuir-Blodgett troughs are also commonly used as information on the mean molecular area, compression modulus and interactions occurring between components at the air-water interface can be analysed using pressure-area isotherms.<sup>83</sup> Liposomes can also be used as model lipid membranes,<sup>43</sup> as diffusion in and out of the core can be used to study diffusion across cell membranes, and can be used to study the effect of various membrane components on stability through examination of their zeta potential.<sup>84</sup>

However, studying mesophases and the transitions between them can also provide valuable information into the behaviour of biological lipid membranes and be used as models to glean insight into the effects of individual components. While the  $L_{\alpha}$  phase is the state in which lipid membranes usually exist within cells, other mesophases and the transitions

between them have also been suggested to play a biological role. For example, it has been suggested that saddle deformations as seen in bicontinuous cubic phases may be induced by some membrane proteins,<sup>85</sup> while the non-bilayer H<sub>II</sub> and Q<sub>II</sub> phases have been proposed to resemble intermediates in the modified stalk theory of lipid membrane fusion.<sup>86</sup>

Studying mesophases with composition resembling the compositions of lipid membranes can be used to construct phase diagrams to observe the effect of various environmental changes such as pressure and temperature as well as the presence of specific membrane components on the behaviour of various lipid systems and how these factors may affect cell processes such as fusion.

### **1.11 Project Justification**

Cardiolipin, PE and PG are all lipids commonly found in bacterial membranes and have been used previously as bacterial membrane mimics,<sup>87, 88</sup> including DOPE, DOPG and CL specifically.<sup>54</sup> These lipids can be used to mimic a bacterial membrane, and so were chosen for this project for that purpose. These lipids are all available in an easy to use, high-purity form from Avanti Polar Lipids and are readily soluble in water. The lipids were used in proportions analogous to those found in bacterial lipid membranes<sup>53, 89</sup>- 70:20:10 DOPE:DOPG:CL.

The effect of cardiolipin's presence on bacterial membrane mimics specifically has not been widely studied, despite the knowledge that it plays a role in shaping the properties of lipid membranes. Therefore, there exists an opportunity to gain greater insight into the effect of this unique molecule on bacterial membranes and thus gain a deeper understanding of the properties of bacterial membranes in general. Mesophases in excess water were chosen as model membranes to investigate the effect of cardiolipin's presence firstly because of the

proposed biological relevance of mesophases in important cellular processes and secondly because they can be investigated using high-pressure SAXS, which provides quantitative structural information about the system and can be used to construct a pressure-temperature phase diagram to obtain a clear overview of the phase transitions the system undergoes and the effect of cardiolipin on these transitions. Three different pH values were also chosen for investigation- 12.1, 5.1 and 1.3. The  $pK_a$  values of the two head groups of cardiolipin are approximately 2.8 and 7.5-9.5, and so the values chosen are above both head group  $pK_a$  values, above one, or below both, with a view to investigate the effect of differing protonation states of the head groups on the behaviour of cardiolipin within the membrane. Polarised light microscopy can also be used to identify lipid mesophases,<sup>90</sup> and so was used to obtain images of all systems identified via HP-SAXS to aid in characterisation and help confirm the assigned mesophases from the HP-SAXS measurements. Liposomes were also used as a model membrane system to investigate the effect of cardiolipin on the stability of liposomes over time at different pH values, as the role cardiolipin plays in the stability of liposomes and in particular the role it plays in membrane stability under differing pH is another interesting area for investigation that has not been widely investigated, particularly as cardiolipin can act as a proton trap within membranes and may be able to act as a buffer.<sup>68</sup>

Given that cardiolipin is a unique, significant and pH-responsive component of the membrane, it is a clear target for investigation. Investigating its role in shaping both the phase behaviour, stability and response to pH of bacterial membrane mimics can help to shed light on the behaviour of bacterial membranes under different conditions, an area that is important to investigate in light of the ongoing need to better understand the bacterial membrane and how it can be disrupted.

## Chapter 2. Methods & Experimental

---

### 2.1 Introduction to X-Rays

X-Rays lie in the section of the electromagnetic spectrum with wavelengths between 0.01 and 10 nm, or corresponding frequencies  $3 \times 10^{16}$  -  $3 \times 10^{19}$  Hz. They were first discovered in 1895 by Wilhelm Röntgen, who named them 'X-rays' to signify the fact that at the time they were an unknown type of radiation, having been previously detected as an unidentified discharge occurring during experiments with cathode rays. Only later were they identified as electromagnetic radiation with a shorter wavelength than visible light.<sup>91</sup> Following their discovery as part of the electromagnetic spectrum, their potential for use in medicine was quickly developed in the years before the first world war, as it was found that they were able to penetrate different tissues within the body to differing extents, allowing for images of bones and foreign objects within the body to be obtained. This property was used in the location of foreign objects and diagnosis of fractures, breaks, disease and tumours, and X-rays remain an essential tool in medicine in modern day. In the 1920s, it was found that X-rays could be used not just in the imaging but in the treatment of cancers, and their ubiquity in the medical field including screening for tuberculosis in the 1930s and 1940s only increased.<sup>91</sup> However, X-rays have found use beyond the field of medicine- 17 years after the discovery of X-rays, and it was discovered by Max von Laue that, when X-rays are shone through a crystal, a diffraction pattern is produced, composed of specific wavelengths with intense peaks of radiation.<sup>92</sup> Following on from this discovery, in 1913 Sir William Henry Bragg and Sir William Lawrence Bragg determined that this phenomenon was a result of constructive interference



arising from reflections by parallel planes within the crystal, and from this they proposed Bragg's Law (**equation 5**):<sup>93</sup>

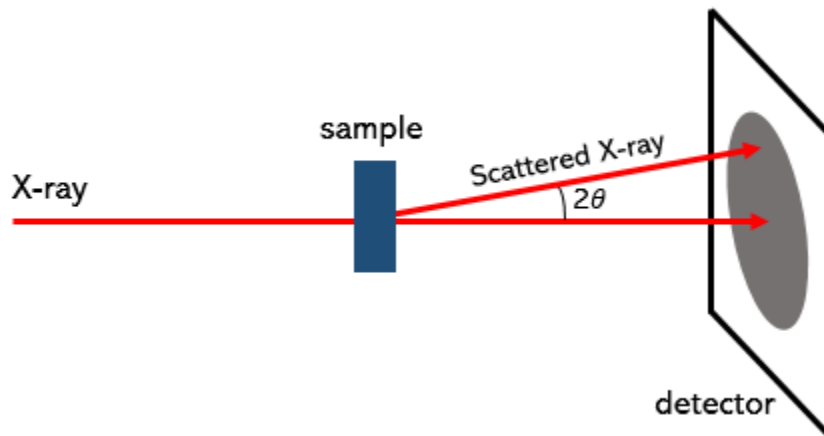
$$2d \sin \theta = n\lambda \qquad \text{Equation 5}$$

where  $n$  is a positive integer,  $\lambda$  is the wavelength of the incident wave, and  $d$  is the interplanar distance, which can be used to find the interplanar spacing present in a crystal for identification or structure determination. Unlike visible light, the wavelength of X-rays is comparable to the distances between atoms within molecules, and so X-rays were found to be able to provide unprecedented insight into the structure of molecules.

Following this realization in the first half of the 20th century, techniques such as X-ray crystallography, famously used to confirm the structures of penicillin and vitamin B12 by Dorothy Hodgkin, X-ray powder diffraction, and small-angle X-ray scattering were developed and are used in the present day to great effect in the determination of the structures of molecules, proteins, and other biological and chemical structures.

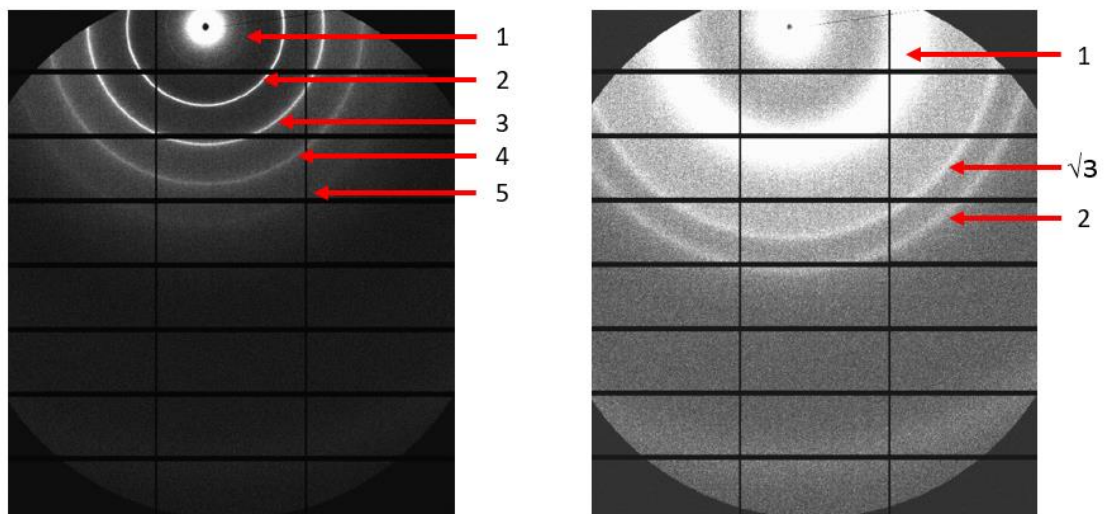
## 2.2 Introduction to SAXS

Small-angle X-ray scattering is an analytical technique used to determine structural information of a sample on nanoscales. It does this by analysing the elastic scattering of hard X-rays when passed through a sample at small angles. Here, elastic scattering is scattering in which no energy is transferred and hard X-rays are more penetrating, using higher-energy X-rays with a wavelength below approximately 0.2 nm. SAXS is able to determine information about structures ranging in size from approximately 1-100 nm, with smaller scattering angles being required to probe larger structures.



**Fig. 7.** illustration of the general principle of SAXS

The principle of SAXS is that a monochromatic (composed of only one wavelength) beam of X-rays is shone through the sample (**Fig. 7**), where it interacts with the electron cloud present in the sample, undergoes a directional change and interferes constructively and destructively, resulting in a fringe pattern that is characteristic of the phase present (**Fig. 8**).



**Fig. 8.** SAXS patterns obtained during this project. (Left) A pattern from a lipid sample in a lamellar phase, showing the characteristic peak ratio 1:2:3:4:5... (Right) A pattern from a lipid sample in the inverse hexagonal phase, showing the characteristic peak ratio 1:√3:2...

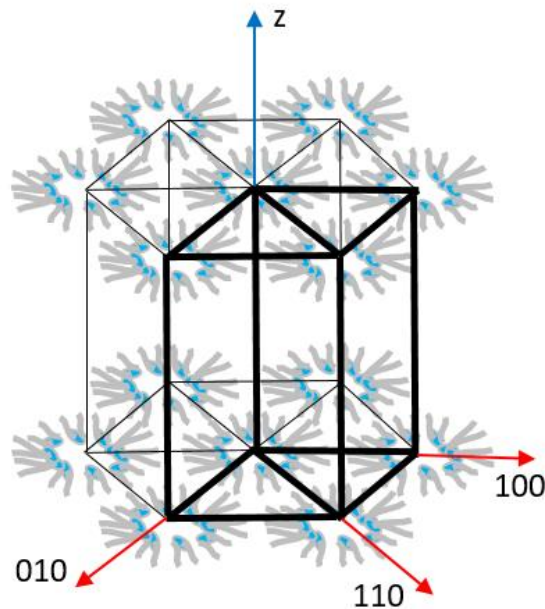
Phases can then be assigned by comparing the scattering vector  $Q$  for each peak.  $Q$  is calculated from the difference between the scattered and the incident wave vectors according to **equation 6** (illustrated in **Fig. 7**):<sup>94</sup>

$$Q = k_i - k_f = \frac{4\pi n \sin \theta}{\lambda} \quad \text{Equation 6}$$

and can then in turn be used to determine the d-spacing present in the sample using **equation 7**.

$$d = \frac{2\pi}{Q} \quad \text{Equation 7}$$

Different mesophases give rise to different peaks according their lattice planes, which can be used to identify them. In the case of lamellar phases, which comprise lipid bilayers separated by water channels, the unit cell consists of a bilayer and the layer of water adjacent to it. All



**Fig. 9.** Illustration of the  $H_{II}$  phase with arrows indicating the positions of the (100), (110) and (010) planes. The bold lines indicate the unit cell, and the blue arrow indicates the z-axis. Adapted from reference 42.

of the planes present are parallel, giving rise to reflections from the (100), (200), (300)... planes, and resulting in evenly spaced peaks with Q ratios of 1:2:3...

Hexagonal phases, however, have a different unit cell (**Fig. 9**).<sup>95</sup> This results in a different set of peaks arising from SAXS, corresponding to reflections from the (100), (110) and (010) planes. As the (100) and (010) planes are parallel to the x and y axes respectively, they are equivalent and so only give rise to a single peak. The characteristic peak ratios of some common lipid mesophases are summarized in **table 2**.<sup>75</sup>

Mesophase	Characteristic peak ratios
Planar bilayer	1, 2, 3...
Inverse hexagonal phase	1, $\sqrt{3}$ , 2...
Bicontinuous cubic Pn3m	$\sqrt{2}$ , $\sqrt{3}$ , 2...
Bicontinuous cubic Ia3d	$\sqrt{6}$ , $\sqrt{8}$ , $\sqrt{14}$ ...
Micellar cubic Fd3m	$\sqrt{3}$ , $\sqrt{8}$ , $\sqrt{11}$ ...

**Table 2.** Characteristic peak ratios produced by various lipid mesophases from SAXS measurements.

As well as being able to characterise mesophases, SAXS peak shapes can be analyzed to determine the coherence length of a sample, that is, the average size of the crystalline domains within the mesophase, through use of the Scherrer equation (**equation 8**):

$$L = \frac{2\pi k}{\Delta Q} \quad \text{Equation 8}$$

where  $k$  is the shape factor of order unity, and  $\Delta Q$  is FWHM.<sup>96</sup>

The radius of gyration  $R_g$ , a measure of the size of the particles present in a sample, can be determined from SAXS using a Guinier plot where scattering is fit to **equation 9**:

$$I(Q) \cong I(0)\exp\left(-Q^2 \frac{R_g^2}{3}\right) \quad \text{Equation 9}$$

where  $I(Q)$  is the scattering intensity,  $I(0)$  is the forward scattering intensity, and  $Q$  is the scattering vector. However, this approximation is only valid when  $qR_g < 1.1$  or  $1.3$  for globular particles.<sup>97</sup>

### 2.3 Synchrotrons and X-ray generation

Synchrotrons are a type of particle accelerator used to generate intense light for various scientific purposes. They have numerous advantages over traditional methods of generating X-rays as they provide very intense beams, the X-ray wavelength can be selected, and the beam is naturally collimated. Synchrotron radiation was first observed by accident in 1947 at the General Electric 70 MeV synchrotron, and following this in the late 1940s theory was developed to allow for accurate predictions about the properties of synchrotron radiation; further experiments were conducted by Pollack et al. on this synchrotron. Further experiments with synchrotron radiation were then conducted throughout the 1950s in Russia, the USA and Germany, the theoretical predictions verified and the first synchrotron storage ring specifically for the purpose of generating synchrotron radiation was created at the university of Wisconsin in 1968.<sup>98</sup>

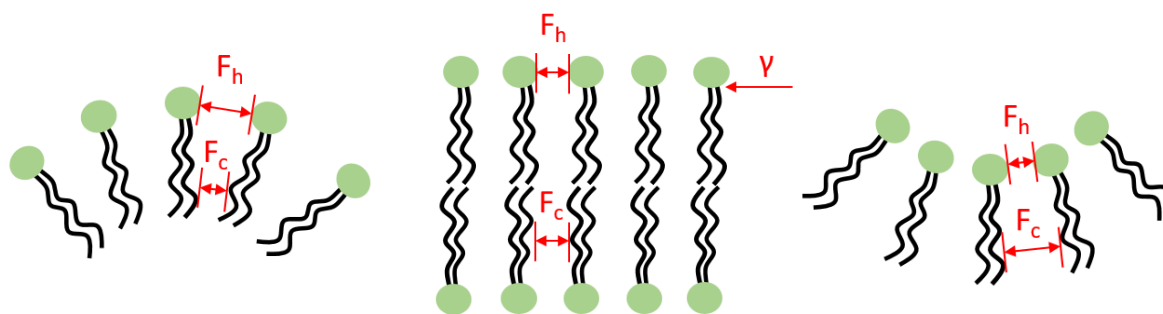
Charged particles generate electromagnetic radiation when they pass through an electromagnetic field. In a synchrotron, electrons in a storage ring are accelerated to close to

the speed of light and forced to change direction by magnets, with a narrow cone of X-rays being emitted perpendicular to the direction of the electrons' acceleration.<sup>99</sup> At Diamond Light Source, a high-voltage cathode is heated under vacuum to cause the thermionic emission of electrons, which are then accelerated by anodes to form a stream of electrons. A linear accelerator is used to accelerate the electrons to 100 MeV, and then up to 3 GeV in a booster synchrotron. The current in the storage ring is then kept constant through regular top-up injections of electrons. The storage ring itself is made up of straight sections followed by corners that the electrons are forced to bend around by magnets, with the radiation emitted by the electrons at these corners passing first into an optics hutch where the required wavelengths of radiation are selected and focused, and then into an experimental hutch where the beam can interact with the sample and measurements be taken. Following the experimental hutch is the control cabin where the equipment in the experimental hutch can be controlled remotely and data can be collected and processed.<sup>100</sup>

## **2.4 The Effect of Pressure on Lipids and the use of HP-SAXS**

SAXS is an enormously useful technique for studying nanoscale structures, allowing for the study of the effects of changes on the physicochemical properties of systems, including lipids. It is useful for the identification of liquid crystalline phases accurately and efficiently,<sup>96</sup> and, when coupled with the use of high-pressure, provides a wealth of information about the phase behaviour of lipid systems.

When pressure is applied to lipid systems, it particularly impacts on the volume of the lipid tails and changes their lateral stress.<sup>96</sup> This results in changes in curvature elastic energy, and pressure can thus be used to induce phase transitions. Lipids can undergo transitions from lamellar to non-lamellar phases or change from a flat bilayer to a curved one due to an



**Fig 10.** Illustration of the forces between head groups and tail groups of lipids.  $F_h$  is the force present between the headgroups, which may be either repulsive due to steric or electrostatic effects, but may also be attractive due to charge or hydrogen bonding.  $F_c$  is the repulsive force present between chains, due to cis-trans rotations and the resulting steric pressure.  $\gamma$  is the interfacial tension due to contact between the tails and the surrounding water, and works to minimise the interfacial area (adapted from reference 9).

imbalance in the effect by the pressure change between the headgroups and tails of the lipids (**figure 10**), with a higher degree of lateral pressure in the chain region causing curvature inwards towards the headgroups and promoting the inverse hexagonal phase, a high degree of lateral pressure between the headgroups causing curvature inwards towards the chain.<sup>101</sup>

It has been observed that increasing pressure has the opposite effect to increasing temperature in lipid systems, as increasing pressure results in a higher degree of constraint on the hydrocarbon tails, restricting their movement<sup>102</sup> and increasing the ordering in the region, i.e. increasing pressure promotes the processes that reduce the volume of the system.<sup>103</sup> As the cross-section of the head group is not as affected by pressure as the tail groups, the magnitude of preferred negative curvature is decreased with increasing pressure in inverse hexagonal systems, resulting in an increase in diameter of the cylinders present (**Fig. 11**) although only up to a point as voids between cylinders cannot form.<sup>103</sup>

The effect of pressure on a lipid system can be quantified with the Clapeyron equation (**equation 10**):

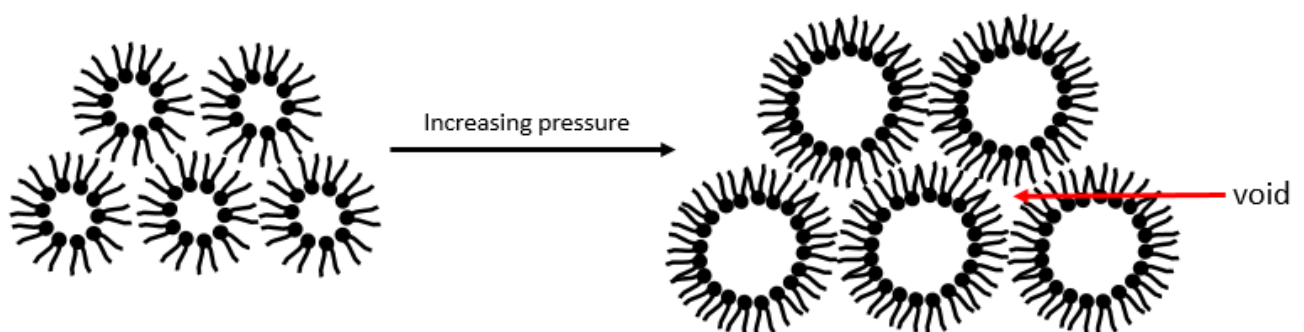
$$\frac{dT_t}{dp} = \frac{\Delta V_m}{\Delta S_m} = \frac{T_t \Delta V_m}{\Delta H_m}$$

Equation

10

where  $T_t$  is the phase transition temperature,  $\Delta S_m$ ,  $\Delta H_m$  and  $\Delta V_m$  are the molar transition entropy, enthalpy and volume changes, respectively, and this linear relationship between pressure and temperature hold for pressure up to approximately 200 MPa.<sup>103</sup>

Using pressure rather than temperature to induce phase changes offers a number of advantages: high pressure does not tend to disrupt intramolecular bonding up to approximately 2 GPa, allowing for substances to be studied as they appear in nature; in addition, pressure can be applied and released on a micro-to-millisecond time frame, which allows for the kinetic effects to be observed in real-time and also for the effects of both increases and decreases in pressure to be observed. In contrast, temperature propagation and equilibrium typically is not established as fast and the time taken to heat and cool a sample is typically not equal.<sup>103</sup>



**Fig. 11.** The effect of increasing pressure on inverse hexagonal lipid phases (adapted from reference 7).



## 2.5 Introduction to Dynamic Light Scattering

Dynamic light scattering (DLS) is a non-destructive, non-invasive analytical technique that can be used to determine structural information about particulate dispersions. It is well-established for collecting information such as size and polydispersity of the particles present and can be coupled with other techniques such as zeta potential as discussed later. As it is noninvasive the collection of data through DLS does not influence the behaviour of the sample. DLS is typically used to determine the Z-average size of particles in solution and their polydispersity index (PDI), where a value approaching zero represents a more monodispersed dispersion, meaning all particles are of a similar size; whereas a value approaching unit (1) reflects a more polydisperse dispersion, indicating the presence of particles of differing sizes. DLS also offers advantages of simple sample preparation and relatively fast measurements.

To carry out DLS measurements, a monochromatic light source, typically a laser, is passed through a polariser and then into a sample, where, given that the particles are sufficiently small, it scatters in all directions in a phenomenon known as Rayleigh scattering. The scatter then passes through a second polariser and is collected by a photomultiplier which converts incident photons into an electrical signal for data processing. This Rayleigh scattering results in what is known as a speckle pattern resulting from constructive and destructive interference of scattered light. As particles in solution are not static but rather subject to the Brownian motion resulting from the collision between particles and the molecules of the solution, this pattern changes over time. This dynamic information about the particles is derived from an autocorrelation of the intensity trace,<sup>104</sup> and so for short time-frames the correlation is high but decays exponentially for a monodisperse sample as the particles move further from their initial position.

As the movement of the particles is a result of collisions with solvent molecules, several factors influence the movement of the particles including temperature, size, and solvent viscosity. The diameter of particles in solution can be derived from DLS through the Stokes-Einstein relation (**equation 11**):<sup>105</sup>

$$D = \frac{k_B T}{6\pi\eta R} \quad \text{Equation 11}$$

where  $R$  is the hydrodynamic diameter or particle size,  $D$  is the translational diffusion coefficient,  $k_B$  is the Boltzmann constant,  $T$  is the temperature, and  $\eta$  is the viscosity of the solution.  $D$  is determined by first plotting the autocorrelation function against the delay time which yields the decay rate  $\Gamma$  (**equation 12**):<sup>106</sup>

$$\Gamma = Dq^2 \quad \text{Equation 12}$$

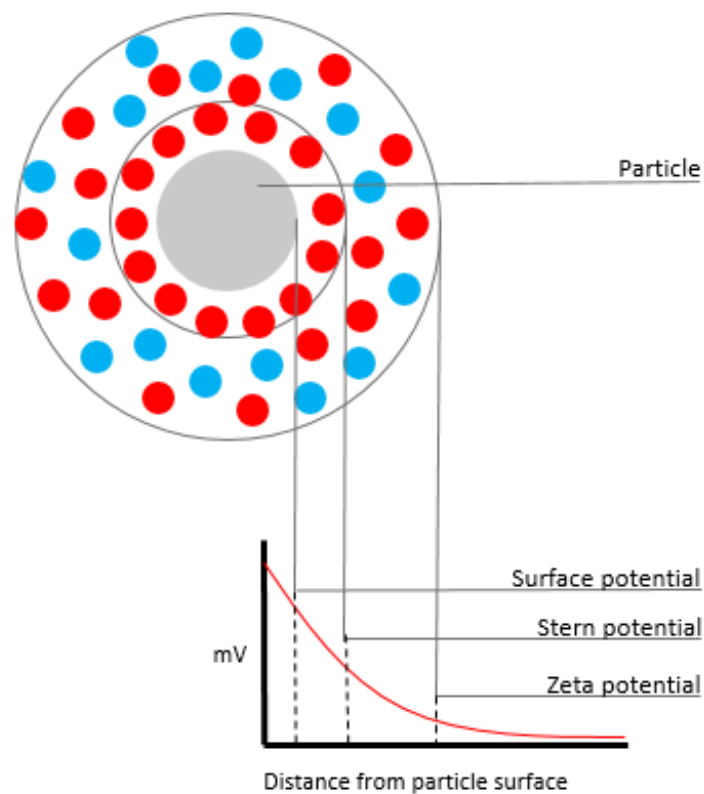
where the wave vector  $q$  is determined via **equation 13**:<sup>107</sup>

$$q = \frac{4\pi n}{\lambda} \sin\left(\frac{\theta}{2}\right) \quad \text{Equation 13}$$

In which  $\lambda$  is the incident laser wavelength,  $n$  is the refractive index of the of the sample and  $\theta$  is the angle at which the detector is positioned relative to the sample cell.<sup>108</sup>

## 2.6 Zeta Potential

The zeta potential is a measure of the electrokinetic potential at a solid-liquid interface, typically measured in mV. When surfaces are exposed to a fluid, a structure known as an electrical double layer arises. The first layer adjacent to the surface, the Stern layer, is composed of adsorbed ions. The second layer or diffuse layer is composed of ions that are more loosely associated with the surface and are attracted to the first layer via the coulomb force. The slipping plane is the name given to the boundary between the diffuse later and the bulk medium, with the zeta potential giving the potential difference between the area bounded by the slipping plane and the bulk medium (**Fig. 12**).<sup>109, 110</sup>



**Fig. 12.** Illustration of the potentials and layers of charge (charged particles represented by red and blue dots) present around a particle (inner ring: stern layer, outer ring: diffuse layer). Adapted from Ref. 13.

The zeta potential ( $\zeta$ ) is a key indicator of colloidal stability. The presence of a large  $\zeta$  indicates a large degree of repulsion between adjacent particles in solution, and therefore indicates a lower chance of particles aggregating and flocculating. Likewise, a small  $\zeta$  indicates that attractive forces may overcome the repulsive forces present and that aggregation is more likely. Zeta potential is therefore a very useful measure of colloidal stability, with a larger  $\zeta$  indicative of a more stable colloid and vice versa.

It is not possible to directly measure zeta potential and so it can be measured indirectly through observing the electrophoretic mobility of particles, that is, how mobile particles are when subject to an electric field. An electric field is applied to the sample and the doppler shift in a laser beam is used to measure the velocity (laser doppler velocimetry, LDV)<sup>111</sup> of the particles by measuring small shifts in the frequency of the scattered light, which is used to calculate the electrophoretic mobility  $U_E$ . The  $U_E$  is then used to calculate the zeta potential  $\zeta$  using the Henry equation (**equation 14**):

$$U_E = \frac{2\varepsilon\zeta F(\kappa a)}{3\eta} \quad \text{Equation 14}$$

Where  $\varepsilon$  is the dielectric constant,  $\eta$  is the viscosity of the medium,  $F(\kappa a)$  is the Henry function, and  $\kappa a$  is the measure of the ratio of the particle radius to the Debye length.<sup>109</sup>

Typically, particles with a zeta potential of +/- 10 mV are considered to be fairly neutral, while a zeta potential of more than +30 mV or less than -30 mV is considered to indicate the presence of highly charged particles.<sup>111</sup>

## 2.7 Introduction to Polarising Light Microscopy

Polarised light microscopy (PLM) is an easy-to-perform microscopy technique that can be used to identify structurally anisotropic crystalline or crystalline-like regions in samples including biological samples and lipids,<sup>112</sup> and has been in use through the 20th century and in modern day. Crystalline materials affect the speed at which light passes through them, and while for isotropic materials the refractive index is the same in all directions, this is not true for crystals, which are termed anisotropic and have more than one refractive index.<sup>112</sup> This results in a property known as birefringence, which cannot be detected by a typical light microscope but can be detected using a polarising light microscope. PLM can thus be used to quickly and easily identify crystalline regions and can complement other more quantitative techniques such as SAXS.<sup>113</sup>

Polarising light microscopes work by having one polariser between the light source and the sample and a second to analyse the polarisation of the light after passing through the sample. Typically, birefringent regions of a sample appear to be brightly lit and coloured while other areas appear dark, making identification of crystalline areas fast and simple. Objects with a greater difference between their two refractive indices appear brighter than objects for which this difference is smaller, and thicker objects will also appear brighter than thinner ones with the same difference between refractive indices. Brightness is also greatest when the object is at 45° to the planes of polarization, and is at a minimum when the object is parallel to one of these planes, i.e. it is not visible.<sup>114</sup>

## **2.8 General Methods**

Cardiolipin, DOPE (1,2-dioleoyl-sn-glycero-3-phosphoethanolamine) and DOPG (1-2,dioleoyl-sn-glycero-3-phospho-(1'-rac-glycerol)) were purchased in chloroform solution from Avanti Polar Lipids and stored at -30°C until use. Glassware used to prepare lipid solutions was cleaned in 10% nitric acid by submerging it in the acid bath for a minimum of one hour, transferred to water purified by a MilliQ advantage a10 purification system and then rinsed with MilliQ water before being dried in a Heraeus Vacuotherm VT 6025 vacuum oven.

### **2.8.1 Preparation of pH solutions**

pH solutions of 1.3, 5.1 and 12.1 were prepared using hydrochloric acid (Fischer Scientific, 37%) or sodium hydroxide pellets (Sigma Aldrich, 99.99%) as appropriate, and measured using a Hanna Instruments HI-2550 pH/ORP & EC/TDS/NaCl benchtop pH meter.

### **2.8.2 Preparation of samples for HP-SAXS**

HP-SAXS samples were prepared by measuring out appropriate volumes of lipid solution into glass vials, which were then dried overnight in a Heraeus Vacuotherm VT 6065 vacuum oven at room-temperature. The dried lipids were re-dissolved in 300  $\mu$ L chloroform with desired and then dried at room temperature overnight again. Samples were then rehydrated with 100  $\mu$ L of the pH appropriate solution before being vortexed vigorously for approx. 10 s and then sonicated for 90 minutes at room temperature. Samples were then left overnight (approx. 18 h) in an incubator shaker at 45 C, 600 rpm, before being vortexed for a further 10 s each and then subjected to five freeze-thaw cycles between warm water (approx. 40 °C) and an acetone/dry-ice bath (approx. -78°C).

### **2.8.3 HP-SAXS Measurements**

HP-SAXS measurements were carried out at beamline I22 at Diamond Light Source, Oxfordshire, UK. The X-ray beam was positioned 5.76 m from the sample, sized 180 x 100  $\mu\text{m}$  and had an energy of 18 keV. The detector used was a Pilatus P3-2M. A high-pressure cell as described by Brooks et al.<sup>115</sup> was used to hold the samples, which were contained in polycarbonate capillary tubes of approximately 20 mm length, outer diameter  $2.08 \pm 0.01$  mm, and  $0.10 \pm 0.03$  mm (Spectrum Plastics, Georgia, USA). The tubes were sealed with Araldite Instant 90 s G Resin (Huntsman Advanced Materials, Everberg, Belgium), cured at 60°C for approximately 30 min.

Before measurements were taken, samples were cycled from 1-4000 bar to further homogenise the samples and check for leaks and damage to the sample. Data was collected by increasing the pressure from 1 to 3000 bar in increments of 300 bar at a range of increasing temperatures, with an exposure time of 100 ms per image, before cooling the sample to the initial temperature and completing another pressure cycle to check for any hysteresis and radiation damage. An additional image was also collected again at 1 bar after each temperature for the same reasons. 2D scattering patterns were collected and converted into 1D intensity vs Q plots and the beamline background subtracted using the software DAWN, and the phases were then determined by peak fitting with Voight or Gaussian functions in Igor Pro.

### **2.8.4 Preparation of samples for Polarising Light Microscopy**

HP-SAXS samples were prepared by measuring out appropriate volumes of lipid solution into glass vials, which were then dried overnight in a Heraeus Vacutherm VT 6065 vacuum oven

at room temperature, re-dissolved in 300  $\mu\text{L}$  of chloroform, combined to make samples of the required composition and then dried at room temperature overnight again. Samples were then rehydrated with 100  $\mu\text{L}$  of MilliQ water at a designated pH before being vortexed vigorously for approx. 10 s and then sonicated for 90 minutes at room temperature. Samples were vortexed for a further 10 s each and then subjected to five freeze-thaw cycles between warm water (approx.  $40^{\circ}\text{C}$ ) and an acetone/dry-ice bath (approx.  $-78^{\circ}\text{C}$ ). PLM images were then captured with an Olympus BX53-P microscope, with polarisers crossed at  $90^{\circ}$  and images captured with Stream software (multi-lipid systems) or a Nikon Eclipse E200 microscope, with polarisers crossed at  $90^{\circ}$  and images captured using PikeLINK Capture OEM software. A 530 nm first-order waveplate was used, providing enhanced contrast. All images were processed with Fiji image processing software.

### **2.8.5 Preparation of samples for Dynamic Light Scattering and Zeta potential measurements**

DLS samples were prepared by measuring out the appropriate volumes of lipid solutions into glass vials and then drying overnight in a vacuum oven at room temperature before being rehydrated with 1 mL of water at a designated pH. Samples were then subjected to 5 freeze-thaw cycles between warm water and an acetone/dry-ice bath, sonicated for 90 min and diluted to a concentration of  $0.1 \text{ mg mL}^{-1}$ . Samples were then extruded using a Lipex 10/1.5 mL thermobarrel extruder at  $60^{\circ}\text{C}$ , 10 times through a 200 nm pore size polycarbonate filter and then 10 times through a 100 nm filter. The resulting liposome dispersions were stored in a fridge between measurements. The solutions were divided into two equal portions, with



one portion being sonicated for 90 min at room temperature prior to each DLS measurement and the other not.

## **Chapter 3. HP-SAXS study on the effect of cardiolipin, temperature, pressure and pH on the phase behaviour of a model bacterial membrane**

---

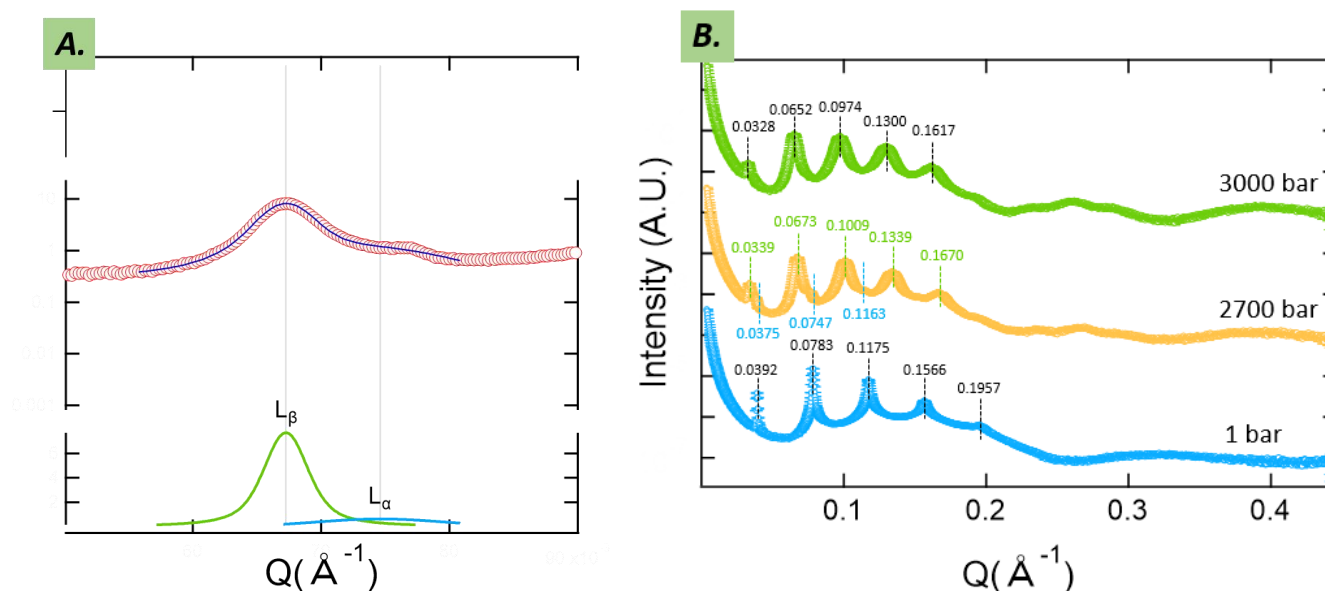
### **3.1 Abstract**

*The effects of cardiolipin and pH on the phase behaviour of a model E. coli bacterial membrane lipid system, consisting of DOPE, DOPG and Cardiolipin in a 70:20:10 ratio, have been investigated. A critical comparison is made with the control sample comprising DOPE/DOPG in a ratio of 78:22. DOPE/DOPG/CL samples were prepared at pH 1.3, 5.1, and 12.1 and DOPE/DOPG at 5.1, to allow for the investigation of the effects of pH on the phase behaviour of the system. Pressure-temperature (p-T) phase diagrams of the lipid systems were obtained using high-pressure small-angle X-ray scattering (HP-SAXS) at Diamond I22 with a pressure range of 1-3000 bar and a temperature range of either 20 - 60°C (for DOPE/DOPG/CL at pH 1.3) or 20 - 45°C (for DOPE/DOPG and DOPE/DOPG/CL at pH 5.1). Peak-fitting was carried out for assigning the mesophases and the analyses of the d-spacing and coherence length L of the samples. For both DOPE/DOPG/CL and DOPE/DOPG at pH 5.1, the lamellar alpha ( $L_\alpha$ ) phase was observed under ambient conditions with a single transition to the lamellar beta ( $L_\beta$ ) phase at high pressure at 20 and 25°C. At pH 12.1, the mesophase behaved in the same manner as at pH 5.1; However, at pH 1.3, the mesophase primarily existed in the inverse hexagonal ( $H_{II}$ ) phase with a transition to an unidentified phase at high pressure at 20 and 30°C. The presence*

of cardiolipin was found to have a small impact on the phase behaviour of the system at pH 5.1, with the  $L_{\beta}$  phase appearing at a lower pressure at 20°C in its presence. The presence of cardiolipin resulted in a larger  $d$ -spacing and  $\Delta d/\Delta p$  gradient at all temperatures and pressures studied at pH 5.1, and a lower  $d$ -spacing and shallower  $\Delta d/\Delta p$  was observed at pH 12.1 compared to pH 5.1. A difference was also observed between the coherence lengths of the pH 5.1 samples, with the presence of cardiolipin resulting in a greater decrease in coherence length with increasing temperature.

### 3.2 Results & Discussion

As previously discussed, small-angle X-ray scattering (SAXS) is a useful tool for characterising lipid mesophases and obtaining a wealth of information including  $d$ -spacing and coherence length. For this chapter, the data obtained at beam line I22 were first plotted and the peaks fitted using Igor Pro (Fig. 13 A.) to establish pressure-temperature ( $p$ - $T$ ) phase diagrams for



**Fig. 13.** Illustration of the peak-fitting process in Igor Pro using data collected in this experiment. On the left (A), part of the process of peak-fitting is shown (taken from CON2 at  $T = 25^{\circ}\text{C}$  and  $p = 2700$  bar), with two peaks identified and assigned to the  $L_{\beta}$  and  $L_{\alpha}$  phase respectively. On the right (B), full SAXS patterns obtained for selected pressures from CON2 at  $T = 25^{\circ}\text{C}$  are shown to illustrate the phase change that occurred.

the samples from  $p = 1\text{-}3000$  bar, with a temperature range  $20 - 60^\circ\text{C}$  (varying with samples). This range was chosen to encompass biologically relevant temperatures (**Table 3 and Fig. 13.**). The  $p$ - $T$  diagram for CON2 was first established as a control, followed by samples CL1, CL2 and CL3 to investigate the effects of the presence of cardiolipin and changes in pH on the phase behaviour of the system.

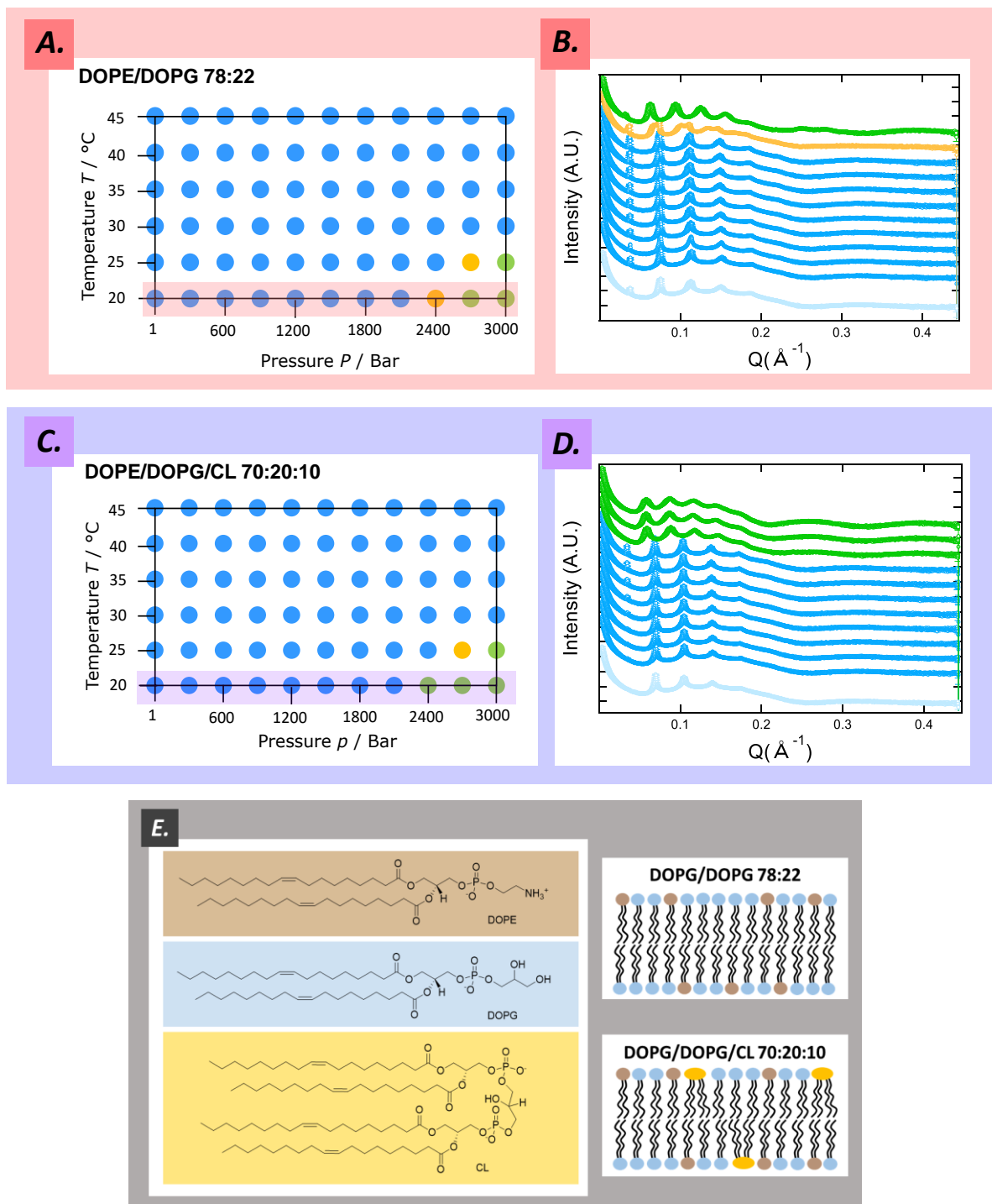
Sample Name	Lipid Composition	Lipid Ratio	pH
CON2	DOPE/DOPG	78:22	5.1
CL1	DOPE/DOPG/CL	70:20:10	1.3
CL2	DOPE/DOPG/CL	70:20:10	5.1
CL3	DOPE/DOPG/CL	70:20:10	12.1

**Table 3.** Samples investigated via HP-SAXS in this work

### 3.2.1 Phase behaviour of lipid systems

Different phases were assigned by examining the  $Q$  values of the peaks to obtain characteristic peak ratios. In **Fig. 13 B.**, at  $p = 1$  bar the peaks are present in a 1:2:3... ratio, indicating the presence of a lamellar phase, identified as the  $L_\alpha$  phase. At  $p = 2700$  bar, a phase transition occurred, evidenced by the emergence of a second set of peaks (shown in green) alongside the peaks arising from the  $L_\alpha$  phase (shown in blue). Peak fitting reveals the presence of a mixed phase, with overlapping peaks belonging to the two different phases obtained. At  $p = 3000$  bar, the peaks belonging to the  $L_\alpha$  phases are no longer present, signalling that at this pressure the phase transition to the  $L_\beta$  phase was complete.

Samples CON2 and CL2 were studied in the temperature range  $20\text{-}45^\circ\text{C}$ , and the  $L_\alpha$  phase were present exclusively at the majority of the  $p$ - $T$  phase diagram (**Fig. 2 A & C**)



**Fig. 14. (A & B)** Pressure-temperature phase diagrams for lipid mesophase systems at pH 5.1. Blue circles indicate the presence of the  $L_\alpha$  phase, yellow circles indicate the presence of a mixed  $L_\alpha/L_\beta$  phase, and green circles indicate the presence of the  $L_\beta$  phase. SAXS patterns for CON2 (**B**) and CL2 (**D**) at pH 5.1 and  $T = 20^\circ\text{C}$ . Blue corresponds to the  $L_\alpha$  phase, yellow to a mixed  $L_\alpha/L_\beta$  phase and green to the  $L_\beta$  phase. The pale blue trace corresponds to the repeated measurement for  $p = 1$  after the pressure cycle was completed. **E:** structures of lipids used in samples and diagrams of lipid mixtures used in samples. Blue lipid headgroups represent DOPE, brown head groups represent DOPG and yellow head groups represent cardiolipin, corresponding to the chemical structures of the lipids shown on the right.

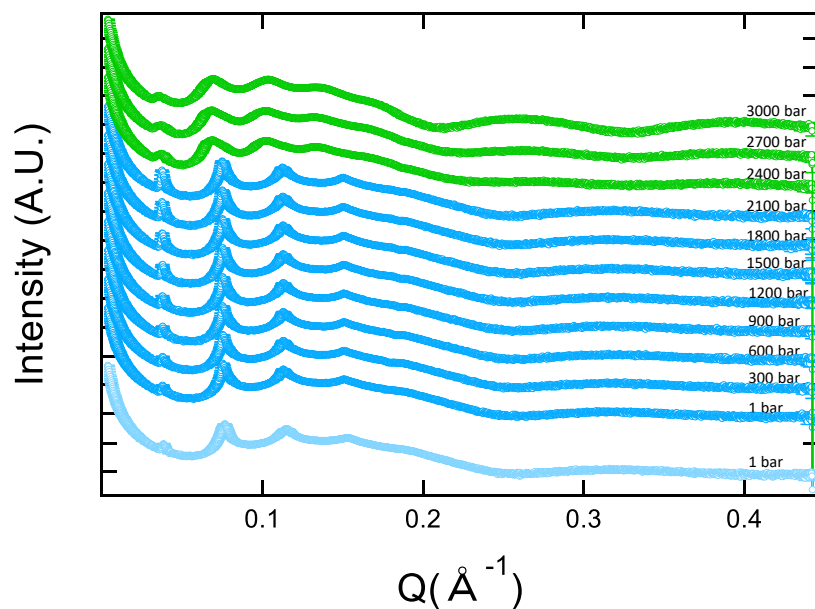
with only the  $L_{\alpha}$  phase observed at temperatures of 30°C and above for both systems. One phase transition was observed in each system from the  $L_{\alpha}$  phase to the  $L_{\beta}$  phase at both 20 and 25°C; however, the pressure at which this transition was complete was slightly lower in the presence of cardiolipin; for CON2 at  $T = 20^{\circ}\text{C}$ , a mixed phase was present at  $p = 2400$  bar between  $p = 2100$  and 2400 bar.

The pressure-temperature phase diagram for pure DOPE has previously been established by Bulpett *et al.*,<sup>96</sup> who found that at ambient pressure and temperature, DOPE forms an inverted hexagonal phase, only transitioning to the  $L_{\alpha}$  phase above approximately  $p = 600$  bar. The  $L_{\alpha} \rightarrow L_{\beta}$  transition was still observed at higher pressures, taking place at ambient temperature at  $p > 2000$  bar. Comparing the findings of Bulpett *et al.* to CL2, which contains DOPE as the major component, it is clear that the addition of DOPG has a significant impact on the phase behaviour of the DOPE, preventing the formation of the inverted hexagonal phase under ambient conditions and increasing the pressure needed to achieve the  $L_{\beta}$  phase from approx. 2000 bar to 2700 bar. This is consistent with the findings of Morein *et al.* however, who found that under ambient conditions and at pH 7.4, DOPE/DOPG in a 7:3 ratio forms the  $L_{\alpha}$  phase.<sup>116</sup> Although DOPE and DOPG have identical tail groups, their head group areas are different. This may explain the difference seen between the established phase behaviour of DOPE and CON2, i.e. changes in the lipid packing due to addition of DOPG wherein the lipids are not able to pack as closely due to the differing headgroup areas and so a greater pressure is required to form the  $L_{\beta}$  phase.

The finding that the addition of cardiolipin slightly lowered the pressure at which the  $L_{\alpha} \rightarrow L_{\beta}$  phase transition is complete from 2700 to 2400 bar (**Fig. 14 A & C**) is likely due to a change in the packing of the lipid chains, possibly due to the increased lateral pressure CL introduces into bilayers.<sup>63</sup> For both CON2 and CL2, increasing temperature increased the

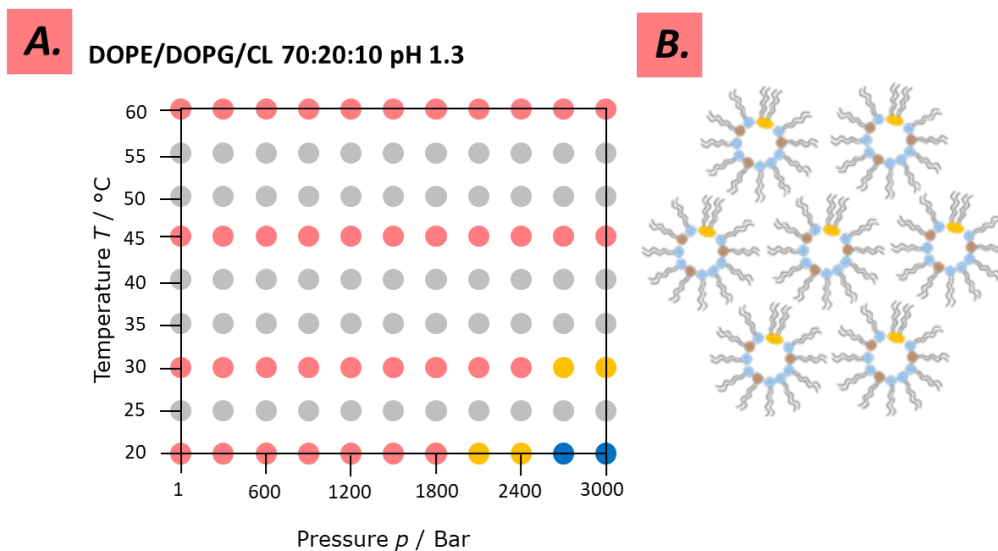
pressure required to produce the gel phase, in line with expectations, as pressure increases the constraint on the hydrocarbon tails and restricts their movement thereby promoting the gel phase, while increasing temperature increases the lateral pressure between tail groups, working to produce the opposite effect.

Aside from the  $L_{\alpha} \rightarrow L_{\beta}$  transition happening at 300 bar lower pressure at  $T = 20^{\circ}\text{C}$  for CON2 (**Fig. 14 A & C**), the  $p$ - $T$  phase diagrams collected for both systems are highly similar suggesting that cardiolipin only had a subtle effect on the phase behaviour of the system at pH 5.1.



**Fig. 15.** SAXS patterns for CL3 at  $T = 20^{\circ}\text{C}$ . Blue corresponds to the  $L_{\alpha}$  phase, and green to the  $L_{\beta}$  phase. The pale blue trace is the repeated measurement for  $p = 1$  bar after the pressure cycle was completed.

As mentioned previously, at pH 5.1, cardiolipin carries a single negative charge, and so repulsion between its two head groups is present but not at a minimum as when no negative charge is present. For pH 12.1, when cardiolipin carries two negative charges, data was only collected for  $T = 20^{\circ}\text{C}$  (**Fig. 15**). It was found that for sample CL3, the system was in the  $L_{\alpha}$  phase from  $p = 1$ -2100 bar, and then in the  $L_{\beta}$  phase from  $p = 2400$  to 3000 bar, behaving in the same way as CL2 (**Fig. 14 A & C**).



**Fig. 16. A:** Pressure-temperature phase diagram for CL1. Red circles indicate the presence of the inverse hexagonal phase, yellow circles indicate the presence of a mixed inverse hexagonal/other phase, and blue circles indicate the presence of an unknown phase. Grey circles represent missing data points, the phase diagram was constructed in this way to allow for easy comparison with the pH 5.1  $p$ - $T$  phase diagram. **B:** Diagram of  $H_{II}$  phase. Blue lipid head groups represent DOPE, brown head groups represent DOPG and yellow head groups represent cardiolipin.

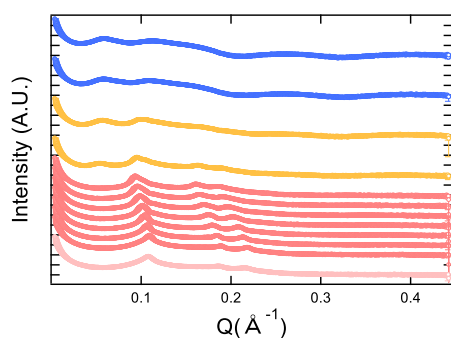
However, the system behaved very differently at pH 1.3 (**Fig. 16. A**), when cardiolipin carries no negative charge and repulsion between its two head groups is at a minimum. At ambient pressure, the system was in the inverse hexagonal phase (**Fig. 16. B**) at all temperatures studied ( $T = 20$ – $60^{\circ}\text{C}$ ). This increased propensity towards the inverse hexagonal phase at acidic pH may be due to the decreased repulsion between the incorporated cardiolipin head groups, allowing for an increase in the packing parameter of the individual molecules and increasing their preference to form inverted phases with negative curvature relative to when only a single or no negative charge is present. However, a control  $p$ - $T$  diagram of DOPE/DOPG only at pH 1.3 would be required to establish this. Increasing the pressure of this system beyond approximately  $p = 1800$  bar at  $T = 20$  and  $30^{\circ}\text{C}$  resulted in a

mixed system composed partially of the inverse hexagonal phase, and partially another phase with peaks positioned at approximately 0.05, 0.07 and 0.11 Å<sup>-1</sup>, with only this phase being present at  $T = 20^{\circ}\text{C}$  at pressures at and above approximately  $p = 2700$  bar. These peak ratios do not appear to correspond to the established peak ratios for the lamellar, inverse hexagonal or any cubic phases and so could not be identified.

As discussed above, the differences seen between the mesophase at pH 1.3 and at pH 5.1 and 12.1 (**Figs. 14, 15 & 16**) are in line with expectations. At higher pH where cardiolipin has one or more negative charges on its two headgroups, the repulsion between the two headgroups is increased, decreasing the packing parameter as the flexibility of the molecule is reduced. At lower pH, with no charge and so minimal repulsion between the headgroups, the increased packing parameter causes a greater tendency towards negative curvature.

As well as cardiolipin, the potential contributions of the other two lipids in the system-DOPE and DOPG- cannot be overlooked. DOPE is a neutral lipid that, due to its two cis double-bonds which introduce kinks into the chains, has a low chain-melting transition temperature relative to many other common lipids, of  $-16^{\circ}\text{C}$ .<sup>117</sup> As observed by Bulpett *et al*<sup>96</sup> pure DOPE exists in the H<sub>II</sub> phase at atmospheric temperature and pressure, transitioning to the L<sub>α</sub> and then the L<sub>β</sub> phase with increasing pressure ( $p = 600$  and  $p = 2100$  bar, respectively, at  $T = 20^{\circ}\text{C}$ ). As the temperature increases, higher pressures are needed to induce the transition to the L<sub>β</sub> gel phase. As DOPE made up the bulk of the model mesophases used in this work, it was predicted that the phase behaviour of these mesophases may approximately follow the observed behaviour of pure DOPE. DOPG also has a low chain-melting transition temperature of  $-18^{\circ}\text{C}$ ,<sup>117</sup> but in contrast to DOPE is anionic and tends to exist in lamellar phases under ambient conditions when not in the presence of divalent cations.<sup>118</sup> The key difference





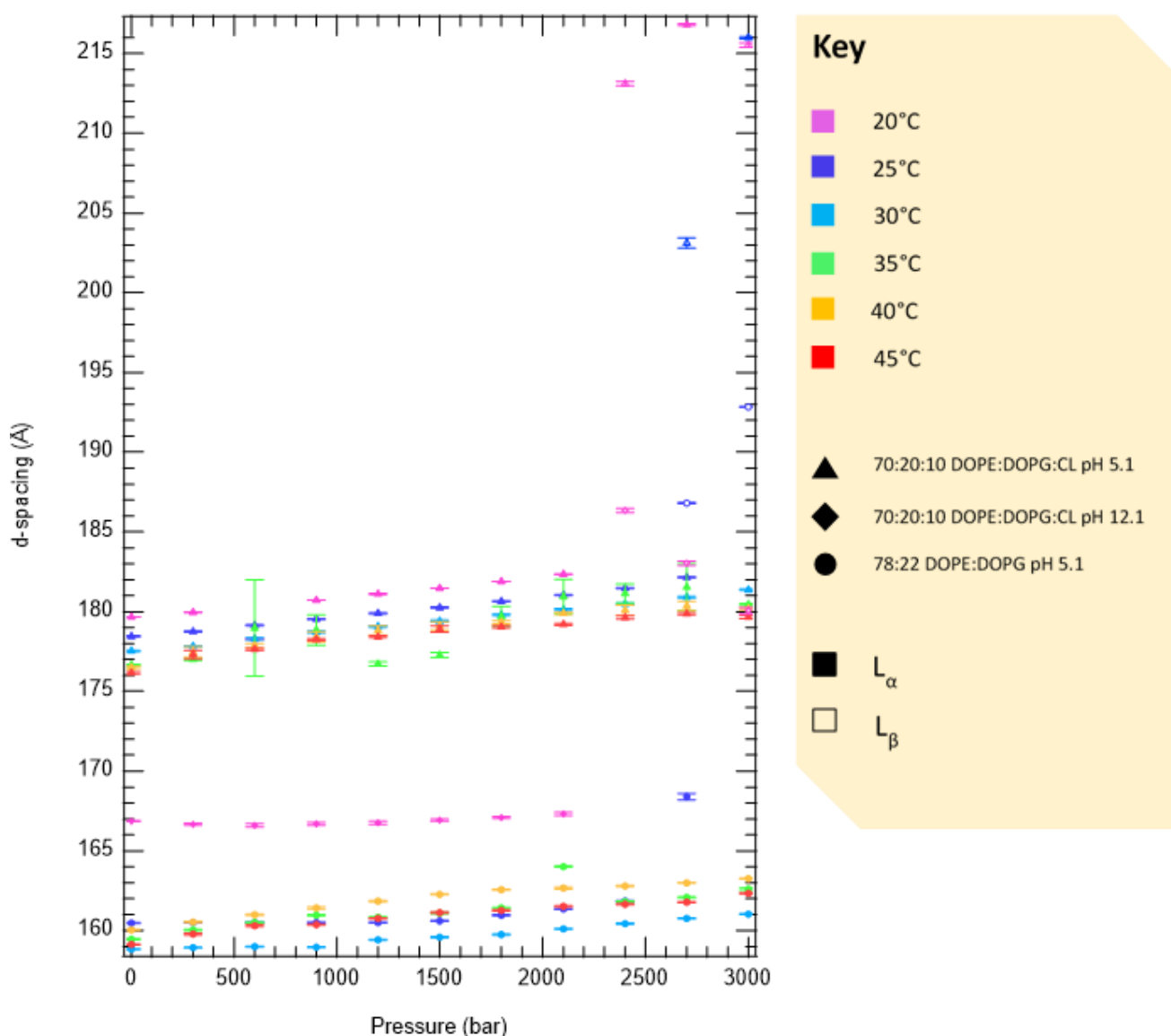
**Fig. 17.** SAXS data for CL1 at  $T = 20^\circ\text{C}$ . Red traces indicate  $p = 1\text{-}1800$  bar (bottom to top) and the presence of the  $H_{II}$  phase, orange traces indicate the presence of a mixed phase at  $p = 2100$  and  $2400$  bar and blue traces indicate the presence of a new phase at  $p = 2700$  and  $3000$  bar.

observed with the addition of DOPG alone to DOPE was the disappearance of the inverted hexagonal phase observed under ambient conditions in pure DOPE,<sup>96</sup> with only lamellar phases appearing, demonstrating the stabilising effect DOPG has on the  $L_\alpha$  phase.

Another feature of note in the SAXS measurements obtained is the presence of scattering curves at higher  $Q$  values on the traces at pH 5.1 and 12.1 at all pressures and temperatures studied (**Figs. 14 & 15**), and at  $p = 2400$  and above in the pH 1.3 measurements (**Fig. 17.**), indicating the presence of not just mesophases but particles in the samples studied.<sup>119</sup> It is likely that these particles are vesicles due to the methods of preparation used, formed during the sonication step. The shape and size of the particles could be obtained through fitting, however attempts using SASview software were unsuccessful due to the presence of peaks amongst these curves. Also noticeable is that no vesicles are present at

the same time as the hexagonal phase at pH 1.3, but start to appear at lower temperatures and high pressures when the system undergoes a phase transition.

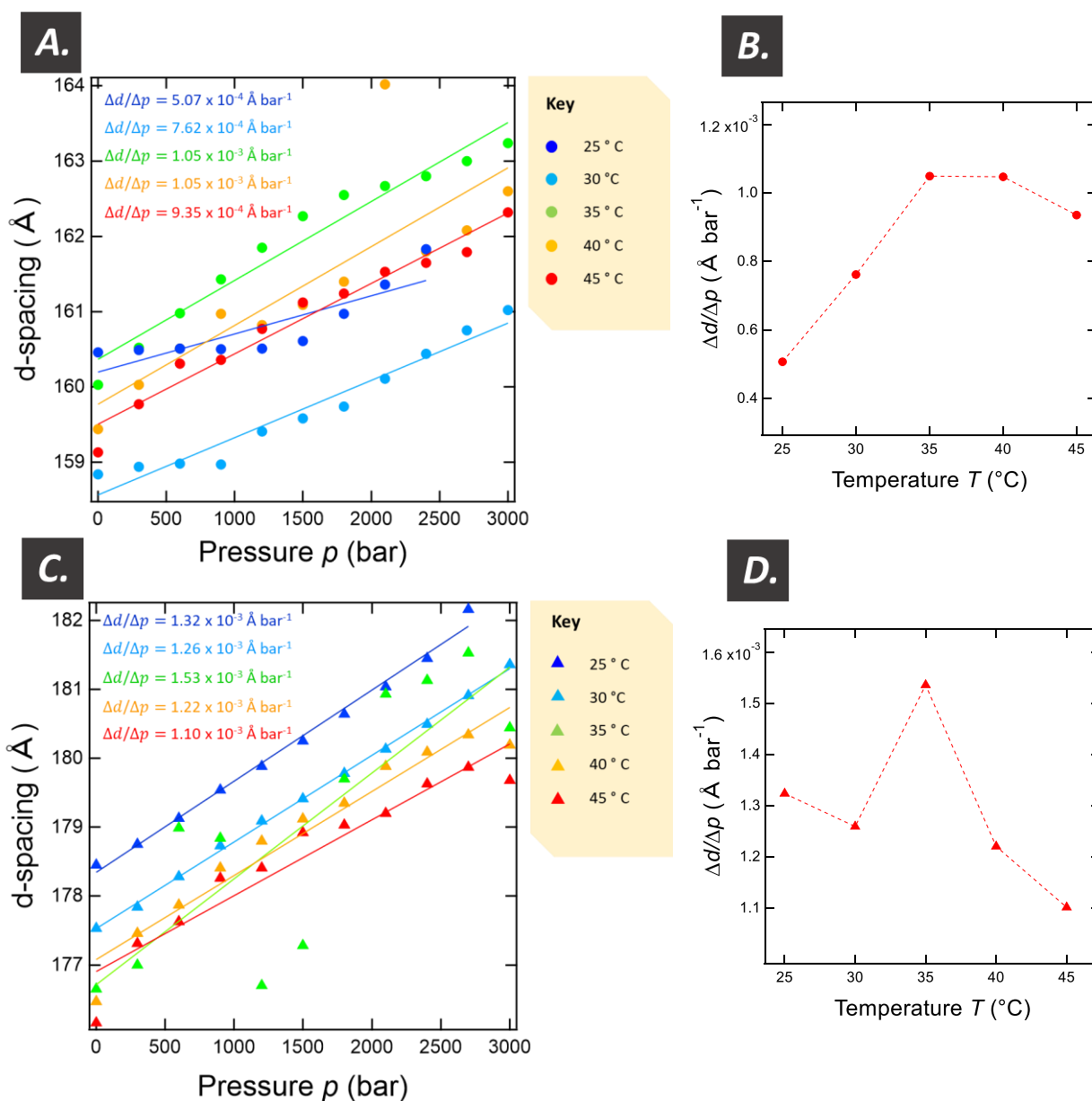
Guinier and Porod fitting could have aided in characterising these particles, however due the lack of validity of the Guinier approximation when applied to this data ( $qR_g$  was not within the accepted limit of  $<1.3$ )<sup>97</sup> and the fact that fitting was difficult due to the presence of multiple peaks in addition to the scattering curves, this analysis was not carried out.



**Fig. 18.** Effect of pressure, temperature and lipid composition on the d-spacing of the lamellar mesophases in samples CON2, CL2 and CL3.

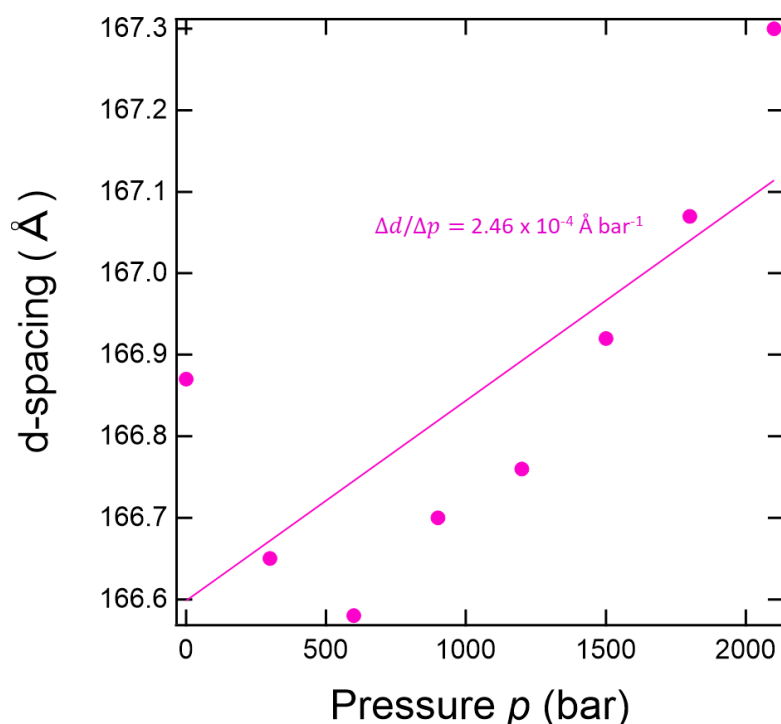
### 3.2.2 d-spacing of lipid systems

However, information on the changes in d-spacing caused by temperature and pressure could be obtained from this data (Fig. 18). It was found that the d-spacing of CL2 was larger relative to CON2, indicating that the cardiolipin played a role in increasing the distance between the lipid bilayers. As seen in Fig. 19. A & C, at all temperatures, the gradient  $\Delta d/\Delta p$  was also greater for CL2 than for CON2, with increasing pressure having a greater effect on the d-



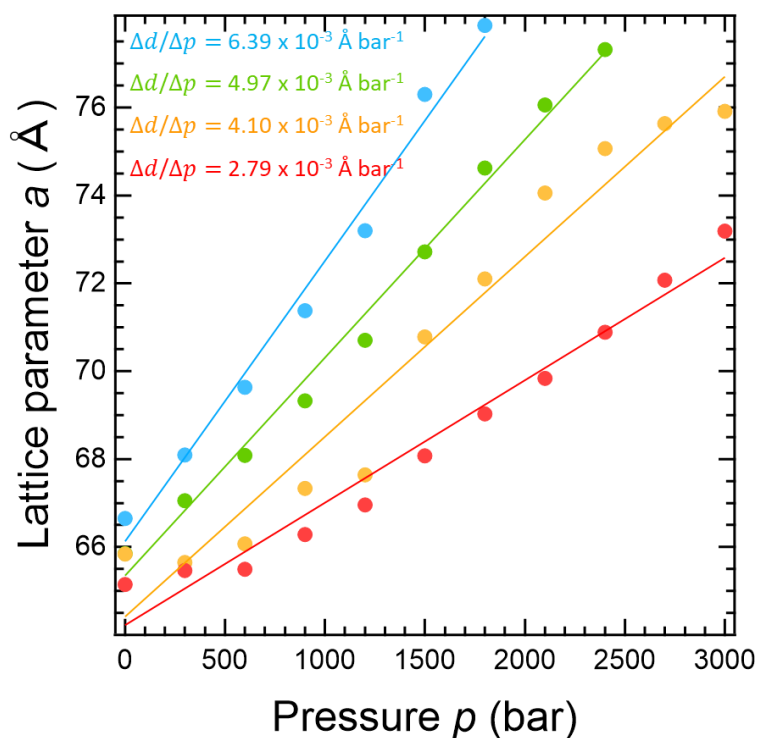
**Fig. 19.** Linear fits carried out for CON2 (A) and CL2 (C) to obtain  $\Delta d/\Delta p$  and  $\Delta d/\Delta p$  against temperature for CON2 (B) and CL2 (D).

spacing of CL2. In **Fig 19. B & D**,  $\Delta d/\Delta p$  against temperature is shown for CON2 and CL2 respectively, with  $\Delta d/\Delta p$  for CON2 increasing between  $T = 25$  and  $35^\circ\text{C}$  before decreasing slightly at  $T = 45^\circ\text{C}$ . Conversely for CL2,  $\Delta d/\Delta p$  decreased with temperature aside from  $T = 35^\circ\text{C}$  where an increase in  $\Delta d/\Delta p$  occurred. The  $\Delta d/\Delta p$  values found are in agreement with literature, with an increase in pressure causing a decrease in the fluidity and disorder of the lipid chains, and an increase in their extension.<sup>120</sup> This was found to be the case for CON2, CL2, and CL3, although  $\Delta d/\Delta p$  for CL3 (**Fig. 20**) at the temperature studied ( $T = 20^\circ\text{C}$ ) was lower than  $\Delta d/\Delta p$  at  $25^\circ\text{C}$  for either CON2 or CL2 at  $2.46 \times 10^{-4} \text{ \AA bar}^{-1}$  vs  $5.07 \times 10^{-4} \text{ \AA bar}^{-1}$  and  $1.32 \times 10^{-3} \text{ \AA bar}^{-1}$  respectively (**Fig. 19. A & C**), suggesting that pH may have influenced the responsiveness of the system to increasing pressure.



**Fig. 20.** Linear fit for CL3 at  $20^\circ\text{C}$  to obtain  $\Delta d/\Delta p$

The transition from the  $L_{\alpha}$  to the  $L_{\beta}$  phase was accompanied by a significant increase in d-spacing, as in gel phases the lipid chains are further extended as the lipids change conformation to accommodate the restriction imposed on their volume by the pressure.<sup>94</sup> Although it was also expected that increasing temperature would result in smaller d-spacing due to the increased fluidity of the chains, this was observed for CL2 but not for CON2. While data for only one temperature was obtained for CL3, it is seen that the d-spacing at this pH is significantly lower than it is at pH 5.1, however, without a control sample it is unclear if this is due to changes in the charge on cardiolipin's head group or other factors related to DOPE and DOPG.



**Fig. 21.** The effect of pressure on the lattice parameter  $a$  for sample CL1 with linear fits used to obtain  $\Delta d/\Delta p$

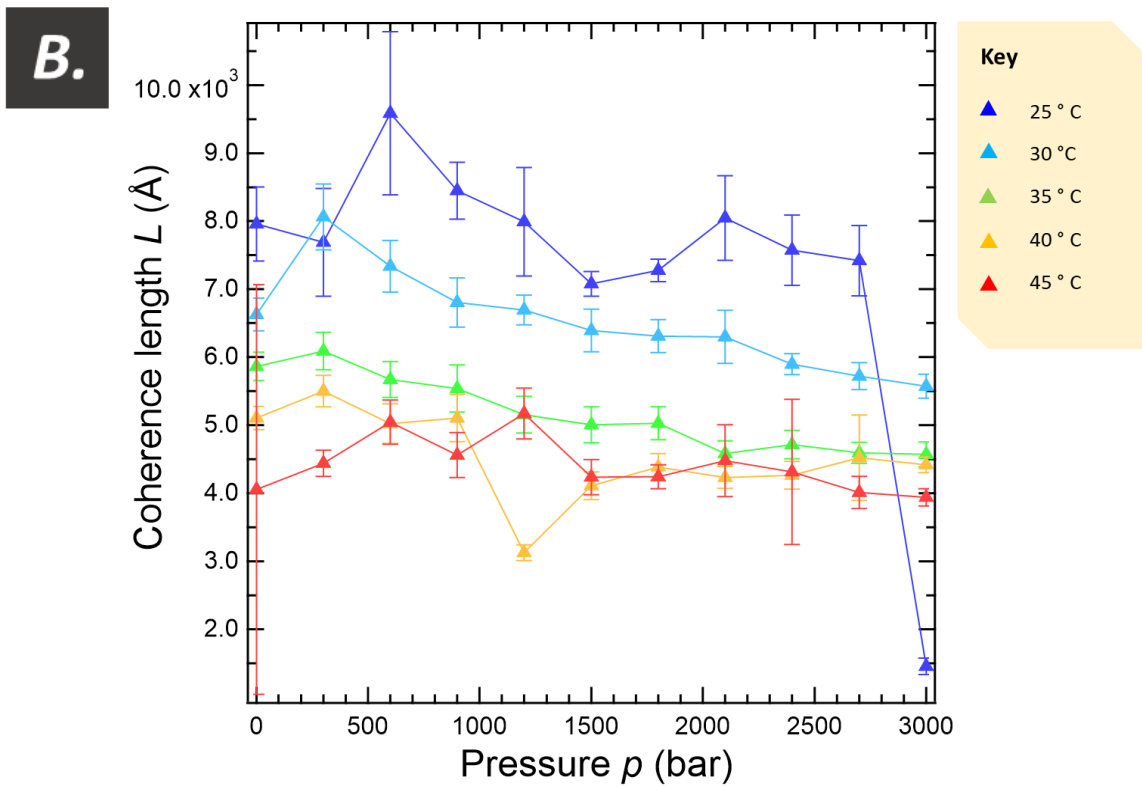
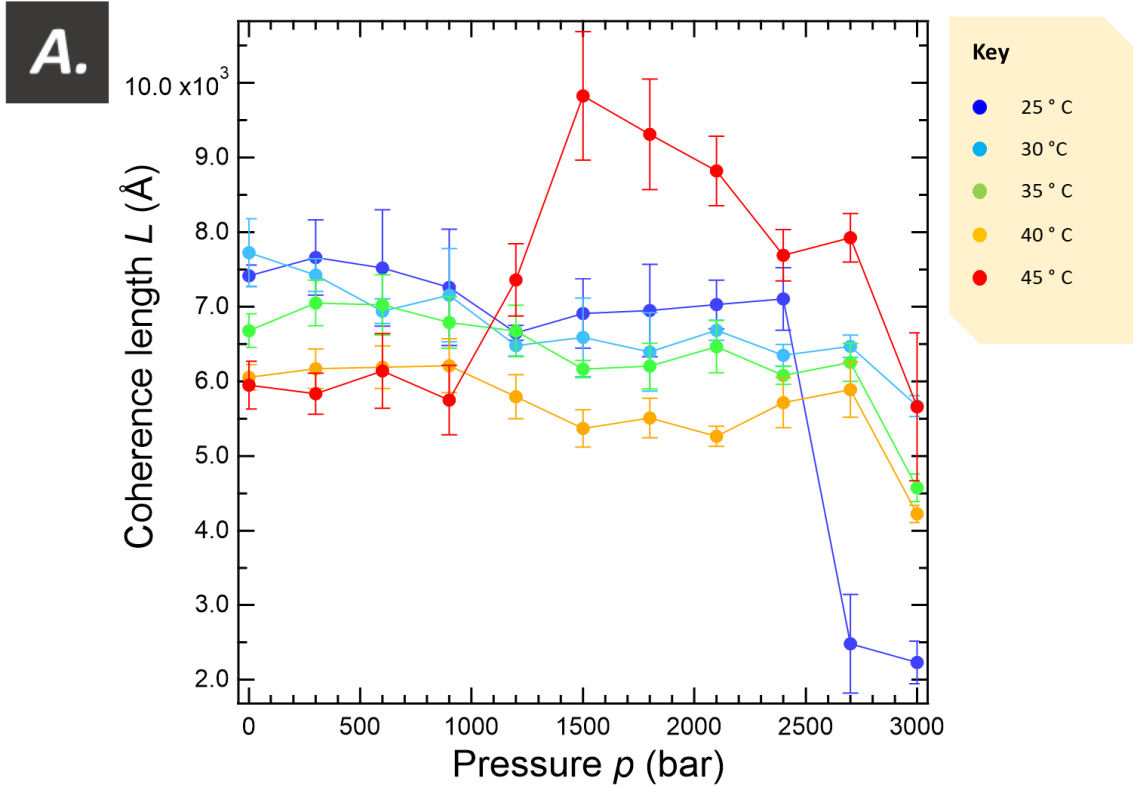
The changes in lattice parameter  $a$  for sample CL1 are shown in **Fig. 21**. As previously mentioned,<sup>72</sup> in hexagonal systems an increase in pressure causes an increase in cylinder diameter, and this was observed here. At all temperatures studied, the lattice parameter  $a$

increased with pressure, and increasing temperature resulted in a decrease in  $a$ , likely due to the increased fluidity of the tail groups.  $\Delta d/\Delta p$  decreased with temperature and was greater than  $\Delta d/\Delta p$  for CON2, CL2 and CL3, these being in the lamellar phase while CL1 was in the  $H_{II}$  phase, indicating that this system was more sensitive to the effects of pressure.

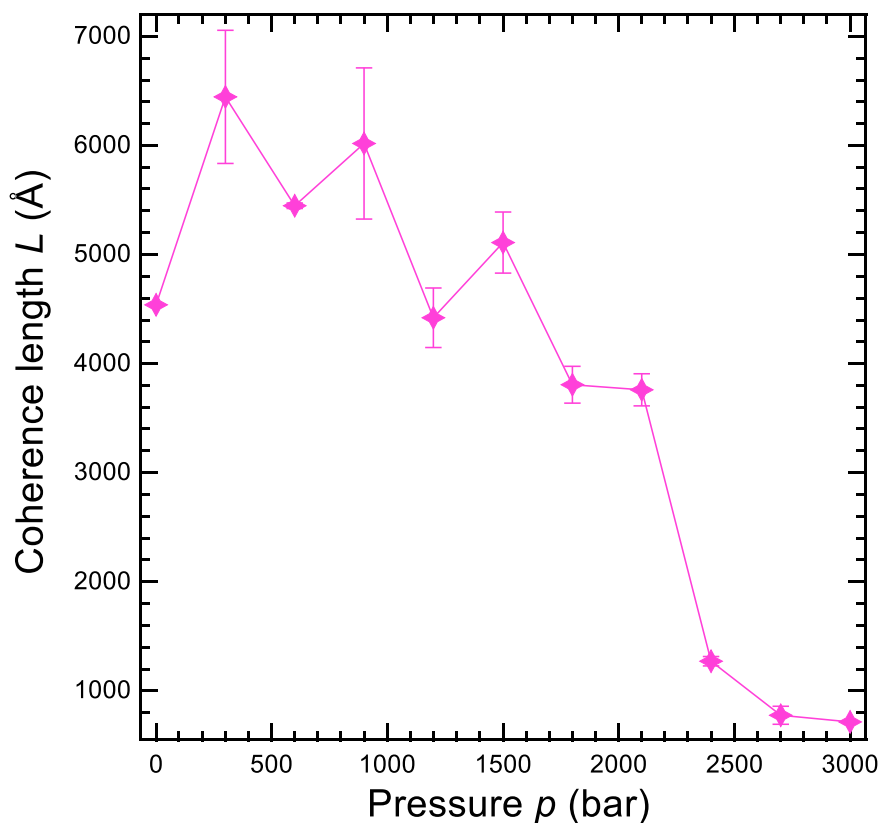
### 3.2.3 Coherence length of lipid systems

The changes in coherence length  $L$  were also obtained from the samples studied. For both CON2 and CL2, the coherence length of the samples roughly increases as temperature decreases (**Fig. 22**), likely due to higher temperatures resulting in a higher degree of chain disorder. A notable exception to this is CON2 at  $T = 45^\circ\text{C}$  (**Fig. 22. A**), it is unclear why the trend is so different at this temperature, and repeat measurements are needed. For both samples, the coherence length for the sample when in the  $L_\beta$  phase is significantly lower than when they are in the  $L_\alpha$  phase. For CL2 (**Fig. 22. B**), the coherence lengths decrease at all temperatures at  $p = 3000$  bar even when the  $L_\beta$  phase is not observed. A noticeable difference between CON2 and CL2 is that increasing the temperature of the system with cardiolipin present appeared to cause a greater decrease in coherence length than without the presence of cardiolipin, and this may be due to cardiolipin disrupting the packing of the membrane, with the large tail area reducing the efficiency of the packing and decreasing the long-range order of the mesophase.

Although there is no control sample data available to assess the impact of cardiolipin on the coherence length of the sample at pH 12.1 (**Fig. 23**), it is noticeable that at this pH the coherence length is lower on average than the same system at pH 5.1, indicating that pH did have some effect on the ordering of the lipids, although a comparison with a DOPE/DOPG



**Fig. 22.** The effect of pressure and temperature on the coherence length  $L$  of CON2 (**A**) and CL2 (**B**)

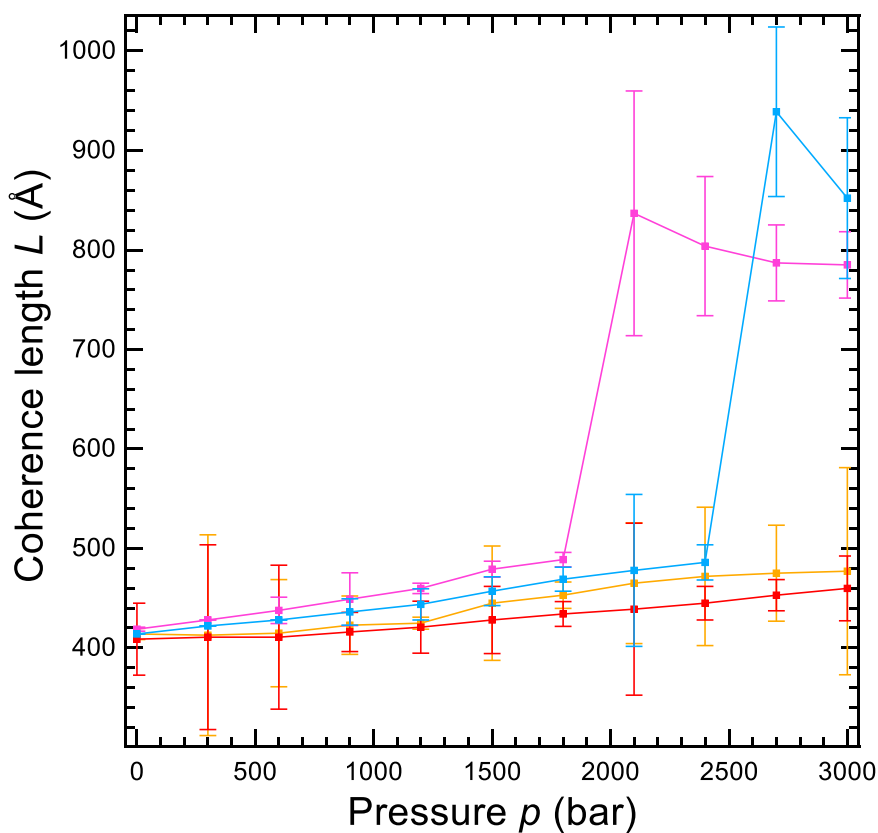


**Fig. 23.** Effect of pressure on the coherence length  $L$  of CL3 at 20°C

system at pH 12.1 would be needed to establish if this effect is due to the differing charge states of cardiolipin or another factor.

For CL1 (**Fig. 24**), the coherence length was significantly lower than for the samples that formed lamellar phases, and also increased gradually with pressure rather than decreasing, with pressure reducing the disorder of the inverse hexagonal phase. After transition to the unknown phase (above  $p = 1800$  bar at  $T = 20^\circ\text{C}$  and above  $p = 2400$  bar at  $T = 30^\circ\text{C}$ ), the disorder decreases significantly compared to when the inverse hexagonal phase is present.





**Fig. 24.** Effect of temperature and pressure on the coherence length  $L$  of sample CL1

### 3.3 Conclusions

In summary, it was found that at pH 5.1, the presence of cardiolipin had subtle but noticeable effects on the behaviour of the system, slightly lowering the pressure required to induce the  $L_\alpha \rightarrow L_\beta$  phase transition at  $T = 20^\circ\text{C}$ , increasing the d-spacing of the lamellar phases formed and increasing the impact of temperature changes on the coherence length of the system. It was also found that pH had a large impact on the behaviour of the DOPE/DOPG/CL system, with an inverse hexagonal phase forming at pH 1.3 and lamellar phases forming at pH 5.1 and above. The d-spacing and coherence length for CL3 were lower than for the same

system at pH 5.1 at the same temperature, also hinting at a potential effect of very high pH on the organisation of the lamellar phase of the system.

As previously discussed, cardiolipin has been shown to have a significant effect on the behaviour of lipid systems<sup>47</sup> in vesicles<sup>72</sup> and lipid bilayers,<sup>61, 62</sup> however no studies examining impact on the bulk phase behaviour of model membrane systems could be found. The finding that the presence of cardiolipin has an effect on the behaviour of the system, albeit a small one, as well as the finding that pH had a significant impact on the behaviour of the system, gives an incentive for further investigation into the role cardiolipin and pH play in shaping the phase behaviour of this lipid system.

Biomembrane models comprising of three or more components can serve as a more accurate model for studying the phase behaviour of lipid systems,<sup>121</sup> and so additional further work following on from this investigation would be the incorporation of additional lipids in order to more accurately model the bacterial membrane. *E. coli* specifically has been found to contain additional lipids beyond PG, PE and CL,<sup>55</sup> and contains a range of different lipid chain lengths.<sup>122</sup> *E. coli* polar lipid extract and *E. coli* cardiolipin extract are also available from Avanti Polar Lipids,<sup>117</sup> both of which contain a range of lipids with differing chain lengths and could potentially be used to provide a more accurate model of the behaviour of the *E. coli* membrane.

The use of buffers that mimic biological conditions such as Phosphate-buffered saline may also provide a better model for the behaviour of bacterial membranes in nature, with other buffers previously used with similar cardiolipin-containing systems including sodium citrate and tris-HCL, and<sup>69</sup> HEPES and EDTA<sup>123</sup>.

## Chapter 4. Stability of cardiolipin-containing liposomes: Effect of pH

---

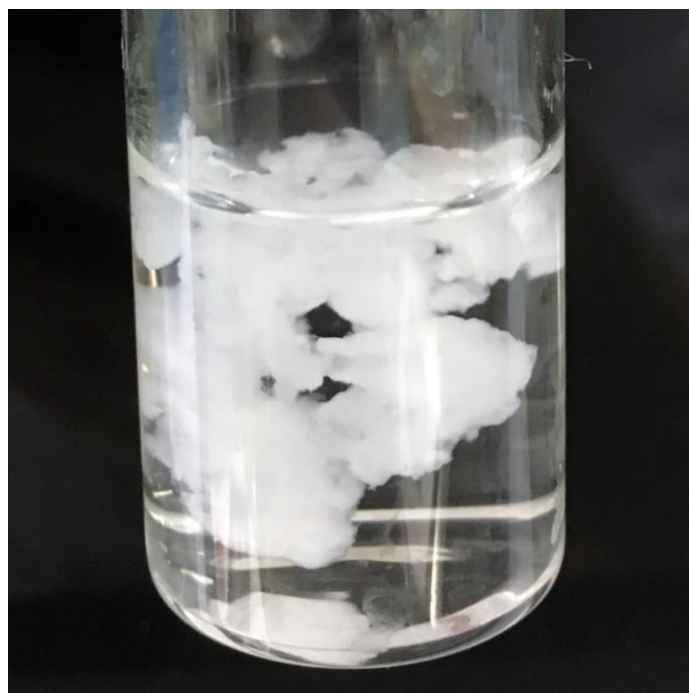
### 4.1 Abstract

*To further investigate the effects of cardiolipin on the behaviour of a model bacterial membrane, liposomes were produced using DOPE/DOPG/CL 70:20:10 and DOPE/DOPG 78:22 as another model for the bacterial membrane. In particular, the effects of pH were investigated. The liposomes were produced using the extrusion method at pH 5.1 and 12.1, and dynamic light scattering (DLS) and zeta potential measurements were used to characterise the liposome dispersions over a period of 44 days to assess their stability. At both pH 5.1 and 12.1, no significant change in either the diameter  $D$  or the zeta potential  $\zeta$  was observed for the DOPE/DOPG or DOPE/DOPG/CL liposomes over 44 days. Whilst the average  $\zeta$  potential of the DOPE/DOPG and DOPE/DOPE/CL liposomes were similar at pH 12.1, at pH 5.1 these values for the DOPE/DOPG liposomes were lower than those for the DOPE/DOPG/CL liposomes, with pH having little effect on the  $\zeta$  of DOPE/DOPG/CL liposomes, pointing to the effect of cardiolipin on the structural response to pH of the mixed liposomes.*

## 4.2 Results & Discussion

As well as mesophases, liposomes can also be used as model for the bacterial membrane as they mimic the basic structure of a bilayer encapsulating a liquid core, and liposomes with a specific composition mimicking a particular membrane can be produced with relative ease.<sup>124</sup> Following on from the HP-SAXS investigation, the effect of cardiolipin and pH on the size, stability and zeta potentials of liposomes mimicking bacterial membranes was studied using dynamic light scattering (DLS). The hydrodynamic diameter, reported through DLS, gives the diameter of a sphere that would produce the scattering pattern obtained during a measurement. As liposomes are spherical, the reported hydrodynamic diameter is likely to closely match the real diameter of the liposomes. Zeta  $\zeta$  potential provides a measure of the stability of liposomes, as if the  $\zeta$  potential is low, there will be little repulsion between liposomes leading to aggregation due to van der Waals forces.

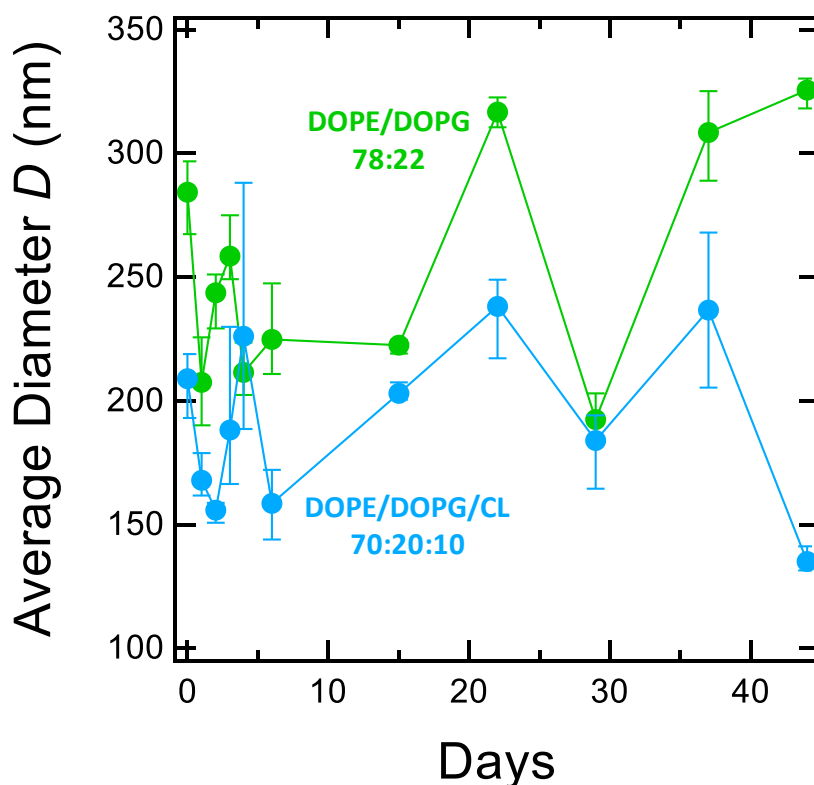
The samples prepared used the same compositions as the mesophase samples in Chapter 3 (DOPE/DOPG/CL 70:20:10 and DOPE/DOPG 78:22) with DOPE/DOPG samples at pH 12.1 and 5.1 as controls. However, it was found during the sample preparation that DOPE/DOPG 78:22 and DOPE/DOPG/CL 70:20:10 would not form liposomes at pH 1.3, even with additional sonication and vortexing. Instead, both systems formed a mesophase pictured in **Fig. 25**, which based on the HP-SAXS data collected likely comprised an inverse hexagonal  $H_{II}$  phase. Liposomes were successfully formed from DOPE/DOPG 78:22 and DOPE/DOPG/CL 70:20:10 mixtures at pH 5.1 and 12.1, confirmed using DLS. The diameter of the liposomes ( $D$ ) and their zeta potentials ( $\zeta$ ) were then measured over a period of 44 days.



**Fig. 25.** The mesophase formed by DOPE/DOPG 78:22 and DOPE/DOPG/CL 70:20:10 at pH 1.3.

#### **4.2.1 Effects of pH and cardiolipin on liposome hydrodynamic diameter**

In **Fig. 26**, the average diameters  $D$  of the DOPE/DOPG and DOPE/DOPG/CL liposomes at pH 5.1 are compared. Despite having been extruded using 100 nm-pore membranes, on the day of first measurement the average diameter of the liposomes was found to be  $D = 283.4$  nm for DOPE/DOPG and 209.00 nm for DOPE/DOPG/CL, which may be due to aggregation of liposomes already occurring as observed via PLM in Chapter 5. While there were changes from week-to-week in the average diameter, there was not a large overall change in the diameter despite some apparent fluctuations in either sample. Also present in almost all DOPE/DOPG/CL and DOPE/DOPG samples at this pH were larger peaks indicating the presence of particles with diameter  $D$  over 1000 nm and up to approximately 5400 nm, likely

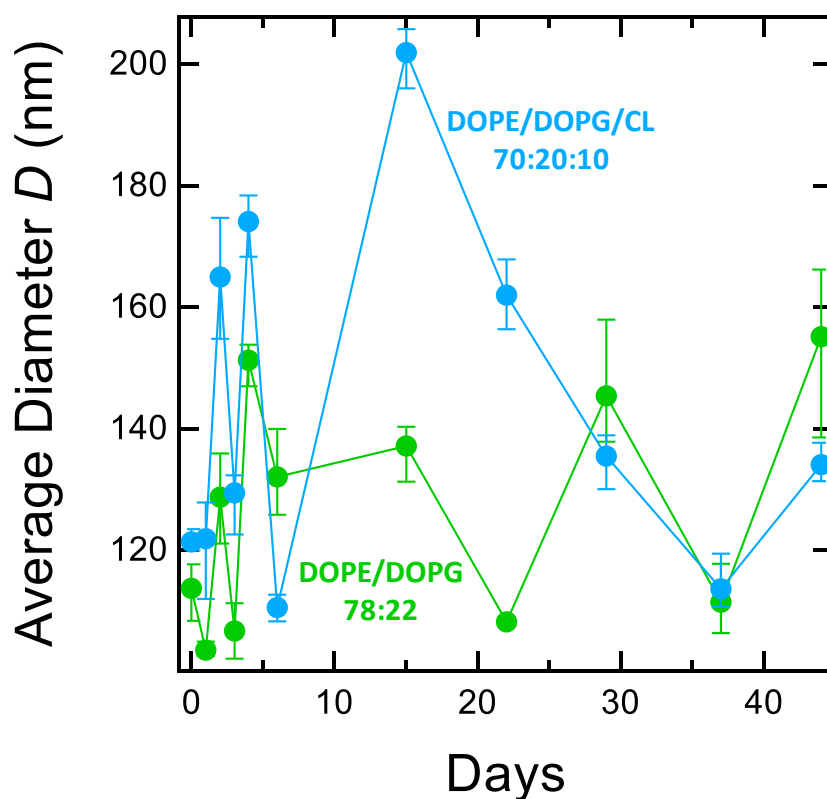


**Fig. 26.** Average diameter of DOPE/DOPG (green) and DOPE/DOPG/CL (blue) liposomes at pH 5.1.

caused by a small number of large liposome aggregates. However, there was some difference in the average  $D$  of the DOPE/DOPG and DOPE/DOPG/CL across the 47 days, at  $D = 254.2$  nm and 191.2 nm respectively.

**Fig. 27.** shows the comparison between the average  $D$  of DOPE/DOPG and DOPE/DOPG/CL liposomes at pH 12.1. As was the case for these systems at pH 5.1, there was little overall change in the average  $D$  of the liposomes over time, and large particles of a similar size to those in the samples at pH 5.1 were observed, again likely due to larger aggregates. The average  $D$  of the DOPE/DOPE/CL liposomes is particularly inconsistent at this pH, with relatively large average diameter of 201.9 nm observed at 15 days before returning to diameters comparable to the initial average  $D$  of 121.3 nm afterwards. It is possible that this large diameter at 15 days is simply due to the particular sample taken on this day. Conversely to the liposomes at pH 5.1 (**Fig. 26**), for these samples at pH 12.1 the average  $D$  of

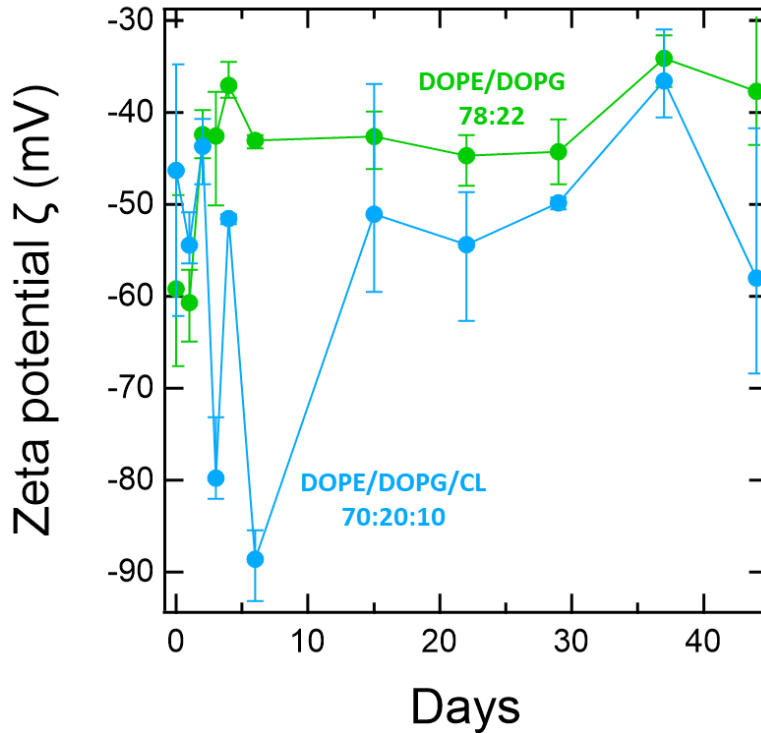
the DOPE/DOPG/CL liposomes across all 44 days was larger than the DOPE/DOPG sample, at  $D = 142.7$  and  $126.7$  nm respectively.



**Fig. 27.** Average diameter of DOPE/DOPG (green) and DOPE/DOPG/CL (blue) liposomes at pH 12.1

#### 4.2.2 Effects of pH and cardiolipin on liposome zeta potential $\zeta$

In **Fig. 28**, the zeta potentials of DOPE/DOPG/CL and DOPE/DOPG at pH 5.1 are compared. For both samples, the zeta potential  $\zeta$  was found to be below  $-30$  mV throughout the 44 days of measurement, considered to be highly charged particles and indicative of liposome stability.<sup>125</sup> The average  $\zeta$  of the DOPE/DOPG liposomes became less negative between 0 and 6 days from an initial value of  $\zeta = -59.2$  mV to a plateau of around  $\zeta = -42$  to  $-43$  mV until another small increase at 37 days. Unlike the DOPE/DOPG/CL liposomes, there was an initial

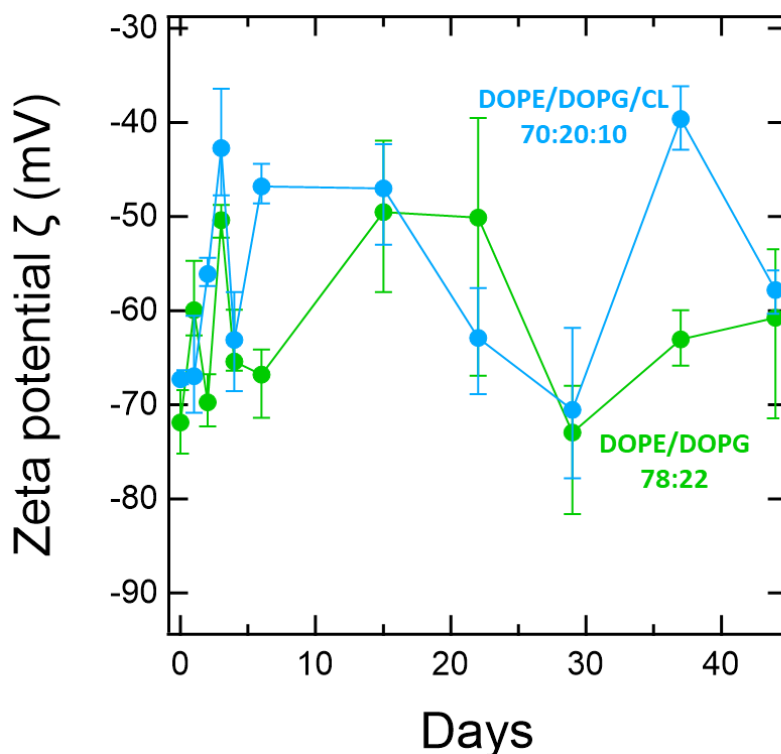


**Fig. 28.** Average zeta potential  $\zeta$  of DOPE/DOPG (green) and DOPE/DOPG/CL (blue) liposomes at pH 5.1.

decrease in  $\zeta$  between 0 and 6 days, with notably large decreases at 3 and 6 days. It is possible that these large decreases were due to the particular samples taken on those days rather than representing the behaviour of the liposomes on the whole. The DOPE/DOPG/CL liposomes then behaved similarly to the DOPE/DOPG liposomes from 15 days onwards but at more negative  $\zeta$  values of approximately -50 mV until 37 days and a large decrease at 44 days, with the  $\zeta$  of the cardiolipin-containing liposomes remaining consistently lower than the control liposomes across the time period studied likely due to the single negative charge cardiolipin carries at pH 5.1.

**Fig. 29.** shows the average  $\zeta$  of DOPE/DOPG and DOPE/DOPG/CL liposomes at pH 12.1, where cardiolipin carries two negative charges. As observed at pH 5.1, neither the DOPE/DOPG or DOPE/DOPG/CL liposomes underwent a significant change in  $\zeta$  over the course of the 44 days studied, with the charge remaining below -30 mV for both samples indicating



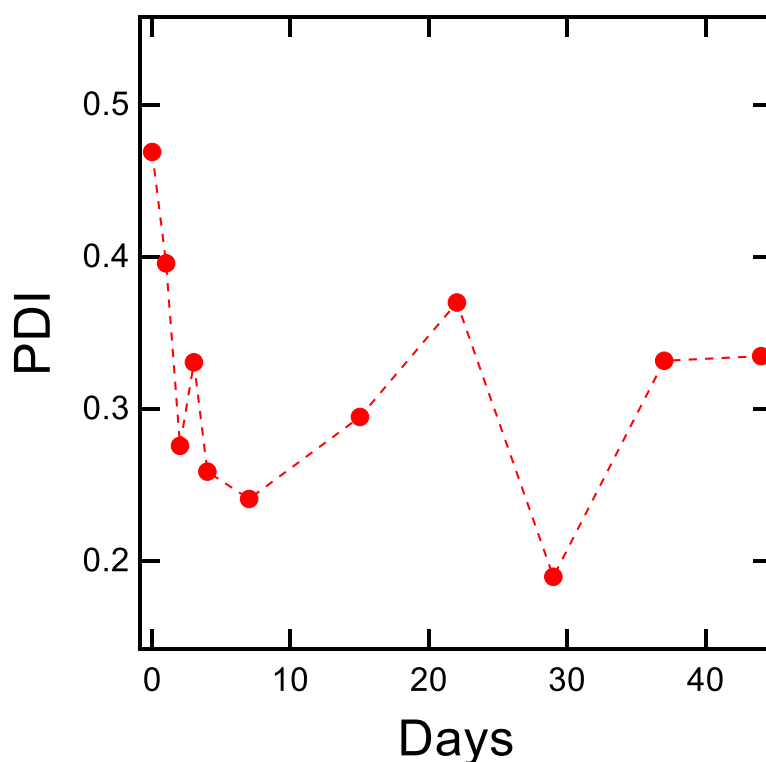


**Fig. 29.** Average zeta potential  $\zeta$  of DOPE/DOPG (green) and DOPE/DOPG/CL (blue) liposomes at pH 12.1.

that they remained stable throughout the time period studied. In contrast to the measurements taken at pH 5.1, there was no difference between the  $\zeta$  values of the DOPE/DOPE or of DOPE/DOPG/CL liposomes. Another notable difference is that the  $\zeta$  value appeared less stable over time for these samples than for the samples at pH 5.1. With cardiolipin carrying two negative charges at pH 12.1, it is somewhat surprising that a larger difference was not observed between the  $\zeta$  value of the DOPE/DOPG and DOPE/DOPG/CL liposomes. At pH 5.1, the average  $\zeta$  values across all 44 days were  $\zeta = -44.4$  mV and  $\zeta = -55.9$  mV for DOPE/DOPG and DOPE/DOPG/CL, respectively, whereas they were  $\zeta = -61.9$  mV and  $\zeta = -56.4$  mV for DOPE/DOPG and DOPE/DOPG/CL at pH 12.1. Thus, it is seen that the change in pH from 5.1 to 12.1 had little effect on the charge and stability of the DOPE/DOPG/CL liposomes, while actually having a larger effect on the DOPE/DOPG liposomes, which were more highly charged and stable at pH 12.1.

### 4.2.3 Effects of pH and cardiolipin on polydispersity index (PDI) of liposomes

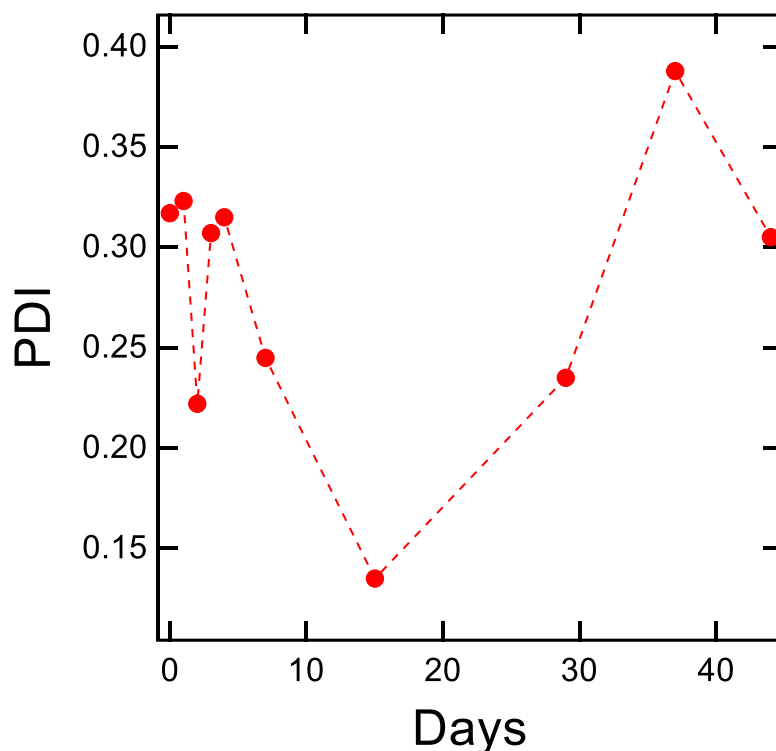
The polydispersity index (PDI) is a measure of the size distribution of particles in a solution, with a high PDI indicating a highly polydisperse solution with a range of different particles sizes present, while a low PDI indicates a monodisperse sample where all particles are the same size. PDI values below 0.05 are considered to be monodisperse, while values of 0.7 and above indicate a broad range of different particle sizes, i.e. a very polydisperse sample, however PDI values of 0.3 and below are considered acceptable for liposomes used in drug-delivery applications.<sup>126</sup>



**Fig. 30.** Polydispersity index (PDI) of DOPE/DOPG liposomes at pH 5.1.

**Fig. 30.** Shows how the polydispersity index (PDI) of DOPE/DOPG liposomes at pH 5.1 changed over time. There was a higher initial PDI of 0.469 before dropping below 0.4 after 24 hours and remaining below 0.4 for the remaining time studied. There was an increase in PDI between 7 and 22 days with a peak at 0.370 before another drop. However, this apparent

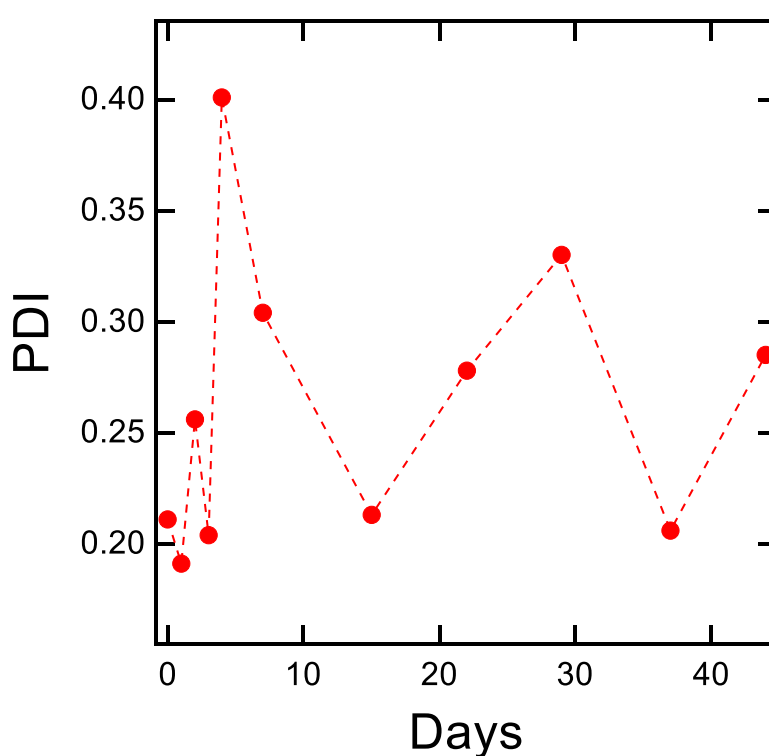
instability in PDI was likely due to different samples taken on different days. There were large particles likely arising from large aggregated present in small numbers. As no large or persistent change in PDI was observed across the 44 days, it is likely that any aggregation or changes in the composition of the sample were minimal.



**Fig. 31.** Polydispersity index (PDI) of DOPE/DOPG/CL liposomes at pH 5.1.

**Fig. 31.** Shows the PDI of DOPE/DOPG/CL at pH 5.1 over time. As with DOPE/DOPG at this pH, the PDI saw a decrease from 0.317 to 0.135 at 15 days, before increasing to 0.388 at 37 days and then returning to a PDI similar to the initial value of 0.305. This sample also showed instability in PDI, again likely resulting from difference in individual samples and aggregation. One notable difference between DOPE/DOPG/CL at pH 5.1 and DOPE/DOPG is that the average PDI across 44 days for DOPE/DOPG/CL was 0.279 compared to 0.347 for DOPE/DOPG. Although repetition would be needed to confirm the difference observed and whether the presence of cardiolipin has an effect on PDI.

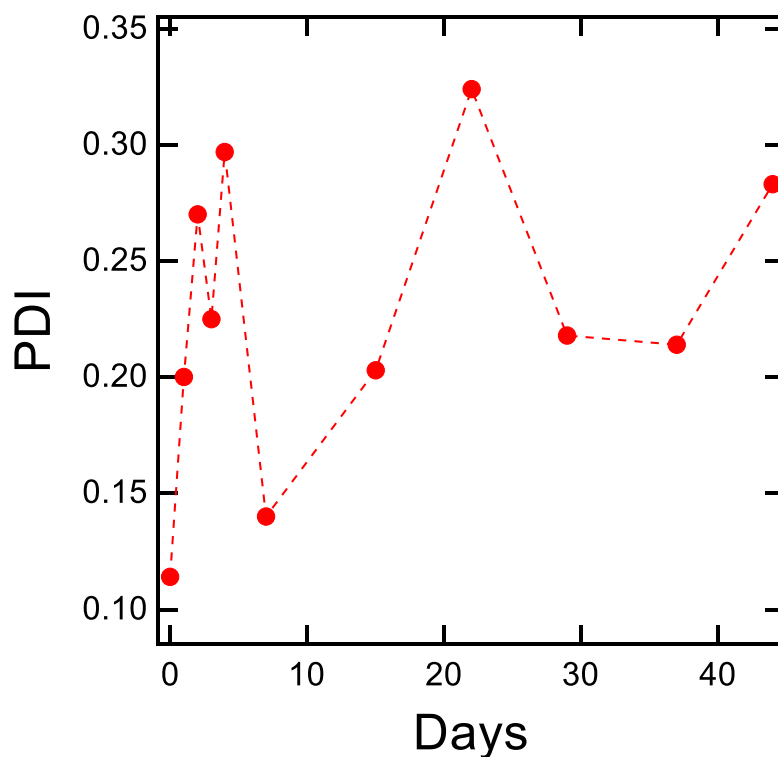
In **Fig. 32**, the PDI of DOPE/DOPG liposomes at pH 12.1. In contrast to the same system at pH 5.1, there was a large increase in PDI from a lower initial value of 0.211 to 0.401 at 4 days. The PDI was similarly unstable across the 44 days, returning to values comparable to the initial value of 0.213 and 0.206 at 15 and 37 days. As with the previous samples, this instability is likely due to sample differences and the presence of aggregated. The average PDI value across the 44 days was 0.288, lower than the average value of 0.347 for DOPE/DOPG at pH 5.1 and closer to the average PDI for DOPE/DOPG/CL at pH 5.1 of 0.279.



**Fig. 32.** Polydispersity index (PDI) of DOPE/DOPG liposomes at pH 12.1.

In **Fig. 33**. The PDI of DOPE/DOPG/CL at pH 12.1 are shown, and as with the previous samples the PDI appeared to be unstable, assumed to be for the same reasons as the other samples. However, for this sample the initial PDI was comparatively low at 0.114, before

increasing to values comparable to those obtained for the other samples. The average PDI across the 44 days was 0.249, the lowest of the four samples.



**Fig. 33.** Polydispersity index (PDI) of DOPE/DOPG/CL liposomes at pH 12.1.

### 4.3 Conclusions

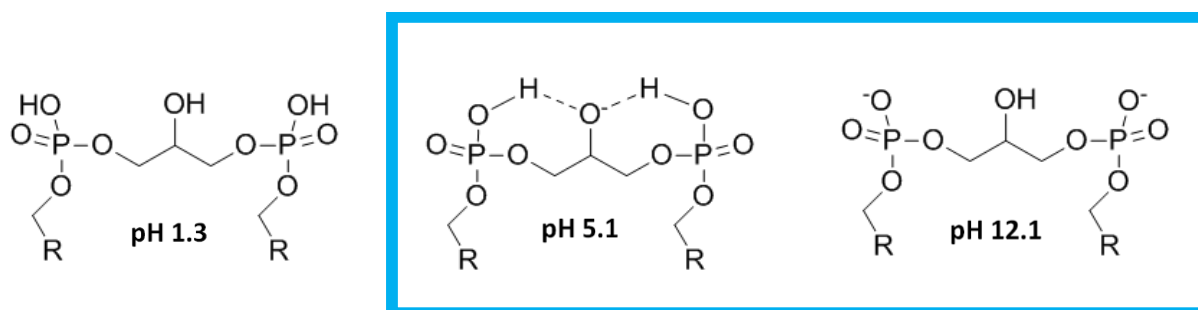
In summary, the average hydrodynamic  $D$  of both DOPE/DOPG and DOPE/DOPG/CL liposomes were smaller at pH 12.1 than at pH 5.1, as summarised in **Table 4**. No clear trends in the hydrodynamic diameter over time were observed; however, differences in the average  $D$  of the samples were observed. As the charge of cardiolipin varies with pH (**figure 34**)<sup>127</sup>, this may have played a role in the average  $D$  values of the different samples. Cardiolipin is known to promote and stabilise negative curvature by segregating into the inner leaflet of

Lipid Composition	pH	Average $D$ / nm	Average $\zeta$ / mV	Average PDI
DOPE/DOPG	5.1	254.2	-44.1	0.347
	12.1	126.7	-61.9	0.288
DOPE/DOPG/CL	5.1	191.2	-55.9	0.279
	12.1	142.7	-56.4	0.249

**Table 4.** summary of DLS results

bilayers,<sup>128</sup> and it is possible that cardiolipin played a role in stabilising smaller liposomes with a larger curvature at pH 5.1 where it carries a single negative charge. Compared to the DOPE/DOPG liposomes, the DOPE/DOPG/CL liposomes underwent a smaller reduction in the average  $D$  between pH 5.1 and 12.1. This smaller negative curvature may again be explained by cardiolipin's pH-responsiveness, as at pH 12.1 it carries two negative charges and headgroup repulsion is at a maximum, potentially decreasing cardiolipin's propensity towards negative curvature.

The  $\zeta$  measurements showed that, while both systems at both pH values studied produced moderately charged and therefore stable liposomes with  $\zeta$  values averaging below -30 mV, pH had a different effect on the DOPE/DOPG and DOPE/DOPG/CL liposomes. At pH



**Fig. 34.** Different behaviours of cardiolipin at the two pH values examined. Adapted from reference 123

5.1, DOPE has no charge, whereas DOPG<sup>129</sup> and cardiolipin both carry a single negative charge. At pH 5.1, the DOPE/DOPG/CL liposomes had a larger charge than the DOPE/DOPG liposomes, owing to the additional negative charge from the cardiolipin present.

At pH 12.1 where cardiolipin has an even greater negative charge of -2, unexpectedly it was the DOPE/DOPG liposomes which had a lower average  $\zeta$  value. A drop in  $\zeta$  at lower pH was expected for both lipid compositions as pH greatly influences  $\zeta$ . However, pH appeared to have little effect at all on the  $\zeta$  values of the DOPE/DOPG/CL liposomes, with  $\zeta = -55.85$  mV at pH 5.1 and  $\zeta = -56.43$  mV at pH 12.1. The PDI values for the samples also showed little change over time with the exception of the DOPE/DOPG/CL liposomes at pH 12.1 where an increase from the initial PDI was observed. It would be expected that because these samples all had a large negative  $\zeta$  indicating stability, the PDI values obtained would also be low due to the low amount of aggregation that would be expected with this stability. The largest average PDI of 0.347 was obtained for DOPE/DOPG liposomes at pH 5.1, which also had the smallest average  $\zeta$ , in agreement with expectations that a smaller  $\zeta$  would lead to more aggregation. The average PDI was also lower for the DOPE/DOPG/CL liposomes at both pH values, potentially pointing to cardiolipin reducing the amount of aggregation due to the additional charge it confers, but additional DLS measurements would need to be carried out to confirm this.

## Chapter 5. Polarised light microscopy (PLM) images of bacterial membrane mimics

---

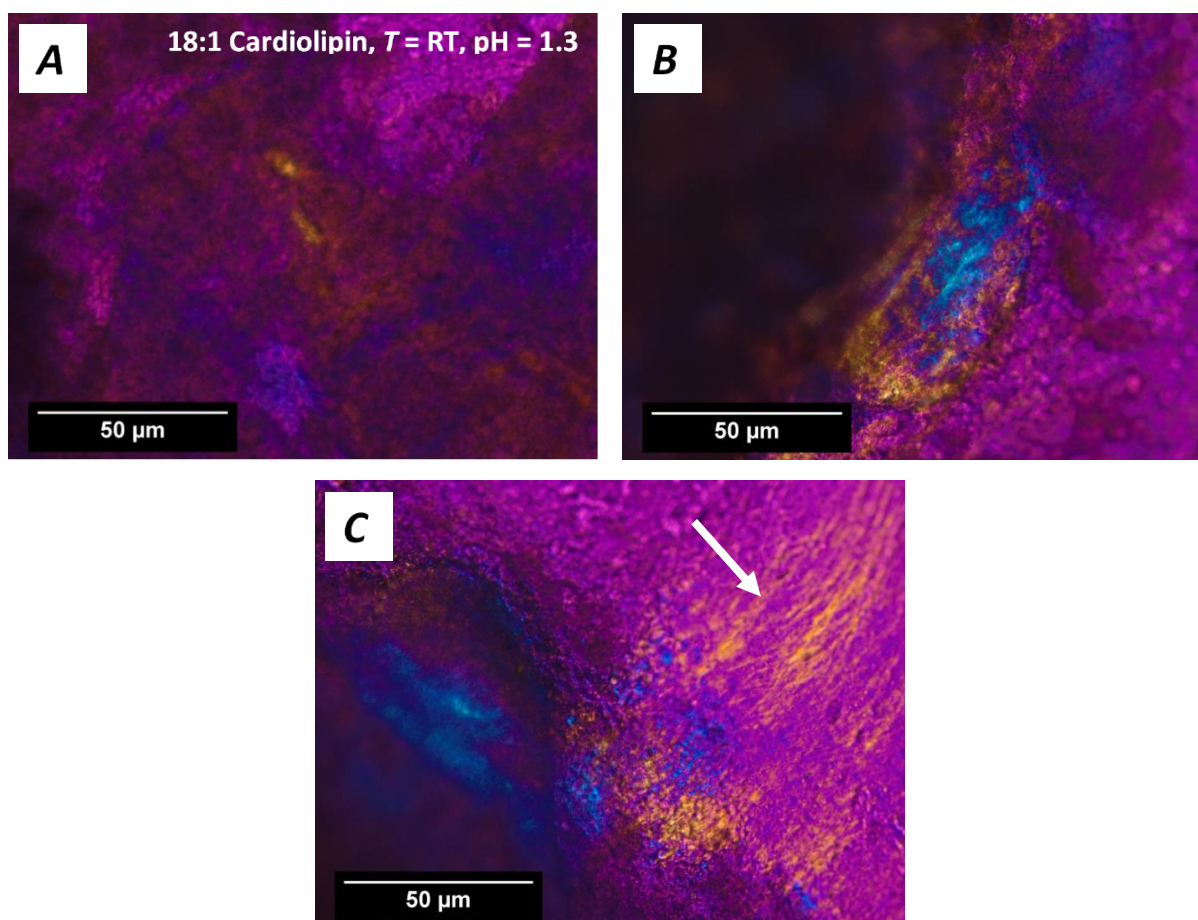
### 5.1 Abstract

*To complement the HP-SAXS data, polarised light microscopy (PLM) images of DOPE/DOPG 78:22 and DOPE/DOPG/CL 70:20:10 were obtained at pH 1.3, 5.1 and 12.1. Control PLM images were also obtained for pure DOPG and pure cardiolipin at pH 1.3, 5.1 and 12.1. It was found that the PLM images for both bacterial membrane mimic systems showed a clear difference in behaviour between pH 1.3, and pH 5.1 and 12.1. This is consistent with the HP-SAXS data showing a difference in phase behaviour at pH 1.3 for both DOPE/DOPG and DOPE/DOPG/CL. Liposomes and their aggregates were observed in the samples, also consistent with the HP-SAXS data from these samples. In addition, pure cardiolipin and pure DOPG samples were found to behave differently at pH 1.3 than at higher pH values, highlighting the important role of pH in determining the phase behaviour of these lipids and lipid systems.*



## 5.2 Results & discussion

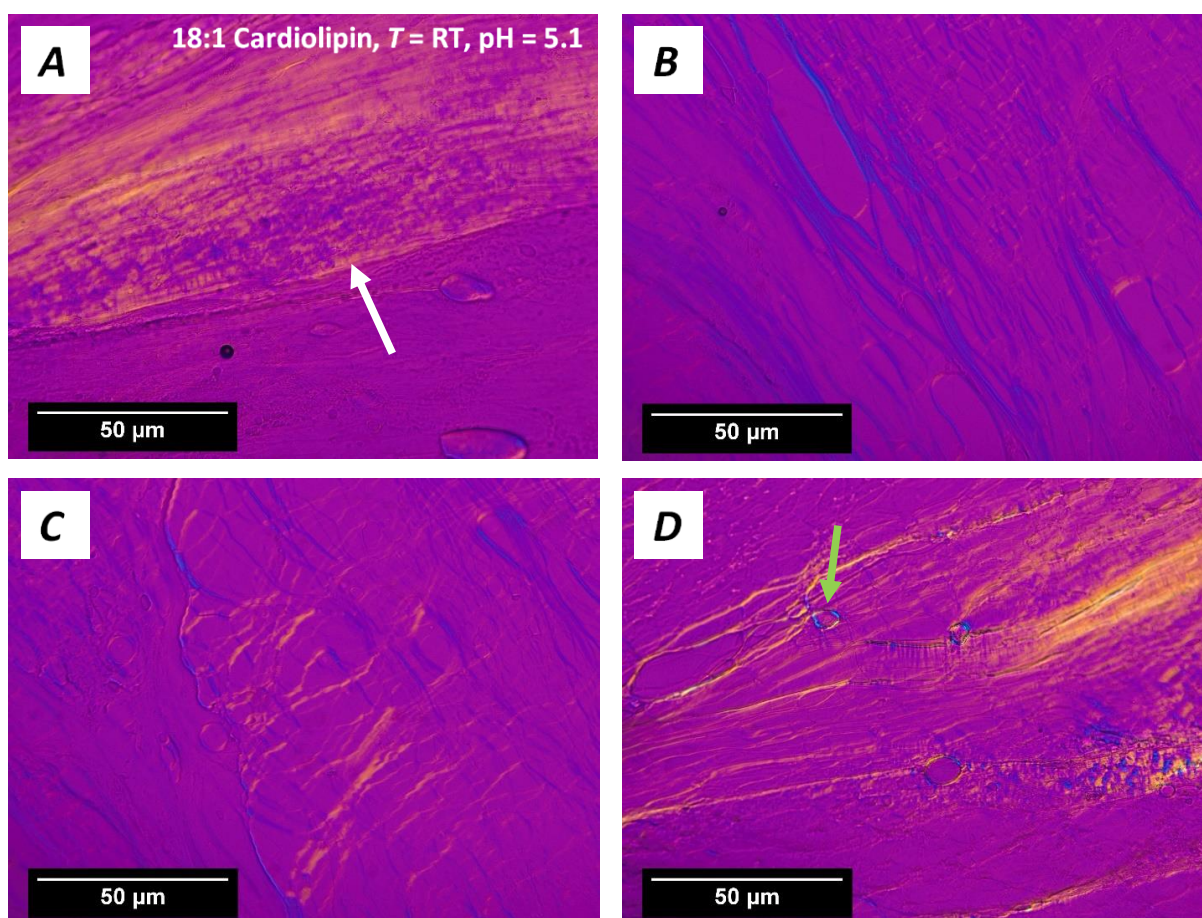
Polarised light microscopy (PLM) is an optical technique that can be used to identify mesophases, which exhibit different visible textures with polarised light.<sup>130</sup> Other structures such as liposomes in samples can also be visually identified. It is particularly useful in conjunction with SAXS for phase characterisation and thus chosen in this project, supporting the phase assignment from SAXS peaks. DOPE/DOPG 78:22 and DOPE/DOPG/CL 70:20:10 mesophases at pH 1.3, 5.1 and 12.1 were prepared following the same method as that of the HP-SAXS samples. In addition, pure DOPG and CL mesophases were examined using PLM for comparison.



**Fig. 35.** PLM images of pure cardiolipin at pH 1.3 taken with a 530 nm waveplate inserted, at 10x magnification. White arrow indicates striation.

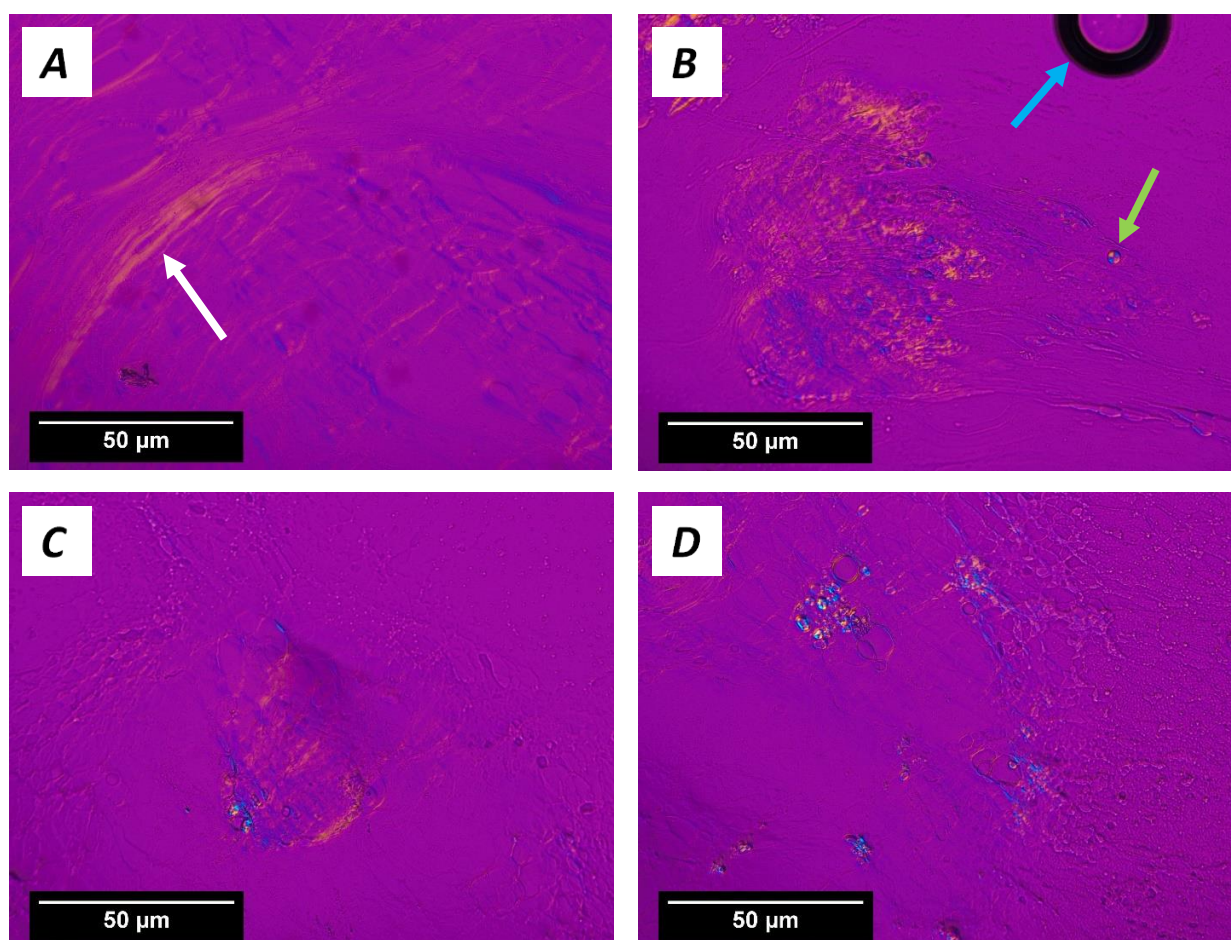
### 5.2.1 Individual lipids

PLM images of pure cardiolipin at pH 1.3, 5.1 and 12.1 were obtained in order to compare the behaviour of cardiolipin alone with DOPE/DOPG and with DOPE/DOPG/CL. **Fig. 35.** shows cardiolipin at pH 1.3, displaying a texture similar to that observed in DOPE/DOPG and DOPE/DOPG/CL at pH 1.3, suggesting that pure cardiolipin also forms the  $H_{II}$  phase at pH 1.3. Some striation was also observed (indicated by white arrow in **Fig. 34. C**), which is also observed in  $H_{II}$  phases.<sup>130</sup> Cardiolipin has a propensity towards forming the  $H_{II}$  phase due to its  $>1$  packing parameter, particularly at low pH where the repulsion between the two headgroups is minimised.

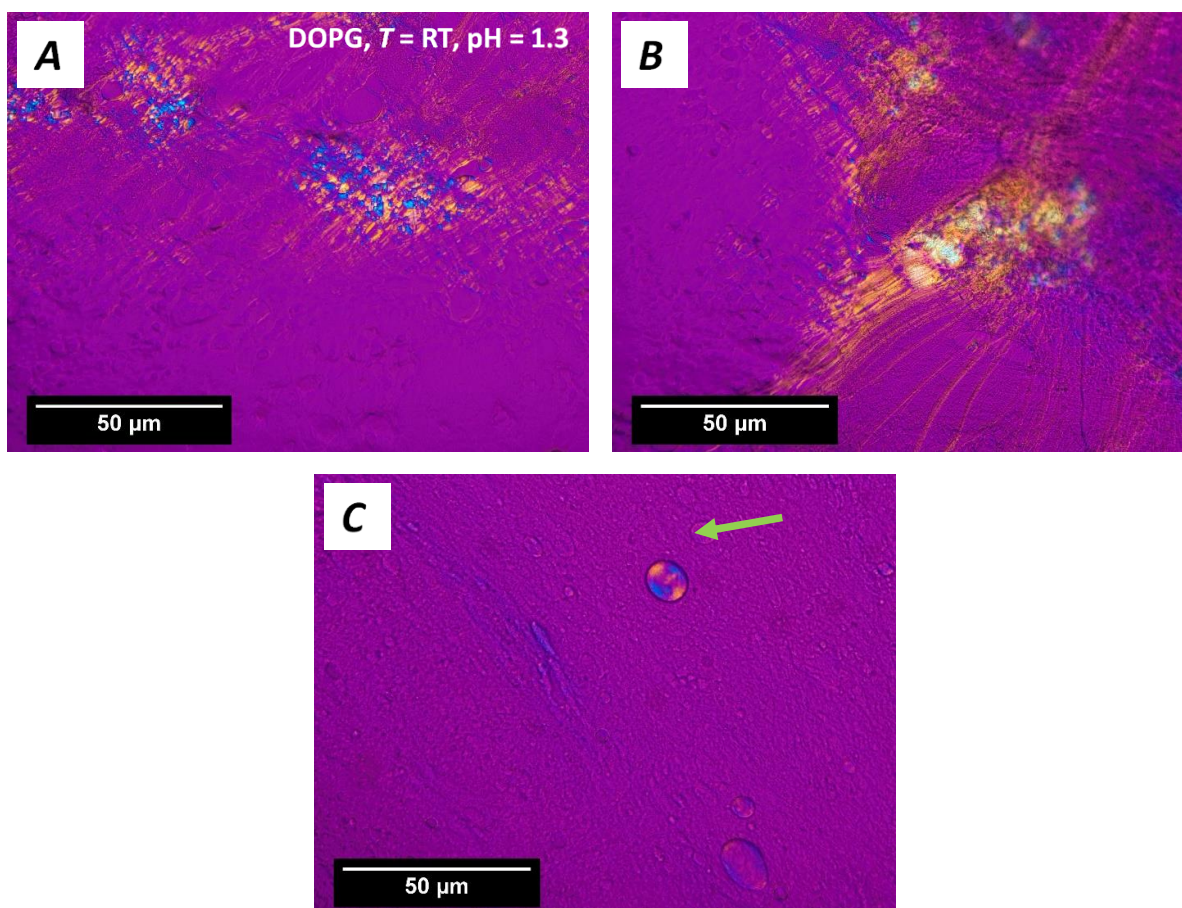


**Fig. 36.** PLM images of pure cardiolipin at pH 5.1 taken with a 530 nm waveplate inserted, at 10x magnification. White arrow indicates striation, green arrow indicates a liposome.

In **Fig. 36**, PLM images of pure cardiolipin at pH 5.1 are shown. For this sample, it is less clear what phase the cardiolipin has formed. Due to issues with the sample drying quickly on the slide, it is unclear if these images accurately represent the behaviour of pure cardiolipin in a hydrated mesophase as was the case for the HP-SAXS samples. Despite this, there are still some notable features of interest including striations as indicated in **Fig. 36. A** which could result from either a  $H_{II}$  or lamellar phase, and a small number of liposomes as indicated in **Fig. 36. D**.

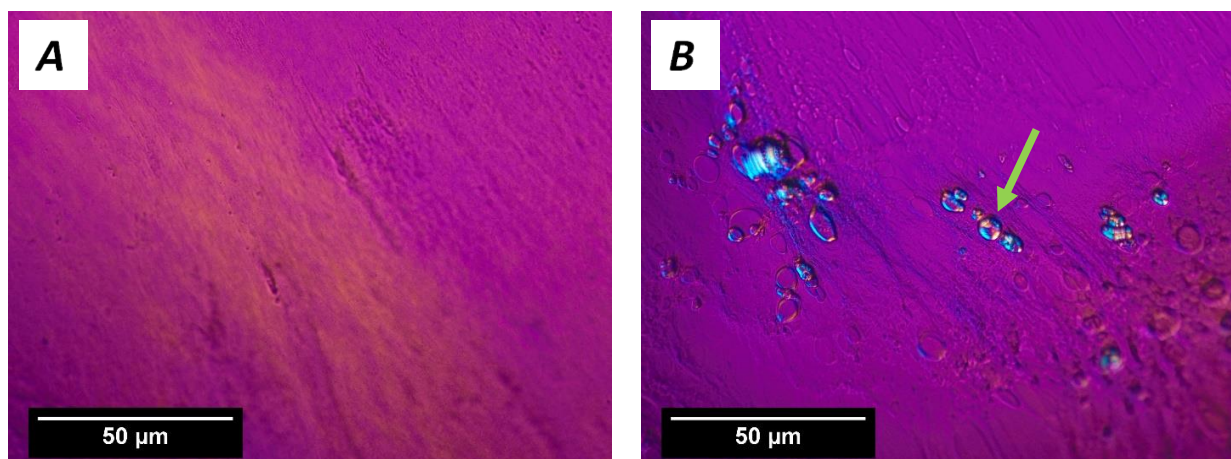


**Fig. 37.** PLM images of pure cardiolipin at pH 12.1 taken with a 530 nm waveplate inserted, at 10x magnification. The white arrow indicates striation, the green arrow indicates a liposome and the blue arrow indicates an air bubble.



**Fig. 38.** PLM images of pure DOPG at pH 1.3 taken at different locations (**A & C**) with a 530 nm waveplate inserted, at 10x magnification. The green arrow indicates a liposome.

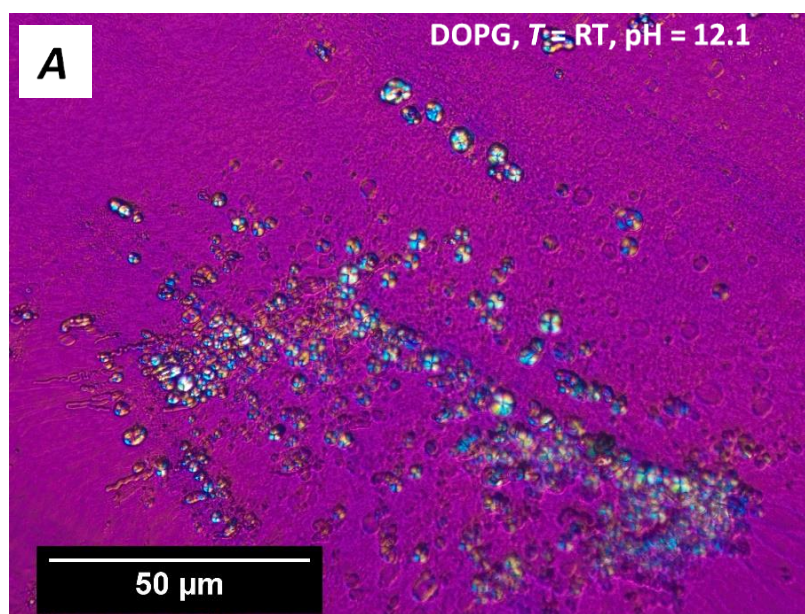
**Fig. 37.** Shows that the PLM images for pure cardiolipin at pH 12.1 were very similar to pure cardiolipin at pH 5.1, also containing a small number of small liposomes, patches of birefringent mesophase and striations as indicated by arrows in **Fig. 37. A & B**. It is notable that this sample and pure cardiolipin at pH 5.1 have a very different texture to pure cardiolipin at pH 1.3, indicating that the cardiolipin is likely at least partially in a different phase (the  $H_{II}$  phase) at pH 1.3. Also notable is the presence of liposomes at pH 5.1 and 12.1, but not at 1.3. PLM images were also taken for pure DOPG at pH 1.3 as shown in **Fig. 37**. As with pure cardiolipin at pH 5.1 and 12.1, this sample suffered from the issue of drying rapidly; however, comparisons can still be made with pure cardiolipin at pH 1.3. Liposomes were present in this sample (**Fig. 38. C**), as well as birefringent mesophases (**Fig. 38. A & B**),



**Fig. 39.** PLM images of pure DOPG at pH 5.1 taken with a 530 nm waveplate inserted, at 10x magnification. The green arrow indicates a liposome.

although it is unclear what phase(s) were present and HP-SAXS measurements would be required to identify this accurately.

The striations in **Fig. 39. A** indicate the presence of a lamellar phase, with liposomes also observed as shown in **Fig. 39. B**. This is similar to the results obtained for both DOPE/DOPG and DOPE/DOPG/CL at this pH, suggesting that similar HP-SAXS results may be obtained for pure DOPG at this pH. This would not be surprising given the fact that

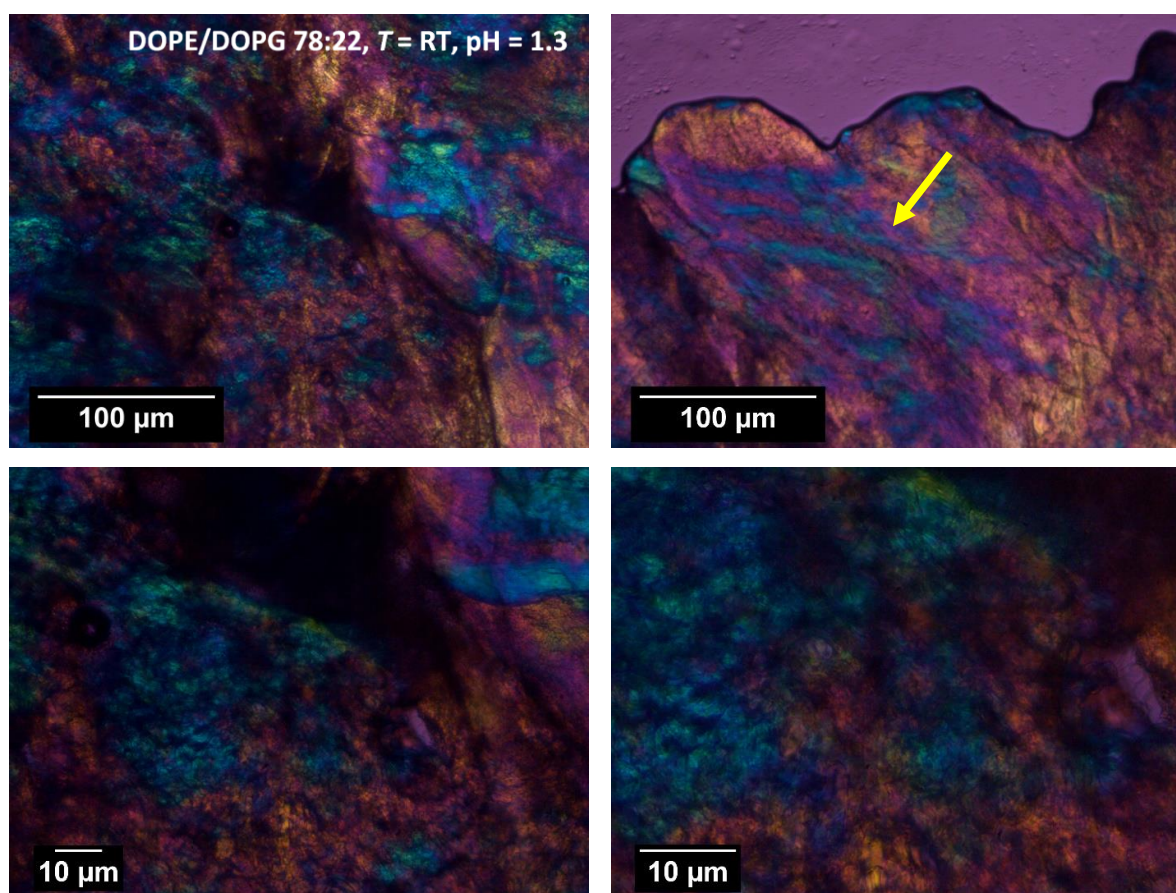


**Fig. 40.** PLM image of pure DOPG at pH 12.1 taken with a 530 nm waveplate inserted at 10x magnification.

DOPE/DOPG alone formed a lamellar phase with liposomes. Some liposome aggregation was also observed in this sample (**Fig. 39. B**).

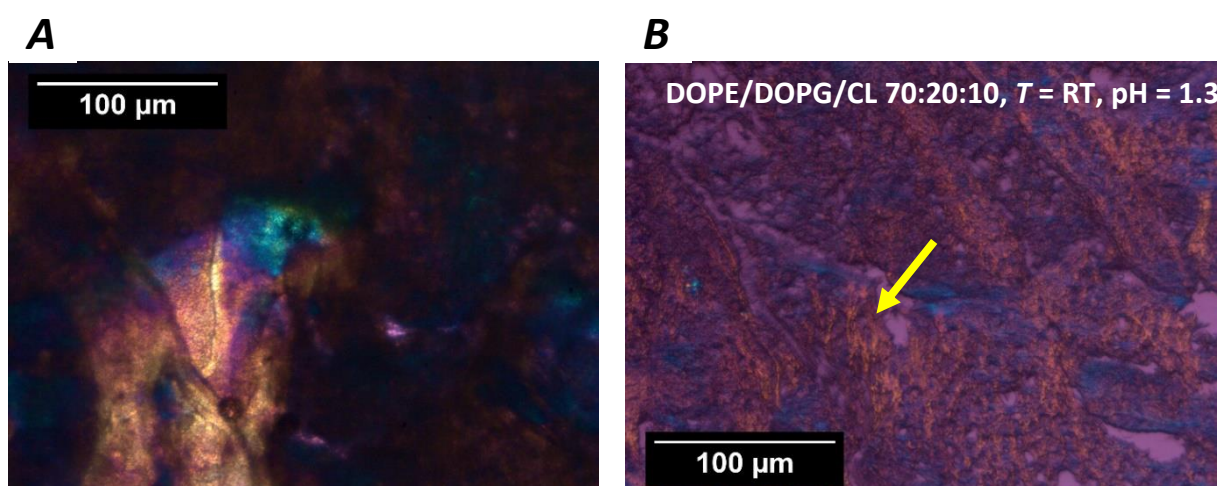
Finally, pure DOPG at pH 12.1 was also examined via PLM (**Fig. 40**). Notable in this sample was the large number of liposomes and their aggregation, and apparent lack of birefringent mesophase.

### 5.2.2 Lipid systems

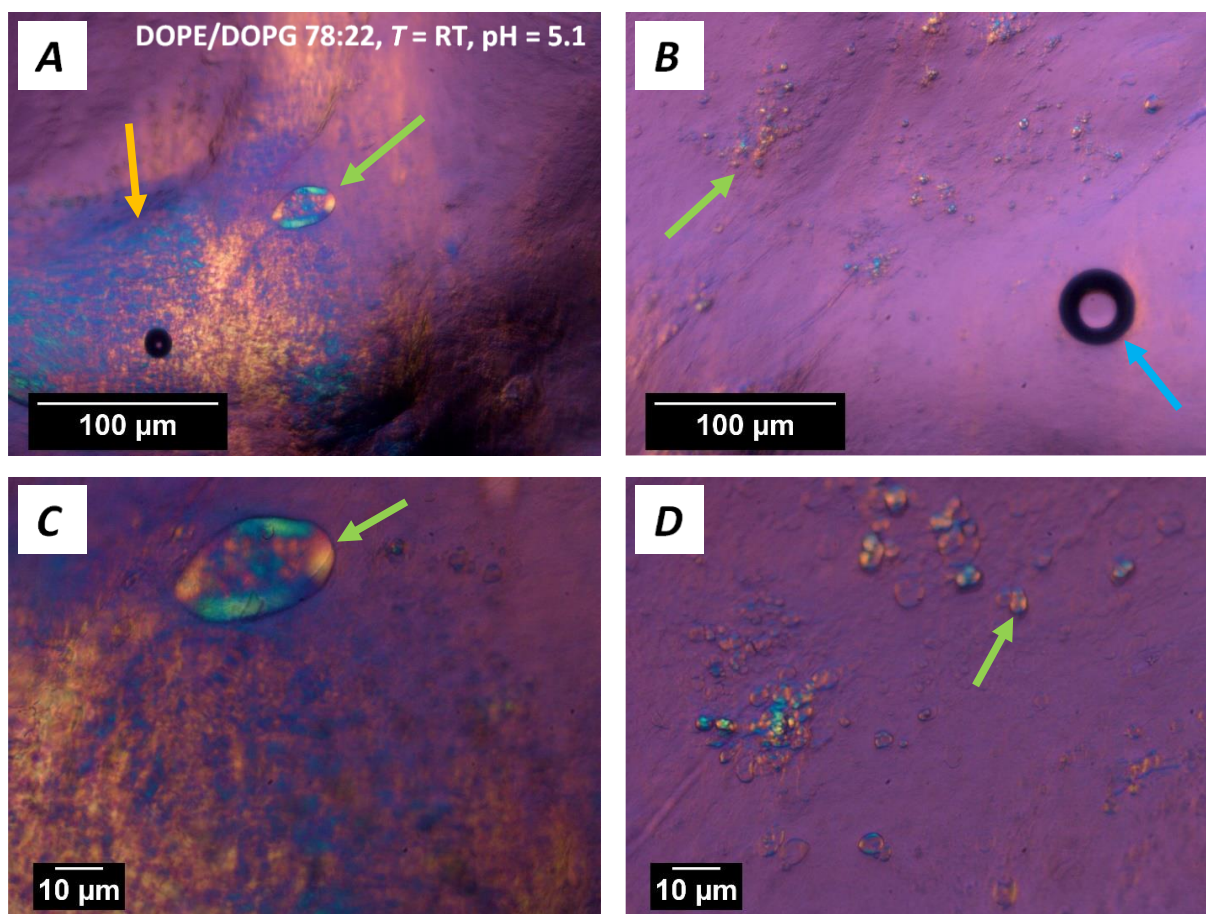


**Fig. 41.** PLM images of DOPE/DOPG at pH 1.3 taken with a 530 nm waveplate inserted, at 4x magnification (A, B), 10x magnification (C) and 20x magnification (D). Example of striations indicated with yellow arrow.

**Fig. 41.** and **Fig. 42.** Show PLM images of DOPE/DOPG and DOPE/DOPG/CL samples, respectively, at pH 1.3. At this pH, DOPE/DOPG/CL was found to be in the inverse hexagonal  $H_{II}$  phase via HP-SAXS. The images obtained are dark due to the thickness and viscosity of the mesophase samples used, this viscosity being characteristic of the presence of the  $H_{II}$  phase.<sup>130</sup> Both images are noticeably different in texture and appearance from the samples prepared at pH 5.1 and 12.1 (**Fig. 43-46**). Yellow arrows in **Fig. 41 B** and **Fig. 42 B** have been used to indicate the presence of striations in both samples, which is indicative of the  $H_{II}$  phase and observed with other lipids in this phase;<sup>131, 132</sup> at higher magnifications for DOPE/DOPG, a fan-like texture is visible which is also characteristic of the  $H_{II}$  phase.<sup>133</sup> The PLM images for these samples are thus supportive of the assignment of the  $H_{II}$  phase to the HP-SAXS measurements of the DOPE/DOPG/CL sample at  $p = 0-3000$  bar and  $T = 45$  &  $60^{\circ}\text{C}$ ,  $p = 1-2400$  bar at  $T = 30^{\circ}\text{C}$ , and  $p = 1-1800$  bar at  $T = 20^{\circ}\text{C}$  (**Fig. 41. A**), and also suggest that an HP-SAXS measurement of DOPE/DOPG alone at this pH would show the presence of a  $H_{II}$  phase under ambient conditions. No evidence of the presence of any liposomes was found for these samples using PLM, in agreement with the HP-SAXS measurements taken.



**Fig. 42.** PLM images of DOPE/DOPG/CL at pH 1.3 taken with a 530 nm waveplate inserted at 4x magnification. Example of striation indicated with yellow arrow.

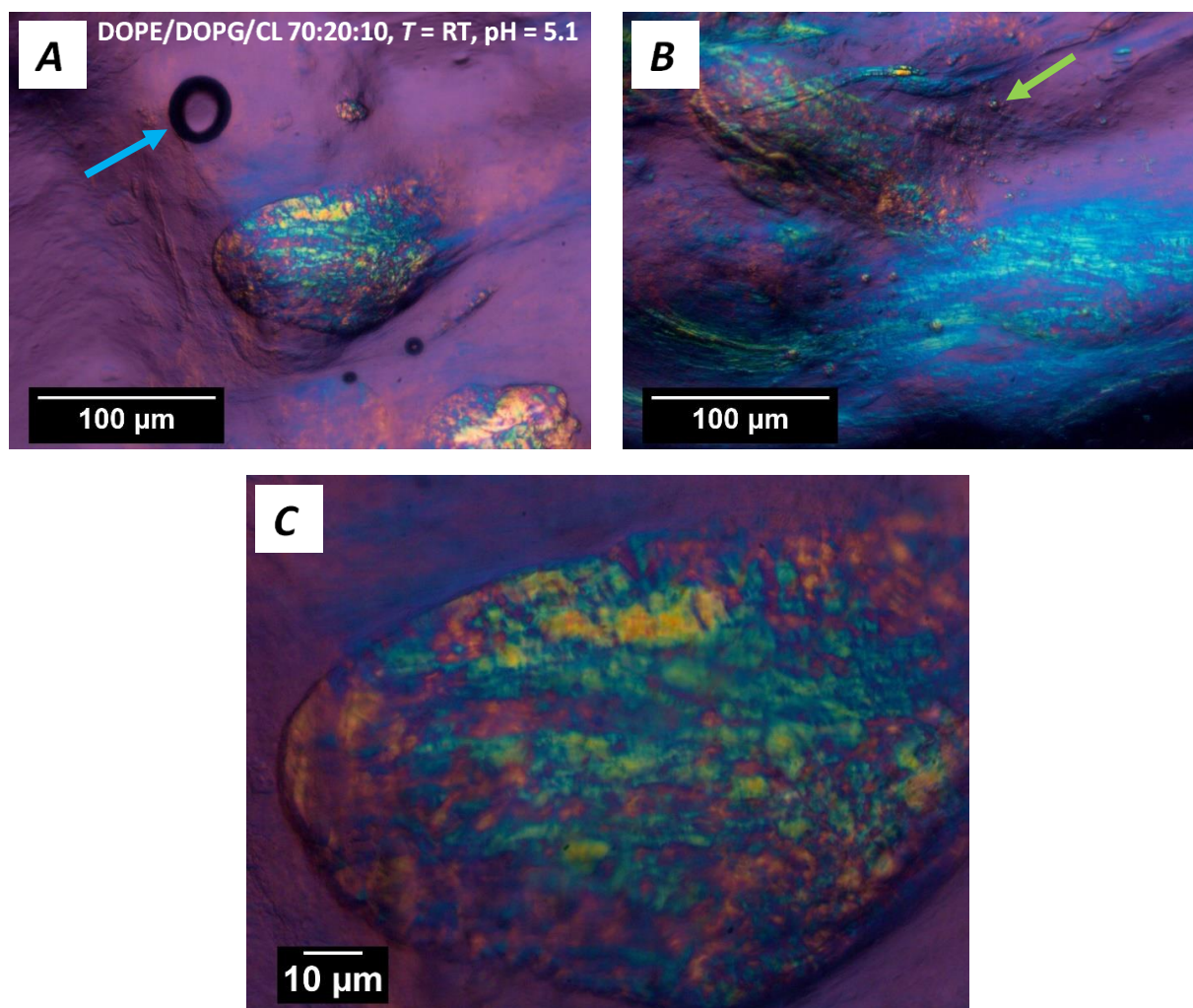


**Fig. 43.** PLM images of DOPE/DOPG at pH 5.1 taken with a 530 nm waveplate inserted, at 4x magnification (A & B) and 10x magnification (C & D). Green arrows indicate examples of vesicles in the samples, orange arrow indicates oily streak texture, and blue arrows indicate air bubbles.

**Fig. 43.** shows PLM images for the DOPE/DOPG sample at pH 5.1. In agreement with the HP-SAXS measurements for this sample, both mesophases and vesicles were present in this sample, with some vesicles such as the one indicated in **Fig 43. A & C** being approximately 36  $\mu\text{m}$  in diameter - very large and likely a multilamellar vesicle, while others such as the one indicated in **Fig. 43. D** are far smaller. An aggregate of liposomes is also visible in **Fig. 43. C**. The mesophase observed resembles lamellar phases observed previously in literature<sup>134</sup> supporting the assignment of an  $L_{\alpha}$  phase to the HP-SAXS data for this sample under ambient



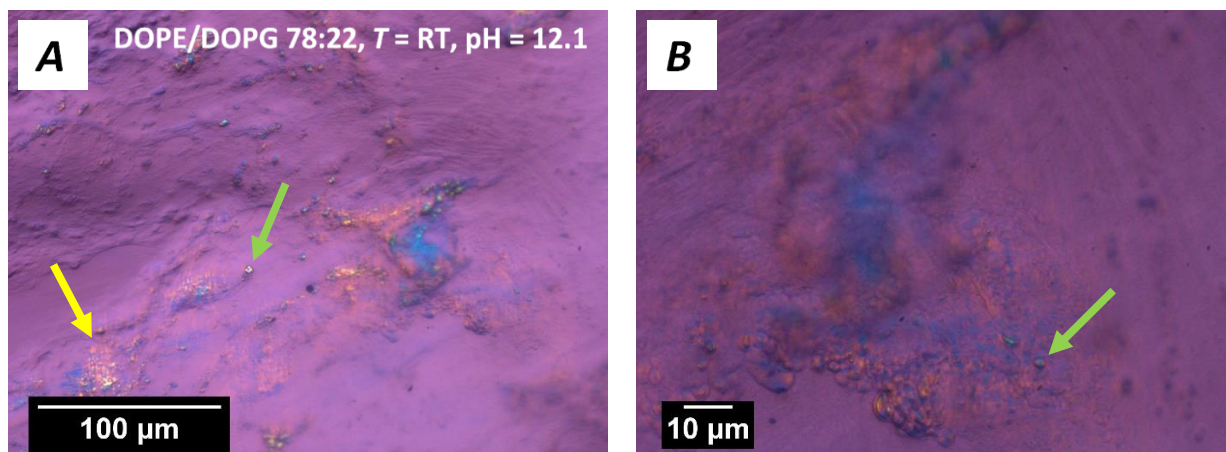
conditions. The 'oily streaks' texture observed in **Fig. 43. A & C** (orange arrow) is often observed in lamellar phases.<sup>135</sup>



**Fig. 44.** PLM images of DOPE/DOPG/CL at pH 5.1 taken with a 530 nm waveplate inserted, at 4x magnification (**A&B**) and 10x magnification (**C**). The green arrow indicates an example of vesicles in the sample, and the blue arrow indicates an air bubble.

**Fig. 44** shows DOPE/DOPG/CL at pH 5.1. No very large vesicles such as the one present in the DOPE/DOPG sample (**Fig. 43**) were observed in this sample, but smaller vesicles as indicated with the green arrow in **Fig. 44. B** were present, as predicted from the HP-SAXS results. In **Fig. 44. A** in bright blue, striations typical of a lamellar phase are present,<sup>132, 136</sup> in further support of the assignment of this phase to the HP-SAXS data. In **Fig. 44. A** and **Fig. 44.**

C (a higher magnification image of the central birefringent area) an oily streaks texture similar to that observed in DOPE/DOPG is present, again likely a lamellar phase.

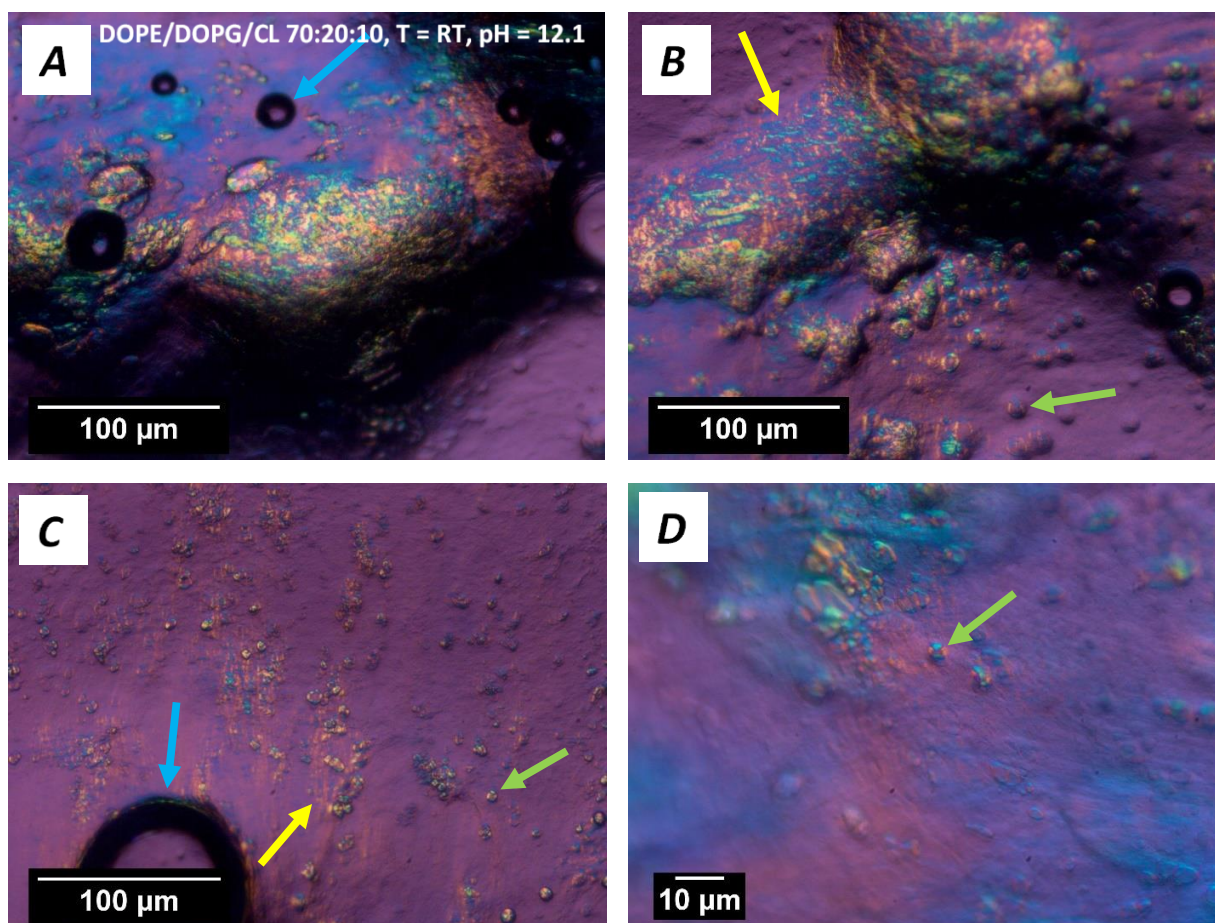


**Fig. 45.** PLM images of DOPE/DOPG at pH 12.1 taken with a 530 nm waveplate inserted, at 4x magnification (top row) and 10x magnification (bottom row). Green arrows indicate examples of vesicles in the sample, yellow arrow indicates striation typical of lamellar phase.

**Fig. 45.** shows DOPE/DOPG at pH 12.1. As with the samples at pH 5.1, vesicles were present of a similar size to the small ones observed in these samples, with no very large vesicles resembling the one in DOPE/DOPG observed (**Fig. 43**). There were fewer areas of birefringence observed in this sample, although some small areas of striations characteristic of a lamellar phase were observed (indicated by yellow arrows in **Fig. 45**). HP-SAXS data was not obtained for this sample. However, this combination of lamellar phase and vesicles was observed via HP-SAXS for DOPE/DOPG/CL at this pH, and so this suggests that HP-SAXS measurements of this sample may be similar.

**Fig. 46.** shows DOPE/DOPG/CL at pH 12.1, and in agreement with the HP-SAXS data for this sample, both vesicles and striations indicating the presence of the lamellar phases identified via HP-SAXS, and similarly to both samples at pH 5.1 and DOPE/DOPG at pH 12.1 (**Fig. 43, 44 & 45**). A noticeable difference with DOPE/DOPG at pH 12.1 is the much larger

prevalence of birefringent mesophase and the greater number of vesicles observed in the sample. It is possible that this difference is due to the presence of cardiolipin, and a comparison with DOPE/DOPG at pH 12.1 via HP-SAXS would shed light on whether this is a significant difference between the two samples.



**Fig. 46.** PLM images of DOPE/DOPG/CL at pH 12.1 taken with a 530 nm waveplate inserted, at 4x magnification (A, B & C) and 10x magnification (D). Green arrows indicate examples of vesicles in the sample, yellow arrow indicates striation typical of the lamellar phase, blue arrow indicates example of air bubble in the sample.

### 5.3 Conclusions

The PLM images taken for the samples studied via HP-SAXS (DOPE/DOPG at pH 5.1, and DOPE/DOPG/CL at pH 1.3, 5.1 and 12.1) all appear to support the phase assignment in chapter

3 from the HP-SAXS data, summarised in **table 5**, as well as showing the liposomes responsible for the shape of the HP-SAXS graphs.

Lipid composition	pH	Phase
DOPE/DOPG 78:22	1.3	H <sub>II</sub>
DOPE/DOPG 78:22	5.1	Lamellar
DOPE/DOPG 78:22	12.1	Lamellar
DOPE/DOPG/CL 70:20:10	1.3	H <sub>II</sub>
DOPE/DOPG/CL 70:20:10	5.1	Lamellar
DOPE/DOPG/CL 70:20:10	12.1	Lamellar

**Table 5.** Phase assignment of lipid samples observed via PLM

The PLM images for DOPE/DOPG at pH 1.3 (**Fig. 41**) and 12.1 (**Fig. 42**) suggest that the behaviour of this system is likely similar to the behaviour of DOPE/DOPG/CL at these pH values (**Fig. 41 & 46**), forming an H<sub>II</sub> phase at low pH and a lamellar phase with liposomes at pH 12.1. DOPE forms the H<sub>II</sub> phase under ambient conditions,<sup>96, 137</sup> but as also observed via HP-SAXS in chapter 3, the addition of DOPG resulted in the formation of a lamellar phase instead, in line with the finding of *Morein et al.* that DOPE/DOPG in a 7:3 ratio forms the L<sub>α</sub> phase at pH 7.4.<sup>116</sup> This again indicates that the DOPG played some role in changing the spontaneous curvature of the lipid system at pH 5.1, possibly by increasing lateral pressure between the headgroups present without increasing the lateral pressure between the tail groups, as DOPE and DOPG have identical tail groups. The PLM results showing an H<sub>II</sub> phase at pH 1.3 for DOPE/DOPG (**Fig. 41**) indicate that the same phase behaviour occurs in DOPE/DOPG without the presence of cardiolipin, i.e. DOPE and DOPG are also responding to pH. A possible reason for this is that the phosphate headgroups of DOPE and DOPG are likely

also being protonated at very low pH, producing the same effect observed with cardiolipin wherein a greater negative curvature is favoured.

Comparing the DOPE/DOPG and DOPE/DOPG/CL samples (**Fig. 41-46**) to the pure lipid samples (**Fig. 35-40**), the behaviour of the mixed lipid systems more closely mirrored the behaviour of pure cardiolipin than pure DOPG, with an  $H_{II}$  phase at pH 1.3 and lamellar phases with liposomes at pH 5.1 and 12.1 for both pure cardiolipin and DOPE/DOPG/CL. DOPG alone on the other hand had liposomes present at all pH values studied and did not have a clear phase difference between pH 1.3 and pH 5.1. As previously discussed, at pH 12.1 the repulsion between cardiolipin's two headgroups is greatest as it carries two negative charges, while at pH 1.3 the repulsion is minimal as the headgroup carries no charge, and so it was predicted that the  $H_{II}$  phase would be observed at low pH for these samples due to cardiolipin's greater packing parameter and thus its greater propensity for negative curvature.

These PLM results all highlight the large role pH appears to play in the phase behaviour of these lipids, supporting especially the large differences in behaviour at low pH of these systems also observed via HP-SAXS.

## Chapter 6. Conclusions & Future Work

---

Cardiolipin is a unique four-tailed pH-responsive phospholipid found in the membranes of bacteria, contributing to maintaining the membrane properties in various ways such as increasing propensity for negative curvature and increasing lateral pressure within the membrane. Understanding its role in shaping the properties of bacterial membrane mimics will contribute towards a better understanding of the ways in which bacteria adapt and respond to their environment and therefore may assist in finding new ways to combat them.

pH was found to play a major role in the phase behaviour of DOPE/DOPG/CL mesophases used as bacterial membrane mimics through the use of HP-SAXS. At pH 1.3, the system formed an  $H_{II}$  phase under ambient conditions, while under the same conditions at pH 5.1 and 12.1 an  $L_{\alpha}$  phase formed. Without control samples at pH 1.3 and 12.1, it is unclear the extent to which this phase behaviour was due to the presence of cardiolipin, but it is clear that the system was pH-responsive. Both the  $d$ -spacing and coherence length of the system were lower at pH 12.1 than at pH 5.1 under the same conditions, demonstrating that the system was responsive to both low and high pH.

As well as the effect of pH, the effect of cardiolipin on the behaviour of the system at pH 5.1 was observed, with cardiolipin lowering the pressure required to induce the  $L_{\alpha} \rightarrow L_{\beta}$  phase transition at 20°C that was observed in the samples at pH 5.1 and 12.1 by approximately 300 bar, likely due to the increased lateral pressure introduced by cardiolipin's bulky chains. Cardiolipin also increased the  $d$ -spacing observed at pH 5.1 and increased the sensitivity of the coherence length to temperature changes. Additionally, as expected, the system was found to respond to temperature with the  $L_{\beta}$  phase only appearing at  $T = 20$  and

25°C, as at higher temperatures, the lateral pressure between the tail groups was too great for the transition to occur in the pressure range studied.

These results were supported by PLM images taken of DOPE/DOPG and DOPE/DOPG/CL mesophases, with images of DOPE/DOPG controls taken at pH 1.3 and 12.1 as well as at pH 5.1, providing additional information on the effects of cardiolipin on the system at these pH values not obtained via HP-SAXS. It was found that the DOPE/DOPG controls exhibited the same phase behaviour as the DOPE/DOPG/CL samples at all three pH values studied, indicating that cardiolipin did not have a significant effect on the phase behaviour of the system and its role was likely more subtle. The PLM images also confirmed the presence of liposomes within all of the samples at pH 5.1 and 12.1, evident from the HP-SAXS data. In addition to the mixed lipid systems, individual DOPG and cardiolipin systems were examined for comparison. Although rapid sample drying prevented the clear assignment of phases to many of these samples, a clear difference in morphology was observed between cardiolipin at pH 1.3, and cardiolipin at pH 5.1 and 12.1, suggesting that it may have similar phase behaviour to the lipid systems examined. Meanwhile, there was no clear phase difference between pH 1.3 and 1.5 for DOPG.

The effects of pH and cardiolipin on the stability of DOPE/DOPG and DOPE/DOPG/CL liposomes used as bacterial membrane mimics were also investigated using DLS. Although only two pH values were investigated as liposomes would not form at pH 1.3, both pH and cardiolipin were found to have an effect on the stability and the average diameter of the liposomes. While there was no overall change in the average diameter  $D$  or the zeta potential  $\zeta$  over time, the DOPE/DOPG liposomes showed a much larger decrease in both the  $D$ ,  $\zeta$  and polydispersity (PDI) of the liposomes at pH 12.1

compared to pH 5.1, while the DOPE/DOPG/CL liposomes showed only a small decrease. This points to cardiolipin somewhat moderating the effects of high pH on the size, charge, and aggregation of the liposomes. In the context of bacterial membranes, this implies that cardiolipin could function to moderate the pH variations in the surrounding, thereby reducing its sensitivity pH changes and enhancing the robustness and stability of the bacteria membrane.

In summary, the DOPE/DOPG and DOPE/DOPG/CL bacterial membrane mimic systems were found to be pH responsive, and the presence of cardiolipin caused subtle differences in the phase behaviour,  $d$ -spacing and coherence length - all affected by the presence of cardiolipin at pH 5.1. DOPG/DOPG liposomes were also found to behave differently at pH 12.1 than at pH 5.1, with a greater  $\zeta$  and smaller  $D$ , while DOPE/DOPG/CL liposomes were not very responsive to an increase in pH. These observed effects provided justification for further investigation into the role cardiolipin and pH play in shaping the behaviour of bacterial membrane mimic systems.

On the basis of the HP-SAXS results obtained, a successful proposal was submitted for beamtime at Diamond I22, and further HP-SAXS measurements were obtained for this system in February 2020. Part of the future work for this project will be to fully analyse this data, as data for DOPE/DOPG controls at pH 1.3 and 12.1 as well as were obtained, thereby completing the original set of measurements for the project and allowing for the role of cardiolipin in the system's response to low and high pH to be assessed. In addition to the original three pH values measured, measurements were taken of DOPE/DOPG and DOPE/DOPG/CL at pH 2.0, 3.0 and 4.0 were obtained in order to more ascertain more precisely the pH at which the system transitions from forming the  $H_{II}$  phase to the  $L_{\alpha}$  phase under ambient conditions. Repeat measurements were also obtained for the temperature-



pressure phase diagrams already produced, at an extended pressure range (1-3600 bar) to better observe the  $L_{\alpha} \rightarrow L_{\beta}$  phase transition. This pressure range was also used for the new pH values. In addition, a sample with a new composition (DOPE/DOPG/CL 62:18:20) was measured at pH 5.1 in order to study if increasing the proportion of cardiolipin in the system exaggerated the effects of cardiolipin previously observed, as well as pure cardiolipin at pH 5.1 for comparison.

The bacterial membrane is a complex structure, and so biomembrane models comprising of three or more components can serve as a more accurate model for studying the phase behaviour of lipid systems.<sup>1</sup> The incorporation of additional lipids into mesophases would provide better insight into the behaviour of a real bacterial membrane, and *E. coli* specifically (which was mimicked in this work) has been found to contain additional lipids beyond PG, PE and CL,<sup>2</sup> of varying chain lengths. *E. coli* polar lipid extract and *E. coli* cardiolipin extract are available from Avanti Polar Lipids,<sup>3,4</sup> both of which contain a range of lipids with differing chain lengths and could be used to provide a more accurate model of the behaviour of the *E. coli* membrane. Further studies using liposomes as a model for the *E. coli* membrane could incorporate other bacterial membrane components such as lipopolysaccharide (LPS) which is found in the outer leaflet of gram negative bacteria.<sup>5</sup> The use of buffers that mimic biological conditions such as phosphate-buffered saline may also provide a better model for the behaviour of bacterial membranes in nature, with other buffers previously used with similar cardiolipin-containing systems including sodium citrate and tris-HCL, and<sup>6</sup> HEPES and EDTA<sup>7</sup>.

In addition to changes to the bacterial membrane model itself, the system could be investigated further by extending the HP-SAXS pressure-temperature phase diagrams for the samples to higher pressures and lower temperatures to better observe the  $L_{\alpha} \rightarrow$

$L_{\beta}$  phase boundary, as well as using smaller temperature and pressure steps to better observe mixed phase regions. Obtaining pressure-temperature phase diagrams for pure DOPE, DOPG and 18:1 cardiolipin at pH 1.3, 5.1 and 12.1 would provide a useful comparison for the behaviour of the lipid systems. More insight into the effect of cardiolipin on the system would also be gained by investigating a mesophase consisting of only DOPE and cardiolipin, to be compared with the DOPE/DOPG mesophase and a pure DOPE pressure-temperature phase diagram, and PLM images of these samples could be obtained to support phase assignment.

The effect of the presence of biologically relevant ions such as  $\text{Na}^+$ ,  $\text{K}^+$ , and  $\text{Ca}^{2+}$ , which have been found to play a role in the stability of liposomes,<sup>8,9</sup> would also be interesting to investigate. Further insight into the role cardiolipin plays in the bacterial membrane and its response to the bacterium's external environment could be obtained by investigating the effects of biologically relevant ions on the properties of cardiolipin-containing liposomes through  $D$ , PDI and  $\zeta$  measurements over time.

## References

1. Unsay, J. D.; Cosentino, K.; Subburaj, Y.; Garcia-Saez, A. J., Cardiolipin Effects on Membrane Structure and Dynamics. *Langmuir* **2013**, *29* (51), 15878-15887.
2. Schlame, M., Thematic review series: Glycerolipids - Cardiolipin synthesis for the assembly of bacterial and mitochondrial membranes. *J Lipid Res* **2008**, *49* (8), 1607-1620.
3. Lopes, S. C.; Ivanova, G.; de Castro, B.; Gameiro, P., Revealing cardiolipins influence in the construction of a significant mitochondrial membrane model. *Bba-Biomembranes* **2018**, *1860* (11), 2465-2477.
4. Lemmin, T.; Bovigny, C.; Lancon, D.; Dal Peraro, M., Cardiolipin Models for Molecular Simulations of Bacterial and Mitochondrial Membranes. *J Chem Theory Comput* **2013**, *9* (1), 670-678.
5. Wright, G. D., Opportunities for natural products in 21st century antibiotic discovery. *Nat Prod Rep* **2017**, *34* (7), 694-701.
6. Fleming, A., Nobel Lecture. Nobel Media AB 2020: 1945.
7. Barber, M., Staphylococcal Infection Due to Penicillin-Resistant Strains. *Brit Med J* **1947**, *2* (4534), 863-865.
8. Ventola, C. L., The antibiotic resistance crisis: part 1: causes and threats. *P T* **2015**, *40* (4), 277-83.
9. Cassini, A.; Hogberg, L. D.; Plachouras, D.; Quattrocchi, A.; Hoxha, A.; Simonsen, G. S.; Colomb-Cotinat, M.; Kretzschmar, M. E.; Devleeschauwer, B.; Cecchini, M.; Ouakrim, D. A.; Oliveira, T. C.; Struelens, M. J.; Suetens, C.; Monnet, D. L.; Burden of, A. M. R. C. G., Attributable deaths and disability-adjusted life-years caused by infections with antibiotic-resistant bacteria in the EU and the European Economic Area in 2015: a population-level modelling analysis. *Lancet Infect Dis* **2019**, *19* (1), 56-66.
10. Akova, M., Epidemiology of antimicrobial resistance in bloodstream infections. *Virulence* **2016**, *7* (3), 252-66.
11. O'Neill, J. *Tackling Drug-resistant Infections Globally; The Review On Antimicrobial Resistance*: 2016.
12. Adams, P. G.; Lamoureux, L.; Swingle, K. L.; Mukundan, H.; Montano, G. A., Lipopolysaccharide-Induced Dynamic Lipid Membrane Reorganization: Tubules, Perforations, and Stacks. *Biophys J* **2014**, *106* (11), 2395-2407.
13. Frieri, M.; Kumar, K.; Boutin, A., Antibiotic resistance. *J Infect Public Health* **2017**, *10* (4), 369-378.
14. *The World Medicines Situation Report (Third Edition)*; World Health Organisation: 2011.
15. Berdy, J., Thoughts and facts about antibiotics: Where we are now and where we are heading. *J Antibiot* **2012**, *65* (8), 385-395.
16. Savage, P. B., Multidrug-resistant bacteria: overcoming antibiotic permeability barriers of Gram-negative bacteria. *Ann Med* **2001**, *33* (3), 167-171.
17. Fleming, S. A., Nobel Lecture. 1945.
18. Thomas, C. M.; Nielsen, K. M., Mechanisms of, and barriers to, horizontal gene transfer between bacteria. *Nat Rev Microbiol* **2005**, *3* (9), 711-21.
19. Khameneh, B.; Diab, R.; Ghazvini, K.; Fazly Bazzaz, B. S., Breakthroughs in bacterial resistance mechanisms and the potential ways to combat them. *Microb Pathog* **2016**, *95*, 32-42.
20. Cui, L. Z.; Iwamoto, A.; Lian, J. Q.; Neoh, H. M.; Maruyama, T.; Horikawa, Y.; Hiramatsu, K., Novel mechanism of antibiotic resistance originating in vancomycin-intermediate Staphylococcus aureus. *Antimicrobial Agents and Chemotherapy* **2006**, *50* (2), 428-438.
21. Livermore, D. M.; British Society for Antimicrobial Chemotherapy Working Party on The Urgent Need: Regenerating Antibacterial Drug, D.; Development, Discovery research: the scientific challenge of finding new antibiotics. *J Antimicrob Chemother* **2011**, *66* (9), 1941-4.

22. Berghman, L. R.; Abi-Ghanem, D.; Waghela, S. D.; Ricke, S. C., Antibodies: an alternative for antibiotics? *Poult Sci* **2005**, *84* (4), 660-6.
23. Abedon, S. T.; Garcia, P.; Mullany, P.; Aminov, R., Editorial: Phage Therapy: Past, Present and Future. *Front Microbiol* **2017**, *8*, 981.
24. Subramaniam, S.; Fahy, E.; Gupta, S.; Sud, M.; Byrnes, R. W.; Cotter, D.; Dinasarapu, A. R.; Maurya, M. R., Bioinformatics and Systems Biology of the Lipidome. *Chem Rev* **2011**, *111* (10), 6452-6490.
25. Cevc, G., *Phospholipids Handbook*. CRC Press: 1993.
26. Hannun, Y. A.; Obeid, L. M., Principles of bioactive lipid signalling: lessons from sphingolipids. *Nat Rev Mol Cell Bio* **2008**, *9* (2), 139-150.
27. Lydic, T. A.; Goo, Y. H., Lipidomics unveils the complexity of the lipidome in metabolic diseases. *Clin Transl Med* **2018**, *7*.
28. Russell, N. J., Adaptive Modifications in Membranes of Halotolerant and Halophilic Microorganisms. *J Bioenerg Biomembr* **1989**, *21* (1), 93-113.
29. Hasegawa, Y.; Kawada, N.; Nosoh, Y., Change in Chemical-Composition of Membrane of *Bacillus-Caldotenax* after Shifting the Growth Temperature. *Arch Microbiol* **1980**, *126* (2), 103-108.
30. Ohno, Y.; Yano, I.; Masui, M., Effect of NaCl Concentration and Temperature on the Phospholipid and Fatty-Acid Compositions of a Moderately Halophilic Bacterium, *Pseudomonas-Halosaccharolytica*. *J Biochem-Tokyo* **1979**, *85* (2), 413-421.
31. Huque, E. M., The Hydrophobic Effect. *J Chem Educ* **1989**, *66* (7), 581-585.
32. Israelachvili, J. N.; Mitchell, D. J.; Ninham, B. W., Theory of Self-Assembly of Lipid Bilayers and Vesicles. *Biochim Biophys Acta Biochim Biophys Acta* **1977**, *470* (2), 185-201.
33. Nagarajan, R., Molecular packing parameter and surfactant self-assembly: The neglected role of the surfactant tail. *Langmuir* **2002**, *18* (1), 31-38.
34. Wang, N.; Chen, M. N.; Wang, T., Liposomes used as a vaccine adjuvant-delivery system: From basics to clinical immunization. *Journal of Controlled Release* **2019**, *303*, 130-150.
35. Salton, M. R. J., Structure and function of bacterial cell membranes. *Annual Review of Microbiology* **1967**, *21*, 417-442.
36. Strahl, H.; Errington, J., Bacterial Membranes: Structure, Domains, and Function. *Annu Rev Microbiol* **2017**, *71*, 519-538.
37. Redeker, C.; Briscoe, W. H., Interactions between Mutant Bacterial Lipopolysaccharide (LPS-Ra) Surface Layers: Surface Vesicles, Membrane Fusion, and Effect of Ca<sup>2+</sup> and Temperature. *Langmuir Langmuir* **2019**, *35* (48), 15739-15750.
38. Malanovic, N.; Leber, R.; Schmuck, M.; Kriechbaum, M.; Cordfunke, R. A.; Drijfhout, J. W.; de Breij, A.; Nibbering, P. H.; Kolb, D.; Lohner, K., Phospholipid-driven differences determine the action of the synthetic antimicrobial peptide OP-145 on Gram-positive bacterial and mammalian membrane model systems. *Bba-Biomembranes* **2015**, *1848* (10), 2437-2447.
39. Zasloff, M., Antimicrobial peptides of multicellular organisms. *Nature* **2002**, *415* (6870), 389-395.
40. Vollmer, W.; Holtje, J. V., The architecture of the murein (peptidoglycan) in gram-negative bacteria: Vertical scaffold or horizontal layer(s)? *Journal of Bacteriology* **2004**, *186* (18), 5978-5987.
41. Levy, S. B.; Marshall, B., Antibacterial resistance worldwide: causes, challenges and responses. *Nat Med* **2004**, *10* (12 Suppl), S122-9.
42. Hughes, D.; Karlen, A., Discovery and preclinical development of new antibiotics. *Upsala J Med Sci* **2014**, *119* (2), 162-169.
43. Peetla, C.; Stine, A.; Labhasetwar, V., Biophysical interactions with model lipid membranes: applications in drug discovery and drug delivery. *Mol Pharm* **2009**, *6* (5), 1264-76.
44. Drulis-Kawa, Z.; Dorotkiewicz-Jach, A., Liposomes as delivery systems for antibiotics. *International Journal of Pharmaceutics* **2010**, *387* (1-2), 187-198.
45. Tripathy, A.; Sen, P.; Su, B.; Briscoe, W. H., Natural and bioinspired nanostructured bactericidal surfaces. *Adv Colloid Interfac* **2017**, *248*, 85-104.

46. Ivanova, E. P.; Hasan, J.; Webb, H. K.; Truong, V. K.; Watson, G. S.; Watson, J. A.; Baulin, V. A.; Pogodin, S.; Wang, J. Y.; Tobin, M. J.; Lobbe, C.; Crawford, R. J., Natural Bactericidal Surfaces: Mechanical Rupture of *Pseudomonas aeruginosa* Cells by Cicada Wings. *Small* **2012**, *8* (16), 2489-2494.
47. Lewis, R. N. A. H.; McElhane, R. N., The physicochemical properties of cardiolipin bilayers and cardiolipin-containing lipid membranes. *Bba-Biomembranes Bba-Biomembranes* **2009**, *1788* (10), 2069-2079.
48. Pangborn, M. C., Isolation and purification of a serologically active phospholipid from beef heart. *Journal of Biological Chemistry* **1942**, *143* (1), 247-256.
49. Chicco, A. J.; Sparagna, G. C., Role of cardiolipin alterations in mitochondrial dysfunction and disease. *Am J Physiol Cell Physiol* **2007**, *292* (1), C33-44.
50. Hoch, F. L., Cardiolipins and Biomembrane Function. *Biochim Biophys Acta Biochim Biophys Acta* **1992**, *1113* (1), 71-133.
51. Mileyskaya, E.; Zhang, M.; Dowhan, W., Cardiolipin in energy transducing membranes. *Biochemistry (Mosc)* **2005**, *70* (2), 154-8.
52. Yankovskaya, V.; Horsefield, R.; Tornroth, S.; Luna-Chavez, C.; Miyoshi, H.; Leger, C.; Byrne, B.; Cecchini, G.; Iwata, S., Architecture of succinate dehydrogenase and reactive oxygen species generation. *Science* **2003**, *299* (5607), 700-4.
53. Lind, T. K.; Wacklin, H.; Schiller, J.; Moulin, M.; Haertlein, M.; Pomorski, T. G.; Cardenas, M., Formation and Characterization of Supported Lipid Bilayers Composed of Hydrogenated and Deuterated *Escherichia coli* Lipids. *Plos One Plos One* **2015**, *10* (12).
54. Lombardi, L.; Stellato, M. I.; Oliva, R.; Falanga, A.; Galdiero, M.; Petraccone, L.; D'Errico, G.; De Santis, A.; Galdiero, S.; Del Vecchio, P., Antimicrobial peptides at work: interaction of myxinidin and its mutant WMR with lipid bilayers mimicking the *P. aeruginosa* and *E-coli* membranes. *Sci Rep-Uk Sci Rep-Uk* **2017**, *7*.
55. Lopes, S.; Neves, C. S.; Eaton, P.; Gameiro, P., Cardiolipin, a key component to mimic the *E. coli* bacterial membrane in model systems revealed by dynamic light scattering and steady-state fluorescence anisotropy. *Anal Bioanal Chem Anal Bioanal Chem* **2010**, *398* (3), 1357-1366.
56. Okabe, A.; Hirai, Y.; Hayashi, H.; Kanemasa, Y., Alteration in Phospholipid-Composition of *Staphylococcus-Aureus* during Formation of Autoplast. *Biochim Biophys Acta Biochim Biophys Acta* **1980**, *617* (1), 28-35.
57. Lillich, T. T.; White, D. C., Phospholipid Metabolism in Absence of Net Phospholipid Synthesis in a Glycerol-Requiring Mutant of *Bacillus-Subtilis*. *Journal of Bacteriology* **1971**, *107* (3), 790-&.
58. Short, S. A.; White, D. C., Metabolism of Phosphatidylglycerol, Lysylphosphatidylglycerol, and Cardiolipin of *Staphylococcus-Aureus*. *Journal of Bacteriology* **1971**, *108* (1), 219-&.
59. Cronan, J. E., Phospholipid Alterations during Growth of *Escherichia Coli*. *Journal of Bacteriology* **1968**, *95* (6), 2054-&.
60. Romantsov, T.; Guan, Z. Q.; Wood, J. M., Cardiolipin and the osmotic stress responses of bacteria. *Bba-Biomembranes Bba-Biomembranes* **2009**, *1788* (10), 2092-2100.
61. Nichols-Smith, S.; Teh, S. Y.; Kuhl, T. L., Thermodynamic and mechanical properties of model mitochondrial membranes. *Bba-Biomembranes Bba-Biomembranes* **2004**, *1663* (1-2), 82-88.
62. Wydro, P., The influence of cardiolipin on phosphatidylglycerol/phosphatidylethanolamine monolayers-Studies on ternary films imitating bacterial membranes. *Colloid Surface B Colloid Surface B* **2013**, *106*, 217-223.
63. Etienne, F.; Roche, Y.; Peretti, P.; Bernard, S., Cardiolipin packing ability studied by grazing incidence X-ray diffraction. *Chem Phys Lipids Chem Phys Lipids* **2008**, *152* (1), 13-23.
64. Ohtsuka, T.; Nishijima, M.; Suzuki, K.; Akamatsu, Y., Mitochondrial Dysfunction of a Cultured Chinese-Hamster Ovary Cell Mutant Deficient in Cardiolipin. *Journal of Biological Chemistry* **1993**, *268* (30), 22914-22919.
65. Schlame, M.; Rua, D.; Greenberg, M. L., The biosynthesis and functional role of cardiolipin. *Prog Lipid Res* **2000**, *39* (3), 257-88.

66. Kates, M.; Syz, J. Y.; Gosser, D.; Haines, T. H., Ph-Dissociation Characteristics of Cardiolipin and Its 2'-Deoxy Analog. *Lipids Lipids* **1993**, *28* (10), 877-882.
67. Henderson, T. O.; Glonek, T.; Myers, T. C., Phosphorus-31 Nuclear Magnetic-Resonance Spectroscopy of Phospholipids. *Biochemistry* **1974**, *13* (3), 623-628.
68. Haines, T. H.; Dencher, N. A., Cardiolipin: a proton trap for oxidative phosphorylation. *FEBS Lett* **2002**, *528* (1-3), 35-9.
69. Sidiq, S.; Verma, I.; Pal, S. K., pH-Driven Ordering Transitions in Liquid Crystal Induced by Conformational Changes of Cardiolipin. *Langmuir Langmuir* **2015**, *31* (16), 4741-4751.
70. Lewis, R. N. A. H.; McElhaney, R. N., Surface charge markedly attenuates the nonlamellar phase-forming propensities of lipid bilayer membranes: Calorimetric and P-31-nuclear magnetic resonance studies of mixtures of cationic, anionic, and zwitterionic lipids. *Biophysical Journal* **2000**, *79* (3), 1455-1464.
71. Dahlberg, M., Polymorphic phase behavior of cardiolipin derivatives studied by coarse-grained molecular dynamics. *J Phys Chem B* **2007**, *111* (25), 7194-7200.
72. Khalifat, N.; Fournier, J. B.; Angelova, M. I.; Puff, N., Lipid packing variations induced by pH in cardiolipin-containing bilayers: The driving force for the cristae-like shape instability. *Bba-Biomembranes Bba-Biomembranes* **2011**, *1808* (11), 2724-2733.
73. Rappolt, M., *Advances in planar lipid bilayers and liposomes*. 2007; Vol. 5.
74. Kranenburg, M.; Smit, B., Phase behavior of model lipid bilayers. *Journal of Physical Chemistry B* **2005**, *109* (14), 6553-6563.
75. Kulkarni, C. V.; Wachter, W.; Iglesias-Salto, G.; Engelskirchen, S.; Ahualli, S., Monoolein: a magic lipid? *Phys Chem Chem Phys Phys Chem Chem Phys* **2011**, *13* (8), 3004-3021.
76. Akbarzadeh, A.; Rezaei-Sadabady, R.; Davaran, S.; Joo, S. W.; Zarghami, N.; Hanifehpour, Y.; Samiei, M.; Kouhi, M.; Nejati-Koshki, K., Liposome: classification, preparation, and applications. *Nanoscale Res Lett* **2013**, *8*.
77. Keller, B. C., Liposomes in nutrition. *Trends Food Sci Tech* **2001**, *12* (1), 25-31.
78. Behr, J.; Zimmermann, G.; Baumgartner, R.; Leuchte, H.; Neurohr, C.; Brand, P.; Herpich, C.; Sommerer, K.; Seitz, J.; Keller, M., Lung Deposition of a Liposomal Cyclosporine A Inhalation Solution in Patients after Lung Transplantation. *J Heart Lung Transpl* **2010**, *29* (2), S68-S68.
79. Silverman, J. A.; Deitcher, S. R., Marqibo (R) (vincristine sulfate liposome injection) improves the pharmacokinetics and pharmacodynamics of vincristine. *Cancer Chemoth Pharm* **2013**, *71* (3), 555-564.
80. Schmid, M. H.; Korting, H. C., Therapeutic progress with topical liposome drugs for skin disease. *Adv Drug Deliver Rev* **1996**, *18* (3), 335-342.
81. Chan, Y. H. M.; Boxer, S. G., Model membrane systems and their applications. *Curr Opin Chem Biol* **2007**, *11* (6), 581-587.
82. Tanaka, M.; Sackmann, E., Polymer-supported membranes as models of the cell surface. *Nature* **2005**, *437* (7059), 656-663.
83. Jurak, M., Thermodynamic Aspects of Cholesterol Effect on Properties of Phospholipid Monolayers: Langmuir and Langmuir-Blodgett Monolayer Study. *Journal of Physical Chemistry B* **2013**, *117* (13), 3496-3502.
84. Chibowski, E.; Szczes, A., Zeta potential and surface charge of DPPC and DOPC liposomes in the presence of PLC enzyme. *Adsorption* **2016**, *22* (4-6), 755-765.
85. Seddon, J. M.; Templer, R. H., Cubic Phases of Self-Assembled Amphiphilic Aggregates. *Philos T Roy Soc A Philos T Roy Soc A* **1993**, *344* (1672), 377-401.
86. Siegel, D. P., The modified stalk mechanism of lamellar/inverted phase transitions and its implications for membrane fusion. *Biophys J Biophys J* **1999**, *76* (1), 291-313.
87. Swain, J.; El Khoury, M.; Kempf, J.; Brie, F.; Van Der Smissen, P.; Decout, J. L.; Mingeot-Leclercq, M. P., Effect of cardiolipin on the antimicrobial activity of a new amphiphilic aminoglycoside derivative on *Pseudomonas aeruginosa*. *Plos One Plos One* **2018**, *13* (8).

88. Michel, J. P.; Wang, Y. X.; De, E.; Fontaine, P.; Goldmann, M.; Rosilio, V., Charge and aggregation pattern govern the interaction of plasticins with LPS monolayers mimicking the external leaflet of the outer membrane of Gram-negative bacteria. *Bba-Biomembranes Bba-Biomembranes* **2015**, *1848* (11), 2967-2979.
89. Kakimoto, Y.; Tero, R., Supported Lipid Bilayers of Escherichia coli Extracted Lipids and Their Calcium Dependence. *Front Mater Front Mater* **2018**, *5*.
90. Amar-Yuli, I.; Garti, N., Transitions induced by solubilized fat into reverse hexagonal mesophases. *Colloids and Surfaces B-Biointerfaces* **2005**, *43* (2), 72-82.
91. Hessenbruch, A., A brief history of x-rays. *Endeavour* **2002**, *26* (4), 137-141.
92. Jaskolski, M.; Dauter, Z.; Wlodawer, A., A brief history of macromolecular crystallography, illustrated by a family tree and its Nobel fruits. *Febs J* **2014**, *281* (18), 3985-4009.
93. Bragg, W. H.; Bragg, W. L., The reflection of X-rays by crystals. *P R Soc Lond a-Conta* **1913**, *88* (605), 428-438.
94. Winter, R.; Kohling, R., Static and time-resolved synchrotron small-angle x-ray scattering studies of lyotropic lipid mesophases, model biomembranes and proteins in solution. *J Phys-Condens Mat J Phys-Condens Mat* **2004**, *16* (5), S327-S352.
95. Partridge, P. G., The crystallography and deformation models of hexagonal close-packed metals. *Metallurgical Reviews* **1967**, *12*(1), 169-194.
96. Bulpett, J. M.; Snow, T.; Quignon, B.; Beddoes, C. M.; Tang, T. Y. D.; Mann, S.; Shebanova, O.; Pizzey, C. L.; Terrill, N. J.; Davis, S. A.; Briscoe, W. H., Hydrophobic nanoparticles promote lamellar to inverted hexagonal transition in phospholipid mesophases. *Soft Matter Soft Matter* **2015**, *11* (45), 8789-8800.
97. Putnam, C. D., Guinier peak analysis for visual and automated inspection of small-angle X-ray scattering data. *J Appl Crystallogr* **2016**, *49*, 1412-1419.
98. Herman Winick, S. D., *Synchrotron Radiation Research*. 1st ed.; Plenum Press: Stanford University, 1980.
99. Synchrotron Light. [https://www.iop.org/publications/iop/2011/file\\_47457.pdf](https://www.iop.org/publications/iop/2011/file_47457.pdf) (accessed November).
100. Welcome to I22. <https://www.diamond.ac.uk/Instruments/Soft-Condensed-Matter/small-angle/I22.html> (accessed November).
101. Seddon, J. M., Structure of the Inverted Hexagonal (H<sub>II</sub>) Phase, and Non-Lamellar Phase-Transitions of Lipids. *Biochim Biophys Acta Biochim Biophys Acta* **1990**, *1031* (1), 1-69.
102. Skanes, I. D.; Stewart, J.; Keough, K. M. W.; Morrow, M. R., Effect of chain unsaturation on bilayer response to pressure. *Physical Review E* **2006**, *74* (5).
103. Brooks, N. J.; Ces, O.; Templer, R. H.; Seddon, J. M., Pressure effects on lipid membrane structure and dynamics. *Chem Phys Lipids Chem Phys Lipids* **2011**, *164* (2), 89-98.
104. Shao, H. L.; Im, H.; Castro, C. M.; Breakefield, X.; Weissleder, R.; Lee, H. H., New Technologies for Analysis of Extracellular Vesicles. *Chem Rev* **2018**, *118* (4), 1917-1950.
105. Pecora, R., Dynamic light scattering measurement of nanometer particles in liquids. *J Nanopart Res* **2000**, *2* (2), 123-131.
106. Cecere, D.; Bruno, A.; Minutolo, P.; D'Alessio, A., DLS measurements on nanoparticles produced in laminar premixed flames. *Synthetic Met* **2003**, *139* (3), 653-656.
107. Bruce J Berne, R. P., *Dynamic Light Scattering With Applications to Chemistry, Biology, and Physics*. Dover Publications: New York, 1976.
108. Stetefeld, J.; McKenna, S. A.; Patel, T. R., Dynamic light scattering: a practical guide and applications in biomedical sciences. *Biophys Rev* **2016**, *8* (4), 409-427.
109. Kaszuba, M.; Corbett, J.; Watson, F. M.; Jones, A., High-concentration zeta potential measurements using light-scattering techniques. *Philos T R Soc A* **2010**, *368* (1927), 4439-4451.
110. Picc, S. L. L., Influence of Nanocomposite Materials for Next Generation Nano Lithography. *Advances in Diverse Industrial Applications of Nanocomposites*: 2011.

111. McNeil, S. E., *Characterization of Nanoparticles Intended for Drug Delivery*. Humana Press: 2011.
112. Chayen, J., Polarized-Light Microscopy - Principles and Practice for the Rheumatologist. *Ann Rheum Dis* **1983**, *42*, 64-67.
113. Lopes, L. B.; Ferreira, D. A.; de Paula, D.; Garcia, M. T. J.; Thomazini, J. A.; Fantini, M. C. A.; Bentley, M. V. L. B., Reverse hexagonal phase nanodispersion of monoolein and oleic acid for topical delivery of peptides: in vitro and in vivo skin penetration of cyclosporin A. *Pharmaceutical Research* **2006**, *23* (6), 1332-1342.
114. Wolman, M., Polarized-Light Microscopy as a Tool of Diagnostic Pathology - Review. *J Histochem Cytochem* **1975**, *23* (1), 21-50.
115. Brooks, N. J.; Gauthe, B. L. L. E.; Terrill, N. J.; Rogers, S. E.; Templer, R. H.; Ces, O.; Seddon, J. M., Automated high pressure cell for pressure jump x-ray diffraction. *Review of Scientific Instruments* **2010**, *81* (6).
116. Morein, S.; Koeppe, R. E.; Lindblom, G.; de Kruijff, B.; Killian, J. A., The effect of peptide/lipid hydrophobic mismatch on the phase behavior of model membranes mimicking the lipid composition in Escherichia coli membranes. *Biophys J* **2000**, *78* (5), 2475-2485.
117. Avanti Polar Lipids, I. Phase Transition Temperatures for Glycerophospholipids. (accessed 10/05/20).
118. Alley, S. H.; Ces, O.; Barahona, M.; Templer, R. H., X-ray diffraction measurement of the monolayer spontaneous curvature of dioleoylphosphatidylglycerol. *Chem Phys Lipids Chem Phys Lipids* **2008**, *154* (1), 64-67.
119. Bouwstra, J. A.; Gooris, G. S.; Bras, W.; Talsma, H., Small-Angle X-Ray-Scattering - Possibilities and Limitations in Characterization of Vesicles. *Chem Phys Lipids Chem Phys Lipids* **1993**, *64* (1-3), 83-98.
120. Kato, M.; Hayashi, R., Effects of high pressure on lipids and biomembranes for understanding high-pressure-induced biological phenomena. *Biosci Biotech Bioch* **1999**, *63* (8), 1321-1328.
121. Kapoor, S.; Werkmuller, A.; Denter, C.; Zhai, Y.; Markgraf, J.; Weise, K.; Opitz, N.; Winter, R., Temperature-pressure phase diagram of a heterogeneous anionic model biomembrane system: Results from a combined calorimetry, spectroscopy and microscopy study. *Bba-Biomembranes Bba-Biomembranes* **2011**, *1808* (4), 1187-1195.
122. Oursel, D.; Loutelier-Bourhis, C.; Orange, N.; Chevalier, S.; Norris, V.; Lange, C. M., Identification and relative quantification of fatty acids in Escherichia coli membranes by gas chromatography/mass spectrometry. *Rapid Commun Mass Spectrom* **2007**, *21* (20), 3229-33.
123. Malyshka, D.; Pandiscia, L. A.; Schweitzer-Stenner, R., Cardiolipin containing liposomes are fully ionized at physiological pH. An FT-IR study of phosphate group ionization. *Vib Spectrosc Vib Spectrosc* **2014**, *75*, 86-92.
124. Grazia Sessa, G. W., Phospholipid spherules (liposomes) as a model for biological membranes. *J Lipid Res* **1968**, *9*, 310-318.
125. McNeil, S. E., *Characterisation of Nanoparticles Intended for Drug Delivery*. 2 ed.; Springer New York: 2017; p 256.
126. Danaei, M.; Dehghankhold, M.; Ataei, S.; Davarani, F. H.; Javanmard, R.; Dokhani, A.; Khorasani, S.; Mozafari, M. R., Impact of Particle Size and Polydispersity Index on the Clinical Applications of Lipidic Nanocarrier Systems. *Pharmaceutics* **2018**, *10* (2).
127. Luzzati, V., Biological significance of lipid polymorphism: the cubic phases - Commentary. *Curr Opin Struc Biol Curr Opin Struc Biol* **1997**, *7* (5), 661-668.
128. Ikon, N.; Ryan, R. O., Cardiolipin and mitochondrial cristae organization. *Bba-Biomembranes Bba-Biomembranes* **2017**, *1859* (6), 1156-1163.
129. Avanti Polar Lipids, I. Ionization Constants of Phospholipids. <https://avantilipids.com/tech-support/physical-properties/ionization-constants> (accessed 24/08/2020).
130. Sulek, M. W.; Bak, A., The Effect of Liquid Crystalline Structures on Antiseizure Properties of Aqueous Solutions of Ethoxylated Alcohols. *Int J Mol Sci* **2010**, *11* (1), 189-205.



131. Angelov, B.; Angelova, A.; Garamus, V. M.; Lesieur, S., Vehicles of inverted hexagonal liquid crystalline lipid phases self-assembled at room temperature. *J Optoelectron Adv M* **2013**, *15* (3-4), 211-215.
132. Garti, N.; Libster, D.; Aserin, A., Lipid polymorphism in lyotropic liquid crystals for triggered release of bioactives. *Food Funct* **2012**, *3* (7), 700-713.
133. Ruela, A. L. M.; Carvalho, F. C.; Pereira, G. R., Exploring the Phase Behavior of Monoolein/Oleic Acid/Water Systems for Enhanced Donezepil Administration for Alzheimer Disease Treatment. *J Pharm Sci-US* **2016**, *105* (1), 71-77.
134. Warriner, H. E.; Idziak, S. H. J.; Slack, N. L.; Davidson, P.; Safinya, C. R., Lamellar biogels: Fluid-membrane-based hydrogels containing polymer lipids. *Science* **1996**, *271* (5251), 969-973.
135. Ruiz-Fernandez, A. R.; Lopez-Cascales, J. J.; Giner-Casares, J. J.; Araya-Maturana, R.; Diaz-Banos, F. G.; Munoz-Gacitua, D.; Weiss-Lopez, B. E., Effect of shape and bending modulus on the properties of nematic lyotropic liquid crystals. *Rsc Adv Rsc Adv* **2016**, *6* (9), 7455-7464.
136. Szutkowski, K.; Jurga, S., Long-Range Ordering in the Lyotropic Lamellar Phase Studied by High-Resolution Magnetic Resonance Diffusion-Weighted Imaging. *J Phys Chem B* **2010**, *114* (1), 165-173.
137. Winter, R.; Jeworrek, C., Effect of pressure on membranes. *Soft Matter Soft Matter* **2009**, *5* (17), 3157-3173.